



United Nations
Educational, Scientific and
Cultural Organization

GRÖ
GTP

Geothermal Training
Programme
Under the auspices
of UNESCO

The Relationship between the Tulu Moya Geothermal System, the Ziway–Asela area and the Tectonic Structure of the Ethiopian Rift

Birhan Abera Kebede



Faculty of Earth Sciences
University of Iceland
2021

The Relationship between the Tulu Moya Geothermal System, the Ziway-Asela Area and the Tectonic Structure of the Ethiopian Rift

Birhan Abera Kebede

60 ECTS thesis submitted in partial fulfillment of a
Magister Scientiarum degree in Geothermal Science

MS Committee

Ásta Rut Hjartardóttir
Páll Einarsson

Master's Examiner
Gylfi Páll Hersir

Faculty of Earth Sciences
School of Engineering and Natural Sciences
University of Iceland
Reykjavik, October 2021

The Relationship between the Tulu Moyo Geothermal System, the Ziway-Asela Area and the Tectonic Structure of the Ethiopian Rift

Tulu Moyo-Ziway Tectonism and the Ethiopian Rift
60 ECTS thesis submitted in partial fulfillment of a *Magister Scientiarum* degree in Geothermal Science

Copyright © 2021 Birhan Abera Kebede
All rights reserved

Faculty of Earth Sciences
School of Engineering and Natural Sciences
University of Iceland
Sæmundargötu 2
101, Reykjavik Iceland

Telephone: 525 4000

Bibliographic information:

Birhan Abera Kebede, 2021, *The Relationship between the Tulu Moyo Geothermal System and the Tectonic Structure of the Ethiopian Rift*, Master's thesis, Faculty of Earth Sciences, University of Iceland, pp. 84.

Printing: Háskólaprent,
Reykjavik, Iceland, October 2021

Abstract

The tectonic features of the Tulu Moye-Ziway area in the Central Main Ethiopian Rift (CMER) were mapped by using Digital Elevation Models, aerial photographs, and field observations. The study area contains various tectonic features, such as normal faults, fissures, eruptive fissures, and caldera structures. Fissures and eruptive fissures are few and mainly trend N-NNE. The faults have different characteristics depending on their localities. In the southern part, between Asela and Lake Ziway, most of them are older, and northeasterly oriented, forming horsts and grabens. They are situated near the eastern escarpment; representing the border fault system of the CMER which is formed by tectonic extension. The faults in the north, and a few in the southeastern part, are younger, volcanotectonically active and belong to the Wonji Fault Belt (WFB). They are formed by extension deformation assisted by magmatic intrusion. The western part of this section includes a NW-striking fault system, while the N-NNE oriented fault swarm dominates in the eastern part. Crosscutting relationships show that the NNE oriented faults predate the NW oriented faults. This section also hosts the active ~N-S striking Salen spreading axis, an aligned ridge of Holocene fissure eruptions and fractures. Three nested and partially visible caldera structures are identified by tracing caldera wall remnants. The Tulu Moye geothermal area is located where the calderas intersect the WFB, and surface hydrothermal alterations follow the caldera lineaments. This suggests that the geothermal activity is linked with the interaction between the caldera structures and the WFB.

Útdráttur

Sprungur og misgengi voru kortlögð á Tulu-Moye-Ziway svæðinu, sem er á miðhluta gliðnunarbeltis Eþíópíu. Notuð voru ný hæðarlíkön og loftmyndir, og voru niðurstöðurnar staðfestar með felvinnu. Á rannsóknarsvæðinu má finna ýmsar tegundir sprungna, s. s. misgengi, opnar gjár, gossprungur og öskjubrot. Opnar sprungur og gossprungur eru fáar og liggur stefna þeirra á milli norðurs og norð-norðausturs. Misgengin eru mismunandi eftir staðsetningu. Á suðurhluta svæðisins, milli Asela og Ziway vatns, eru flest þeirra gömul og stefna í norðaustur. Þau mynda sigdali og rishryggi. Misgengi nærri austurbrún gliðnunarbeltisins eru hluti af jaðarsprungum þess og eru talin mynduð vegna fráreks og gliðnunar. Misgengin norðar, ásamt nokkrum misgengjum á suðausturhluta svæðisins, eru yngri og tilheyra Wonji sprungukerfinu sem er talið myndað og mótað vegna samspils kvikuvirkni og gliðnunar, þegar kvikuinnskot skjótast grunnt inn í jarðskorpuna. Vesturhluti þessa svæðis inniheldur sprungukerfi þar sem sprungur stefna í norðvestur, en í austurhlutanum eru norð- til norð-norðaustlægar sprungustefnur ráðandi. Þar sem sprungustefnurnar skerast sést að norð-norðaustlægu misgengin eru eldri en norðvestlægu misgengin. Á því svæði liggur Salen gliðnunarhryggurinn. Hann stefnir í norður-suður og inniheldur gossprungur og sprungur. Öskjubrot þriggja askja sjást innan rannsóknarsvæðisins. Tulu-Moye jarðhitasvæðið er staðsett þar sem öskjurnar skarast við Wonji sprungukerfið. Auk þess má finna jarðhitaummyndanir sem liggja eftir öskjubrotunum. Þetta gefur til kynna að jarðhitavirknin á svæðinu sé tengd samspili Wonji sprungukerfisins og askjanna.

Dedication

This work is dedicated to the innocent civilians, who suffered and were displaced because of their identity in my country at the time of my study.

Table of Contents

List of Figures	viii
Abbreviations.....	xiii
Acknowledgements	xv
1 Introduction	17
1.1 The geothermal resources of Ethiopia	18
1.2 Objectives of the project	20
2 Tectonics and Structural Setting of the Main Ethiopian Rift System	21
2.1 The northern main Ethiopian rift (NMER)	22
2.2 The central main Ethiopian rift (CMER)	24
2.3 The southern main Ethiopian rift (SMER)	26
3 The Tulu Moye - Ziway-Asela Area.....	27
3.1 Location and physiography	27
3.2 General geology and tectonic setting of the Tulu Moye - Ziway area	28
3.2.1 Tectonic setting	28
3.2.2 Lithology.....	30
3.2.3 Thermal manifestations	35
3.3 Geothermal exploration in Tulu Moye high temperature geothermal field.....	36
3.3.1 Geochemistry	37
3.3.2 Geophysical Exploration	37
3.3.3 Recharge	40
4 Methods	43
5 Results.....	44
5.1 General overview of structural features in the study area	44
5.2 Fissures	46
5.3 Eruptive fissures	48
5.4 Faults.....	48
5.4.1 General pattern.....	48
5.4.2 Types of faults based on orientation	49
5.4.3 Types of faults based on their localities	51
6 Discussion	62
6.1 The crosscutting relationships and volcano-tectonic interaction	62
6.2 . Tulu Moye caldera complex structures.....	64
6.2.1 Scenarios for the mode of collapse of the proposed caldera complex.....	66
6.3 The WNW-NW fracture system	69

6.4 Seismicity and its relationship with fractures	70
6.5 Tectonic structures and its relationship with the geothermal system	72
6.6 Characterisation of the study area with respect to the MER	73
6.7 Conceptual models of the developmental phases of the study area	74
7 Conclusions	77
8 Recommendations	78
References	78

List of Figures

Figure 1. Map of the east African rift system and the Ethiopian rift.	18
Figure 2. Map of the identified geothermal prospects along the Ethiopian rift system (the red triangles) and the location of the Tulu Moyo geothermal field (indicated in the inset map within the black rectangle).....	19
Figure 3. Lithospheric terranes, crustal thickness, and locations of Cenozoic extension following the rheological boundaries (NMER, CMER, YTVL) (Image from Keranen and Klemperer, 2007).	21
Figure 4. Digital elevation model showing the tectonic map of the Main Ethiopian Rift sectors. NMER: Northern MER; CMER: Central MER; SMER: Southern MER; YTVL: Yerer Tulu Welel Volcanic lineament; BTSH: Boru Toru structural high; GBL: Goba–Bonga lineament; BG: Bridge of God; ChB: Chamo Basine; GB: Galana basin;AH: Amaro Horst; ZSMS: Ziway-Shala magmatic segment; AGMS: Aluto-Gedemsa magmatic segment; BKMS: Boseti-Kone magmatic segment; FDMS: Fantale-Dofen magmatic segment; DZ: Debre Zeyit; BT: Butajira; Ms: Munesa. The study area is indicated by the green box1. Most of the information plotted on the map are from Agostini et al., (2011b) and Corti, (2009).	23
Figure 5. Picture on the left shows the upper mantle P-wave tomography at 75 km depth (figure from Bastow et al., 2005) and on the right is a velocity model along the rift axis (figure from Keranen and Klemperer, 2007).	26
Figure 6. Overview map of the central main Ethiopian rift and location of the study area. YTVL: Yerer Tulu Welel Volcanic lineament; BTSH: Boru Toru structural high; AGMS: Aluto-Gedemsa magmatic segment.....	28
Figure 7. a) Fault traces and accommodation zones (cross rift broken lines) of MER (figure from Woldegabriel et al., 1990). b) Fault traces of part of the Central MER-Northern MER transition zone, BTSH (figure from Bonini	

et al., 2005). Thick dark gray dashed line indicates structures extrapolated from the trend of the Yerer Tullu-Wellel (YTVL).	30
Figure 8. Geological map of the research area showing lithology and distribution of surface hydrothermal alteration activity. Lithology is modified from Abebe et al. (1998), Boccaletti et al. (1999) and Abebe et al. (2005). The surface hydrothermal alteration is modified from Ayele et al. (2002) and field observations.....	31
Figure 9. Mt. Bora and the heavily faulted volcanic complex further to the SE (on the left side) and thick succession of stratified pyroclastic deposit near Jarbula crater (on the right).	33
Figure 10. The NNE aligned Salen-Giano deposit, a view from the heavily dissected half caldera situated in the east.	33
Figure 11. Stratigraphy column of the main rock types outcropping in the study area (Modified from Boccaletti et al. 1999).	34
Figure 12. Photos of surface hydrothermal manifestations. The upper photos show fumaroles and the lower are rocks altered to variegated clay deposits. Photo A to C are taken from the western side of Tulu Moye area and photo D to F are taken from the eastern side Arba Bite, between Mt. Jima and Adano.....	36
Figure 13. A map showing model of (a) Electrical conductivity along the E-W cross section and (b) the magmatic system transferring from the lower crust into a shallow partial melt zone driving the convecting hydrothermal system (figures from Samrock et al., 2018).	38
Figure 14. Resistivity map at 1500 m a.s.l. figured from MT survey showing lower resistivity in the eastern part of the survey area, south of Salen Ridge (figure from Varet and Birba, 2018).	39
Figure 15. Earthquake epicentres distribution map around the Bora-Tulu Moye volcanic complex. a) Epicentres indicated by circles that are colored by their cluster location and size of circles denote the magnitude. b) Longitude versus depth cross section of hypocentres. c) Cumulative magnitude distribution. Figure from Greenfield et al. (2019a).	40
Figure 16. Regional and local hydrological map of the Ziway-Asela area and Tulu Moye geothermal system. The major and minor stream flows are indicated by the thick blue colored lines and thin light-blue colored lines, respectively.	41
Figure 17. A map showing extent of the areas used by different images and aerial photo.	43
Figure 18. A tectonic map showing a general overview of the structural features together with the lithology of the area. The lithology is modified from Abebe et al. (1998), Boccaletti et al. (1999) and Abebe et al. (2005). The	

surface hydrothermal alteration is modified from Ayele et al. (2002) and field observations.	45
Figure 19. The graph on the left side shows length vs. orientation of the fissures and the rose diagram on right side represents frequency of the total distribution of the fissures with their respective orientations. The small numbers on the X and Y axis of the circles represents the percentage of frequency of the fissures.....	46
Figure 20. An aerial photo and DEM showing the longest fissure of the area (in the black dashed rectangle) and eruptive fissure (a dashed yellow color) formed during the historic eruption on the Salen spreading axis.....	47
Figure 21. Photo of an extension fissure (a) south east of Giano dome, about 3 m opening towards the direction of the general extension of the MER. (b) a fissure developed an open fault with an opening of ~10 m in the basaltic field of the Wonji group, further south east of Mt. Tulu Moye.	47
Figure 22. The fault density distribution map of the study area.	48
Figure 23. Quantitative data representation of the faults in the study area. Length vs. orientation graph (the left hand side) and rose diagram (the right side) of the faults in the study area. The color bars on the rose diagram represent the frequency of the faults over their orientations. The small numbers on the X and Y axis of the circles represent the percentage of the frequency.	49
Figure 24. Map showing the relationship between the WNW-NW striking faults and surface hydrothermal activity. Information on the hydrothermal activity is modified from Ayele et al. (2002).....	50
Figure 25. Structural map of the research area showing faults, hydrothermal activity and the categorized regions as identified by the white dashed lines. a) the southern region, b) the north-eastern region, c) the north-western region. The letters A, B and C represent the location of pictures used in this report. The white circle shows the highest measured temperature of surface surface manifestation.	51
Figure 26. Length vs. orientation graph (the left hand side) and rose diagram (the right side) of the faults in the southern region. The color bars on the rose diagram represent the frequency of the faults over their orientations. The numbers on the X and Y axis of the circles represent the percentage of the frequency.	52
Figure 27. Map of the throws distribution in the southern region.....	53
Figure 28. Profiles across the faults in the southern region of the research area. The faults and graben/half grabens are indicated by the black and red arrows, respectively.....	54

Figure 29. A map showing the lowest elevated graben (indicated by the black line) between Lake Ziway and Asela and its northern extension towards the Salen volcanic ridge (axis of ridge).....	55
Figure 30. Length vs. orientation graph (the left side) and rose diagram (the right side) of the faults in the north-eastern region. The color bars on the rose diagram represent the frequency of the faults over their orientations. The numbers on the X and Y axis of the circles represent the percentage of the frequency.	56
Figure 31. Photo showing some of the NE and NNE striking faults in the southernmost part of the north-eastern region. The white arrows indicate the faults. Their location is indicated as A, B and C in Figure 24.	57
Figure 32. Map of the Salen intra-rift spreading axis (indicated by black dashed rectangle) with lithology and the surrounding fractures. The lithology is modified from Abebe et al. (1998), Boccaletti et al. (1999) and Abebe et al. (2005).....	58
Figure 33. A photo and image showing the mini graben structures of Tulu Moye (a) and Salen (b) volcanic centres. The white and black arrows on the photo and image point to the mini graben structures. The current drilling site is represented by the black star on the up right image.	59
Figure 34. Length vs. orientation graph (the left side) and rose diagram (the right side) of the faults in the north-western region. The color bars on the rose diagram represent the frequency of the faults over their orientations. The numbers on the X and Y axis of the circles represent the percentage of the frequency.	60
Figure 35. a) Map of the half graben and the surrounding transverse faults at Bora-Arba Bite area. b) The zoomed map of the yellow box on map a, showing the graben. c) A photo showing a transverse fault (black dotted line) near the extensively altered mount Arba Bite.	61
Figure 36. DEM showing examples of the interaction of fractures and faults with the cinder cones and silicic domes at different localities as indicated on the inset map.....	62
Figure 37. DEM image showing crosscutting relationships of the fractures at the northern region; in the southern (b) and in the south-western (a) side of Gnaro dome. The red and blue dotted lines represent the younger and relatively older faults, respectively. Location of the areas are indicated in the inset map.....	63
Figure 38. A photo of the remnant of the half caldera-1 seen from the top center.....	64
Figure 39. Map of the proposed caldera complex structures and the lithology. The lithology is modified from Abebe et al. (1998), Boccaletti et al. (1999) and Abebe et al. (2005). The surface hydrothermal alteration is modified from Ayele et al. (2002) and field observations.	65

Figure 40. Type of caldera collapses A) Piston/Plate B) Piecemeal C) Downsag. Figures from Cole et al. (2004).	66
Figure 41. A) A structural map of Askja central volcano showing the most important tectonic and magmatic features (from Trippanera et al., 2018); B) The fissure swarm crossing Krafla caldera, Iceland (from Hjartardottir et al., 2012); C) Map of the fault swarm and fissures crossing an elongated caldera of Tulu Moye area.....	68
Figure 42. Seismic activity of the Ethiopia since 1960. The triangles show the Quaternary volcanoes in the MER. The image is taken from Keir et al. (2006).	70
Figure 43. A seismic map showing the dostribution of focal mechanisms (from Greenfield et al. 2019 a)	71
Figure 44. Epicentral map with magnitude showing the association of the existing surface structures with the distribution of the earthquakes (indicated by yellow lines) and surface alteration (The seismic data are provided by the TMGO expert, and the surface alteration is from Ayele et al., 2002 and field observtion).	72
Figure 45. Conceptual models showing the development of the study area in the context of the MER.	76

Abbreviations

EARS: East African Rift System

MER: Main Ethiopian Rift

NMER: Northern Main Ethiopian Rift

CMER: Central Main Ethiopian Rift

SMER: Southern Main Ethiopian Rift

WFB: Wonji Fault Belt

YTVL: Yerer Tulu Welel volcanic lineament

BTSH: Boru Turo structural high

GBL: Goba–Bonga lineament

BG: Bridge of God

ChB: Chamo basine

GB: Galana basin

AH: Amaro horst

ZSMS: Ziway-Shala magmatic segment

AGMS: Aluto-Gedemsa magmatic segment

BKMS: Boseti-Kone magmatic segment

FDMS: Fantale-Dofen magmatic segment

DZ: Debre Zeyit

BT: Butajira

Ms: Munesa

GRO-GTP: Geothermal Training Program

GSE: Geological Survey of Ethiopia

RG: Reykjavik Geothermal

TMGO: Tulu Moya Geothermal Operation

USGS: United States Geological Survey

Acknowledgements

I sincerely thank the Icelandic Government and GRO-GTP, the former United Nations University Geothermal Training Program (UNU-GTP) and its staff for giving me the full scholarship to do this master degree. I am greatly indebted to my employer Geological survey of Ethiopia (GSE) for allowing me to use this opportunity. My very sincere gratitude to my supervisors Ásta Rut Hjartardóttir and Páll Einarsson for their guidance.

This research has also benefited from Reykjavik Geothermal (RG), the shareholder of Tulu Moye Geothermal Operation (TMGO) and my special thanks goes to RG and its staff for providing the data and financing my field work. My special thank also goes to Snorri Gudbrandsson for supporting and providing data from RG and Anette Mortensen for the following up, encouragement and support.

I am also thankful for my colleagues and GRO-GTP fellows for their support and friendship. My colleague Zelalem Abebe is also thanked for his experience sharing during the fieldwork. Thanks to my wonderful parents and siblings for their support and care.

Finally, I give all glory and honor to God that made the program possible.

1 Introduction

The East African rift system is a divergent continental rift system consisting of a series of several thousand kilometres long rifts. It extends from Afar in the north to Mozambique, branching into the Eastern and Western branches (Figure 1). It is formed on the ancient weak zones over the super plume, which causes the extensive volcanism and topographic uplifting of the region since the Eocene epoch (e.g., Chorowicz, 2005; Ring, 2014). High altitude plateaus and successive graben structures bound both branches. Both branches are segmented into discrete rifts that are connected to each other by transform fault zones. Each of these rifts consist of aligned volcanic centres and rift Lakes within them. The eastern branch extends over the 2200 km, from the Afar triangle in the north, to the Gregory rift at the Tanzanian divergence zone in the south (Chorowicz, 2005). The western branch runs for over 2100 km from Lake Albert in the north, to Lake Malawi in the south. The western branch is characterized by scattered volcanism, less elevated regional plateau that surrounds the rift and is less mature compared to the eastern branch (e.g., Ring, 2014). The rift maturity increases from south to the north. The northern part of the EARS is characterized by weakened lithosphere, active volcanism and advanced level of rifting; while the south, volcanism and rifting activities are in a relatively less advance stage (e.g., Chorowicz, 2005).

The Ethiopian rift system is a part of the northern segment and the eastern branch of the East African rift system. It extends about 1000 km distance from the Afar depression in the north to the Omo-Turkana low-land in the south (Woldegabriel et al., 1990), in a NE–SW to N–S direction. The Ethiopian rift is developed along the uplifted plateau (the Ethiopian dome), splitting it asymmetrically into two plateaus: the western/ Ethiopian plateau and the eastern/ Somalian plateau. Both plateaus are characterised by Neoproterozoic basement rock overlain by thick Mesozoic sediment succession, which in turn are overlain by Eocene-Late Oligocene flood basalt (trap basalt). On top of the flood basalt, shield volcanoes and rhyolitic eruptions predominate the plateau area. The plateaus are highly elevated on either side of the rift rising up to > 4000 m above sea level, due to the accumulation of volcanic deposit uplift in relation to erosional unloading (e.g., Corti, 2009; Gani et al., 2007).

Based on its tectono-volcanic feature and rifting activity, the Ethiopian rift system is divided into the Afar rift/depression and the Main Ethiopian rift (Figure 1). The Afar rift is formed by subsidence of the Afar dome as a result of subsequent stretching and thinning in late Oligocene - early Miocene (e.g., Beyene and Abdelsalam, 2005) where the present altitude reaches down to ~ 125 m below sea level. The Afar depression is bounded by the Ethiopian Plateau in the west, the Somalian Plateau in the east, the main Ethiopian rift and Danakil block from the south and north sides, respectively (Figure 1, 2). It is a place where a triple junction is formed between the main Ethiopian rift, Red sea, and the Gulf of Aden (Figure 1,2) and represents the matured rift and an on land seafloor spreading of the EARS (Ebinger and Casey, 2001; Beyene and Abdelsalam, 2005). The main Ethiopian rift extends from south of the Afar rift to the low land of Omo-Turkana in the south.

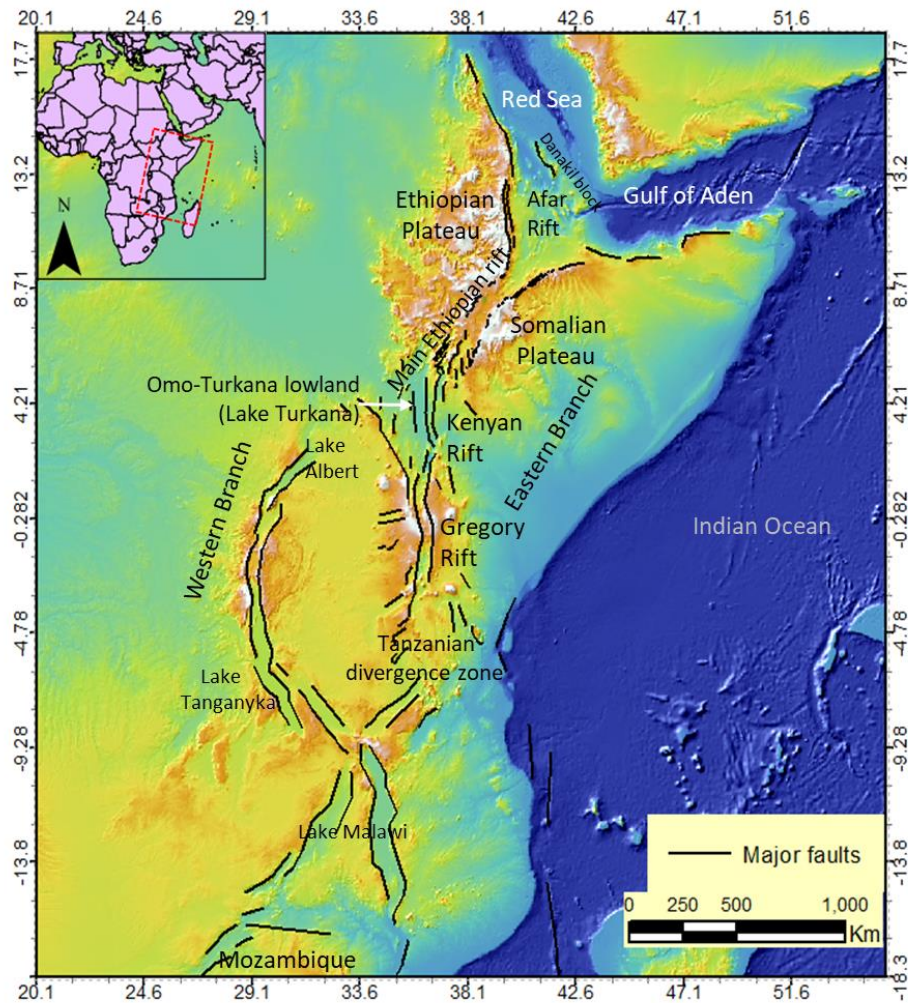


Figure 1. Map of the east African rift system and the Ethiopian rift.

1.1 The geothermal resources of Ethiopia

The EARS is a home of very high enthalpy geothermal resources. Numerous geothermal areas have been identified along the EARS. The Ethiopian rift is one of the promising sites of geothermal resource in East Africa. It has a total estimated electrical power potential of over 10,000 MW (Kebede, 2014).

Previously, the whole Ethiopian rift system went through a preliminary survey. About 120 localities within the rift system were identified to have an independent heating and circulation system and were evaluated to have potential for both high and low enthalpy geothermal resource development (UNDP, 1973). So far, over 23 prospect areas (Figure 2) have been identified as high enthalpy geothermal resource, potential for electricity generation. The prospects are economically valuable due to their good reservoir properties, and the proximity of the resources to the existing infrastructures (Kebede, 2014). The prospects are at different stages of exploration and exploitation.

Since late 1969, surveys mostly comprising geology, geochemistry, and geophysics, were carried out at the southern-central part of the Ethiopian rift and in Afar. In addition, a semi detailed surface exploration of ten sites in the central and southern Afar has been carried out by the Geological Survey of Ethiopia (GSE) and Electroconsult (ELC, 1987). In the 1980s exploratory wells were drilled in Afar Dubti area and in Aluto, in the central sector of the Main Ethiopian rift. The wells in Aluto were productive and produced 7.3 MW, until the recent two appraisal trajectory wells were added. About eight MW of power is estimated from the additional two wells. Tulu Moye - Gedemsa, Tendaho, Corbetti, Abaya, Dofan, Fantale, Meteka and Dallol are a few of the prospect areas in which detailed exploration studies and drilling have started.

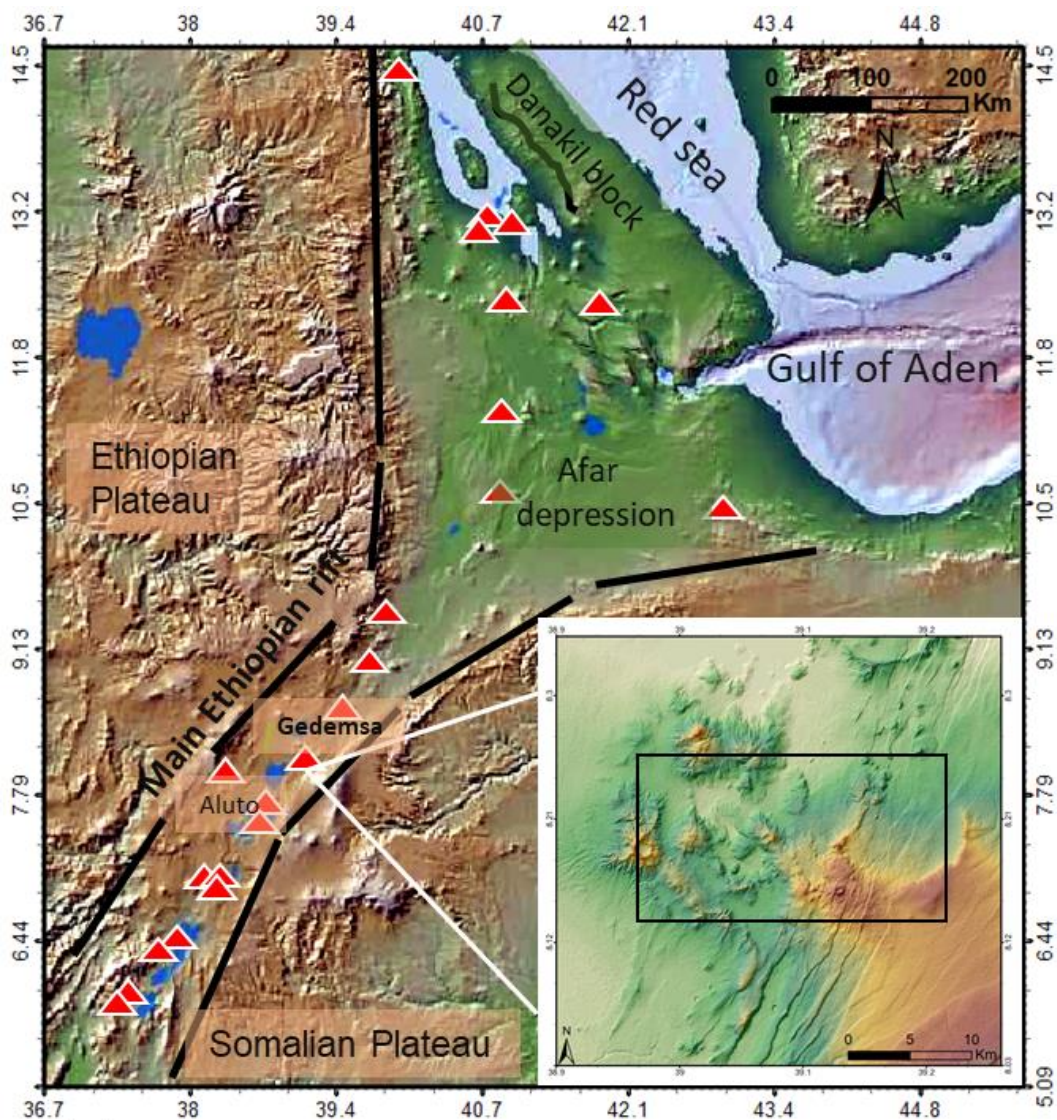


Figure 2. Map of the identified geothermal prospects along the Ethiopian rift system (the red triangles) and the location of the Tulu Moye geothermal field (indicated in the inset map within the black rectangle).

1.2 Objectives of the project

The main objective of this work is to study the tectonic and structural setting of Asela-Ziway area and the Tulu Moyo geothermal system in detail and relate this with the tectonics of the Ethiopian rift. The specific objectives of the project include:

- ✓ To outline the fault and fissure swarms of the study area from satellite images, aerial photographs and field observation,
- ✓ To create a detailed structural map of the area,
- ✓ To illustrate the complex caldera structure/s,
- ✓ To compare the surface structural data with other data available in the area, such as the geophysical data, and characterize the geothermal system of the area.

The thesis will be divided into three parts. The first part will cover a general description of the geology and tectonic features of the main Ethiopian rift system and its sectors, as well as in the study area. The second part will focus on the results and findings of the structural studies in the area from the images and field investigation; and the last will be relating the results of the current study with the existing data, such as seismicity and resistivity.

2 Tectonics and Structural Setting of the Main Ethiopian Rift System

The main Ethiopian rift (MER) is the southern extension of the Ethiopian rift, situated south of the Afar depression, between the two plateaus. The plateaus, east and west of the rift system have different crustal thicknesses. The eastern plateau has a uniform crustal thickness of ~38-40 km, while the western plateau is thicker in its north part and thinner in the south part (Figure 3). The thickness in the north part is due to the underplated mafic (gabbro) material accumulated in association with voluminous flood basalts which were formed 30 Ma years ago (e.g., Mackenzie et al., 2005; Maguire et al., 2006); separating the western plateau into north-western and south-western plateaus (Keranen and Klemperer, 2007; Dugda et al., 2005; Mackenzie et al., 2005). Accordingly, the north-western part is elevated on the surface and has thicker crust, 40-50 km, while the south-western part has lower altitude with thinner crust (34-36 km, e.g., Hayward and Ebinger, 1996; Mackenzie et al., 2005; Dugda et al., 2005). These two plateaus are then separated by the Yerer -Tulu - Wellel volcano tectonic lineament (YTVL), a structurally low area, which propagates from the northern main Ethiopian rift and diverts to the west following the rheological boundary (Figure 3; Abebe et al., 1998; Mackenzie et al., 2005; Keranen and Klemperer, 2007).

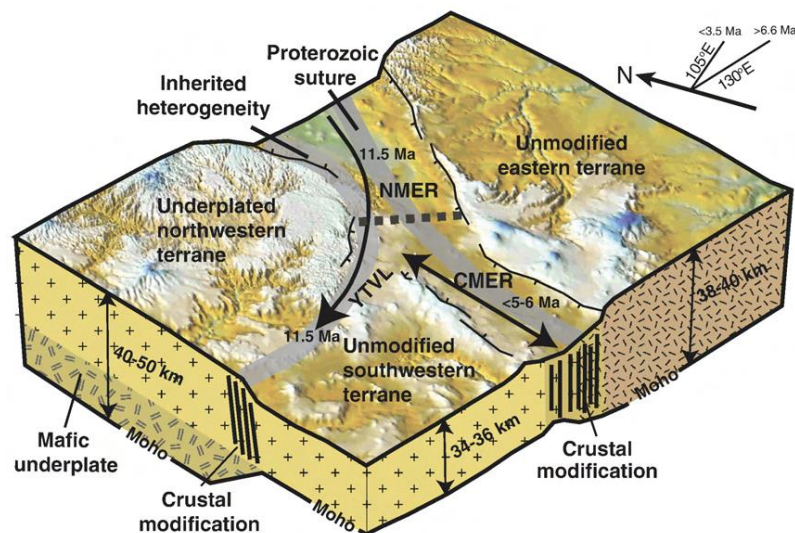


Figure 3. Lithospheric terranes, crustal thickness, and locations of Cenozoic extension following the rheological boundaries (NMER, CMER, YTVL) (Image from Keranen and Klemperer, 2007).

About 80 km wide Ethiopian rift system is formed by the reactivation of pre-tertiary tectonic weakness zone along the Pan African suture. It has NE-SW to NNE-SSW tectonic trends with the extension rate of ~ 6-7 mm/yr, in the direction of ESE-WNW (Mohr, 1962; Berhe, 1990; Keranen and Klemperer, 2007; Keranen et al., 2009; Corti, 2009). Apart from the mentioned orientations, the pre-rifting tectonic activities also played an important role in controlling the traversing NW-SE orientations (Chorowicz et al., 1994). The rift development is diachronous and discontinuous in terms of its propagation as well as its timing of activation. Geological, geochronological and geophysical data suggest that the MER is divided into three sectors, the northern MER (NMER), the central MER (CMER), and the southern MER (SMER). These sectors differ one from the other by their rift trend,

fault pattern, timing and lithospheric characteristics (e.g., Agostini et al., 2011a,b; Bonini et al., 2005; Wolfenden et al., 2004; Woldegabriel et al., 1990; Hayward and Ebinger, 1996; Mohr, 1962).

According to the architecture and activity of the faults, each sector is characterized by two distinct normal fault systems, the border faults and the internal faults (e.g., Agostini et al., 2011a,b). They represent two phases of rifting: the Tertiary and Quaternary rifting phases. The border faults are relatively older than the internal faults and are roughly oriented to the NE. These faults represent the rift boundary. They have large vertical offsets, widely spaced (e.g., Boccaletti et al., 1998; Corti, 2009) and long. The internal faults form the Wonji Fault Belt (WFB), they dominate the floor of the rift and represent the youngest (< 2 Ma) rifting activity in MER in relation with the Quaternary magmatic activity of the rift floor. The WFB is a 20 km wide, consisting tectono-magmatic segments trending NS to NNE, which are arranged in a right-stepping en-echelon fashion obliquely cutting the rift floor. The segments of the WFB characterize the floor of NMER and CMER, but are less exposed on the SMER. The Wonji faults are closely spaced, and are shorter in length and fewer in comparison with the outer border and marginal faults. The WFB shows a general southward decrease in the number and density of faults (e.g., Agostini et al., 2011a,b; Abebe et al., 2007; Ebinger and Casey, 2001; Hayward and Ebinger, 1996; Mohr, 1962; Figure 3).

In the MER, the earliest Early Miocene deformation is observed in the SMER, marked by the development of N-S trending structures with no extensions. These structures are related to the northward propagation of the Kenya Rift (Bonini et al., 2005). Extension related to rifting activity in the MER suggests a southward propagation, from the relatively older rift, NMER to the SMER (e.g., Bonini et al., 2005). The three MER sectors are described in more detail below.

2.1 The northern main Ethiopian rift (NMER)

The NMER extends from the southern Afar rift in the north to the Lake Koka area in the south, where it separates from the Central MER by the Boru Toru structural high (BTSH) as well as the YTVL (Figure 4; Bonini et al., 2005). Rifting in the NMER started in the Late Miocene, ~11 Ma (Wolfenden et al., 2004). It was initiated by the development of the boundary faults and propagated southward (e.g., Bonini et al., 2005).

This rift sector has a general trend of ~N50°E-N55°E, where the border faults are oriented ~N35°E-N40°E and the internal WFB faults are between N20°E and N25°E (e.g., Agostini et al., 2011a, b). The border faults of this sector are mainly eroded and inactive, while the WFB is younger and active.

The WFB is divided into Aluto-Gedemsa, Boseti-Kone and Fantale-Dofen magmatic segments, arranged in a northward right-stepping en-echelon fashion, from the CMER border to the southern part of the Afar depression (Figure 4; Wolfenden et al., 2004). Different geophysical studies show that the lithospheric property of the NMER is different from the other sectors (e.g., Mahatsente et al., 1999; Ebinger and Casey, 2001; Mackenzie et al., 2005; Dugda et al., 2005; Rooney et al., 2005; Maguire et al., 2006; Keranen and Klemperer, 2007; Keranen et al., 2009). There is a northward crustal thinning between the

central and northern MER border and the southern Afar rift depression; as the crustal thickness decreases from ~33-35 km to 24-26 km.

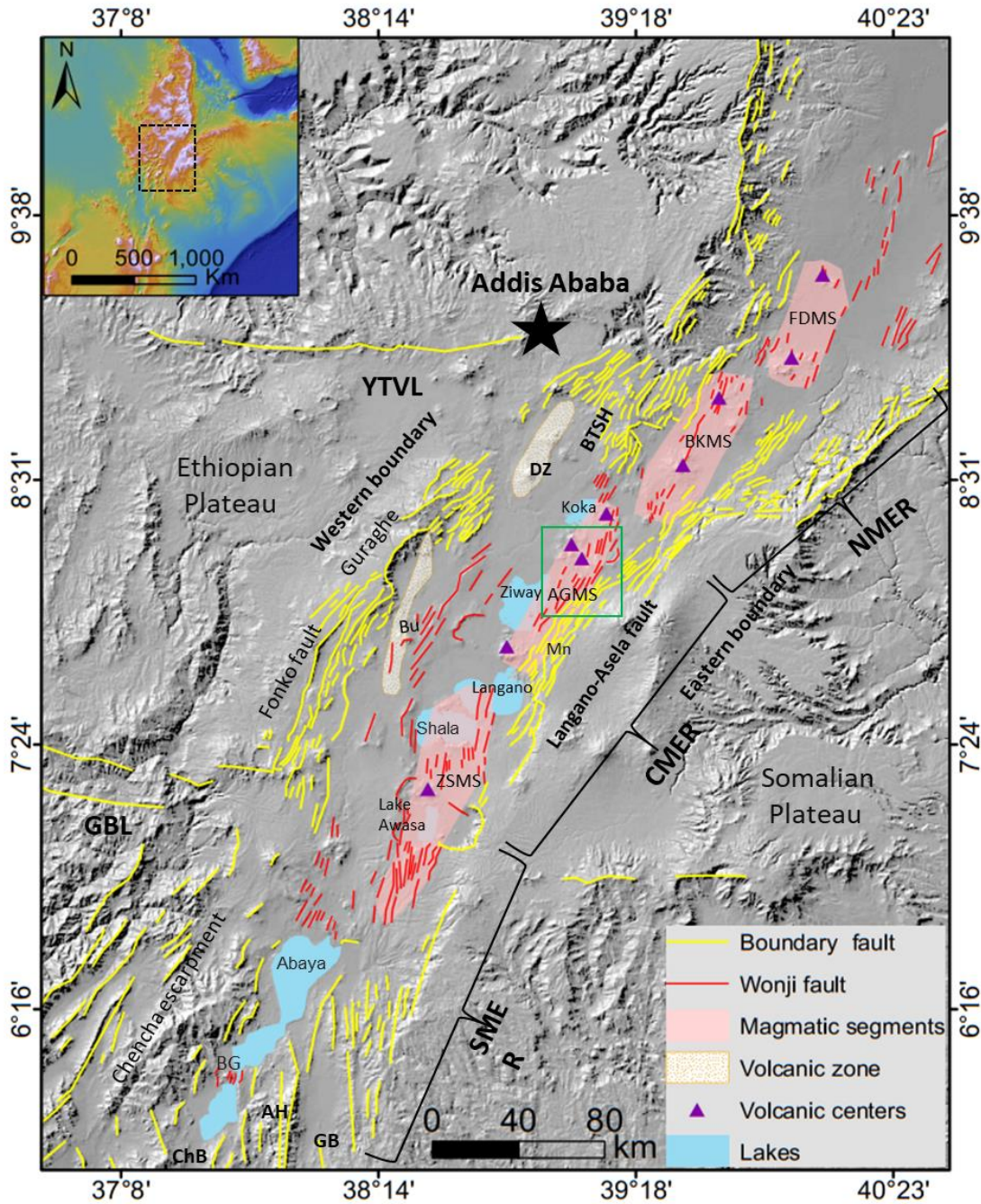


Figure 4. Digital elevation model showing the tectonic map of the Main Ethiopian Rift sectors. NMER: Northern MER; CMER: Central MER; SMER: Southern MER; YTVL: Yerer Tulu Welel Volcanic lineament; BTSH: Boru Toru structural high; GBL: Goba–Bonga lineament; BG: Bridge of God; ChB: Chamo Basine; GB: Galana basin; AH: Amaro Horst; ZSMS: Ziway-Shala magmatic segment; AGMS: Aluto-Gedemsa magmatic segment; BKMS: Boseti-Kone magmatic segment; FDMS: Fantale-Dofen magmatic segment; DZ: Debre Zeyit; BT: Butajira; Ms: Munesa. The study area is indicated by the green box1. Most of the information plotted on the map are from Agostini et al., (2011b) and Corti, (2009).

The NMER is characterized by high seismic velocity, dense lower crust, and high Poisson's ratio, which reaches its maximum beneath the magmatic segments (e.g., Mackenzie et al., 2005; Mickus et al., 2007; Keranen and Klemperer, 2007). These high anomalies are interpreted as mafic intrusions and dike complexes predominantly situated within WFB (e.g., Rooney et al., 2005; Mickus et al., 2007). The upper mantle is characterized by lower velocity and lower density relative to the crust, indicating the presence of a hotter thermal regime with some degree of partial melting. The boundary between the NMER and CMER lithosphere is marked by a sharp and abrupt discontinuity of the upper mantle as indicated by the upper-mantle tomographic models of the geophysical observations (Figure 5). The southerly propagating NMER clearly deflected westward beneath the YTVL rather than continuing into the CMER (Figure 5). Interpretations of the geophysical studies show that YTVL is experiencing strain and crustal mafic intrusions, where crustal melting exists at shallower depth, ~ 20-25 km (e.g., Mackenzie et al., 2005; Keranen and Klemperer, 2007). Overall, the NMER is considered to be at a transitional stage between continental and oceanic lithosphere (e.g., Hayward and Ebinger, 1996; Ebinger and Casey, 2001; Rooney et al., 2005). It is a mature rift and can be compared with the active volcanic zones of Iceland.

The volcanic activity on the MER commenced after the Eocene-Late Oligocene flood basalt activity. The older boundary faults exposed the older rocks while the recent volcanic activity is mainly confined to the axial part of the rift. Volcanism in the NMER is as old as Mid-Miocene (10.5 Ma). Basaltic to trachytic lava flows and associated pyroclastic (Termaber–Megezez formation) from the shield volcanoes of the rift shoulders, overlay the flood basalt (Chernet et al., 1998; Wolfenden et al., 2004). The Nazret Group ignimbrites, with intercalated minor silicic and Mio-Pliocene cover mafic lavas cover a vast area up to the southern Afar transition zone, representing the syn-rift volcanism. The sequence is followed by Late Miocene–Pliocene and upper Pliocene basalt volcanism namely Afar Stratoid Series and Bofa basalts, respectively. During the period of Plio-Pleistocene (2.5 - 1.7 Ma) a number of large caldera pyroclastic flow and fall deposits are recorded (e.g., Abebe et al., 2005; Boccaletti et al., 1999) covering mainly the floor of the rift. It is named differently by different authors, but commonly known as Chefe Donsa and Dino ignimbrite. On top of these successions, Quaternary bimodal volcanic activity called the Wonji Group, also known as Wonji series is deposited in relation with the oblique rifting activity of the Wonji fault belt flooring the axis of the rift (Woldegabriel et al., 1990). This group consists of silicic and mafic lava flows, pyroclasts and phreatomagmatic deposits, erupted mainly from the fissures and calderas mostly aligned with the WFB propagation direction. The products mainly dated as 1.8 Ma to historical (e.g., Woldegabriel et al., 1990; Chernet et al., 1998; Wolfenden et al., 2004). The last eruptions in the NMER sector are historical, such as Kone (1820) and Fentale (1810) (Cole, 1969; Wadge et al., 2016).

2.2 The central main Ethiopian rift (CMER)

The ~N30°E - N40°E oriented CMER extends about 175 km from the southern end of the NMER to the Lake Awasa area, where the northern extension of the SMER starts (Woldegabriel et al., 1990; Figure 4). The transverse tectonic features of YTVL bound it to the north and the Goba–Bonga lineament to the south (Abebe et al., 2010; Bonini et al., 2005). The onset of the CMER is dated as Late Miocene-Early Pliocene (5/6-7 Ma). It is characterized by ~N25°E to N30°E oriented, steeply dipping boundary faults that have large vertical offset of more than 1500 m. Such areas include as an example the Munesa and

Guraghe rift margins, which have N10°E-N15°E trending internal faults (Abebe et al., 2010; Agostini et al., 2011a, b). The floor of the rift is characterized by limited distribution of the faults of the WFB, which are less affected by tectonic-magmatic processes relative to the NMER and mostly localized near the rift margins. The western margin of this rift sector is well expressed by the N25°E-N35°E trending and ESE-dipping Guraghe and Fonko faults and by the off-axis belts near the boundary of Butajira and Debre Zeit volcanic zones (Figure 4; e.g., Boccaletti et al., 1998; Abebe et al., 2007). These volcanic zones are defined by a narrow marginal graben, Quaternary cinder cones and maars aligned to the NNE-NE and NE in the Butajira and Debrezeit volcanic zones, respectively (Woldegabriel et al., 1990; Abebe et al., 2007). The highest values of Poisson's ratios in the CMER, 0.33-0.35 and lower degree of seismicity is observed beneath these volcanic zones (e.g., Keranen and Klemperer, 2007; Keir et al., 2006). The eastern margin is well represented by the N30°E-trending and WNW-dipping Asela-Langano fault system, displaying a complex S or Z-shaped pattern of the Langano (or Haroresa) rhomboidal fault system formed by the intersection between the NE-SW-trending border faults and a local NW-SE trend (e.g., Corti, 2009; Boccaletti et al., 1998). Compared to the NMER, the CMER consists of purely continental lithosphere with a thicker crust, 38-40 km (Figure 3; Dugda et al., 2005; Maguire et al., 2006; Mickus et al., 2007), less defined magmatic segments (Aluto-Gedemsa and Ziway-Shala magmatic segments) and lower seismic velocities (Keir et al., 2006). Keranen and Klemperer, (2007) suggest that the thicker crust is due to the lower amount of extension. The CMER displays lower upper-crustal seismic velocities, reflecting lower degree of magmatic addition to the crust. The Quaternary faulting, magmatic activity, and seismicity is concentrated near the eastern rift boundary (Keranen and Klemperer, 2007).

The oldest tertiary rocks in the CMER are flood basalts, dated to 29 Ma (Bonini et al., 2005). After this was a hiatus, until the Late Miocene basalts, trachy basalt and minor silicic products of Gurage basalt were formed (Woldegabriel et al., 1990; Bonini et al., 2005; Abebe et al., 2005; Chernet et al., 1998). Woldegabriel et al. (1990) reported that intermediate and acidic rocks, Shebele trachyte of ~17–12 Ma age, are exposed locally. On top of the Gurage basalt, intensive volcanic activity was recorded (Abebe et al., 2010) depositing pyroclastic rocks associated with trachytic and rhyolitic lava domes and flows associated with some important central volcanoes of a 5–3 Ma age which cover the shoulders and floor of the rift. This unit is equivalent to the Nazret group of NMER. The last episode of the volcanic activity in CMER is a < 3 Ma bimodal deposits of pumiceous fall and flow, rhyolitic to trachytic lava flows forming central volcanic edifices, fissural basaltic lava flows with associated scoria and phreatomagmatic cones (Wonji group < 1.6 Ma), and interbedded lacustrine deposits (e.g., Abebe et al., 2007; Abebe et al., 2005). The Quaternary volcanic activity, apart from the Wonji group products that are localised in the eastern part, is also situated near the western marginal area, and expressed as the Debrezeit and Butajira volcanic (Abebe et al., 2007). The NNE-NE oriented cinder cones, maars, and some lava phreatomagmatic cones define these zones. They are less mature than the WFB, with less evolved magmatic system and less defined conduits and melt fractionation at various depths within the crust (Rooney et al., 2005). The last eruption in the CMER sector dated to historic time (1800s; Wadge et al., 2016), erupted within the WFB in the Aluto-Gedemsa magmatic segment.

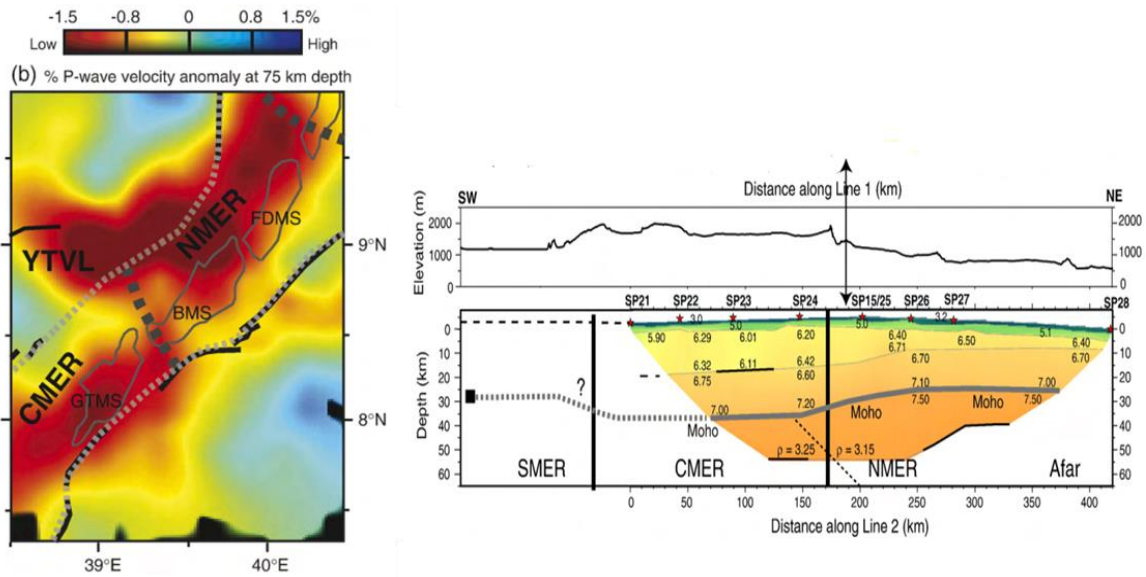


Figure 5. Picture on the left shows the upper mantle P-wave tomography at 75 km depth (figure from Bastow et al., 2005) and on the right is a velocity model along the rift axis (figure from Keranen and Klemperer, 2007).

2.3 The southern main Ethiopian rift (SMER)

The Plio-Pleistocene southern sector of the MER represents an early stage of rift development, where the deformation activity, axial faulting (WFB) and magmatic modification is less active than at the other MER sectors. The subsurface lithospheric property of this sector is poorly constrained. The geophysical data indicate limited volcanic activity and the absence of significant magmatic processes in this sector (Dugda et al., 2005). The transition from the CMER to SMER is marked by a major E-W-trending transverse structure, the Goba-Bonga lineament (Abbate and Sagri, 1980) which is related to the reactivation of a pre-existing lithospheric weakness zone. The rift trend in this sector rotated from NE to NS, dividing the SMER into north and south; SMERn and SMERs respectively (Agostini et al., 2011a, b). The SMERn is N20°E-N25°E oriented, with the same orientation as the border faults, while the SMERs is oriented to N0°-N10°E. The WFB in both SMER is very limited and ~N0°-N10°E oriented. Further south of SMERs, the rift corresponds to a division of the rift valley into two near-parallel grabens, namely the Chamo basin to the west and the Galana basin to the east. They are separated by a horst called the Amaro Horst, a narrow block of Precambrian basement (Figure 4; Corti, 2009).

The oldest Tertiary volcanic rocks outcrop in the SMER is dated at 45-30 Ma (Woldegabriel et al., 1990; Ebinger et al., 1993). This old unit is overlain by the Late Miocene stratoid basalt and dykes, which again is overlain by a Miocene (~11 Ma) basalt, trachyte and rhyolite lava until the minor basaltic lava deposited on the plateau of Chench escarpment ~7 Ma years ago. The bimodal volcanic activity commenced in Pliocene-Early Pleistocene (Zanettin et al., 1978) depositing ignimbrites, which is coeval of the Nazret group. This unit is followed by the Wonji group equivalent of 1.34–0.77 Ma old basalt (Nech sar olivine basalt; Ebinger et al., 1993) and 0.66 Ma old trachy basalts, pumiceous tuffs, obsidian flows

and basalts (e.g., Corti, 2009; Bonini et al., 2005). Fissurally erupted basaltic lava and cinder cones in Chamo basin and Bridge of God (Figure 4) are the historic eruptions encountered on the SMER (Ebinger et al., 1993).

In general, the MER is a spectacular site to study the ongoing divergent rifting activity. The relative Nubia-Somalia motion gives rise to a roughly ESE-WNW spreading direction, at an average vector of $\sim N100^{\circ}E$ (Keir et al., 2006). The overall studies of MER depicts that the rift is generally evolving from mature rifting in the Northern MER to less evolved rifting southward (e.g., Hayward and Ebinger, 1996; Corti, 2009; Agostini et al., 2011a,b).

3 The Tulu Moye-Ziway-Asela Area

3.1 Location and physiography

The research area is located ~ 100 km south of the capital Addis Ababa. It is situated at the boundary of the northern and the central part of the main Ethiopian rift sectors, near to the eastern margin of the CMER. The area is bounded by a rift lake, Lake Ziway in the south and an artificial lake, Lake Koka in the north (Figure 6). The areas near the lakes are of the lowest altitude, while the highest elevation is in the southeastern part of the study area, along the escarpment and Mt. Chilalo (> 4000 m). Mt. Tulu Moye, Bora and Berecha are also elevated (> 2200 m). The area can be accessed via the roads built from Addis – Mojo – Meki, or Addis – Mojo – Adama – Itaya, (Figure 6). Apart from the main roads, dry weather roads are built within the study area to access most parts of it. Topographically, the area is partially rugged and partially flat plain. Farmland and different vegetation with a patchy settlement cover most of the Tulu Moye area. Tulu Moye area is also characterized by extensive hydrothermal activity. It is one of the high temperature geothermal prospects in Ethiopia, and the activity is manifested on the surface in the form of fumaroles, steaming and altered grounds.

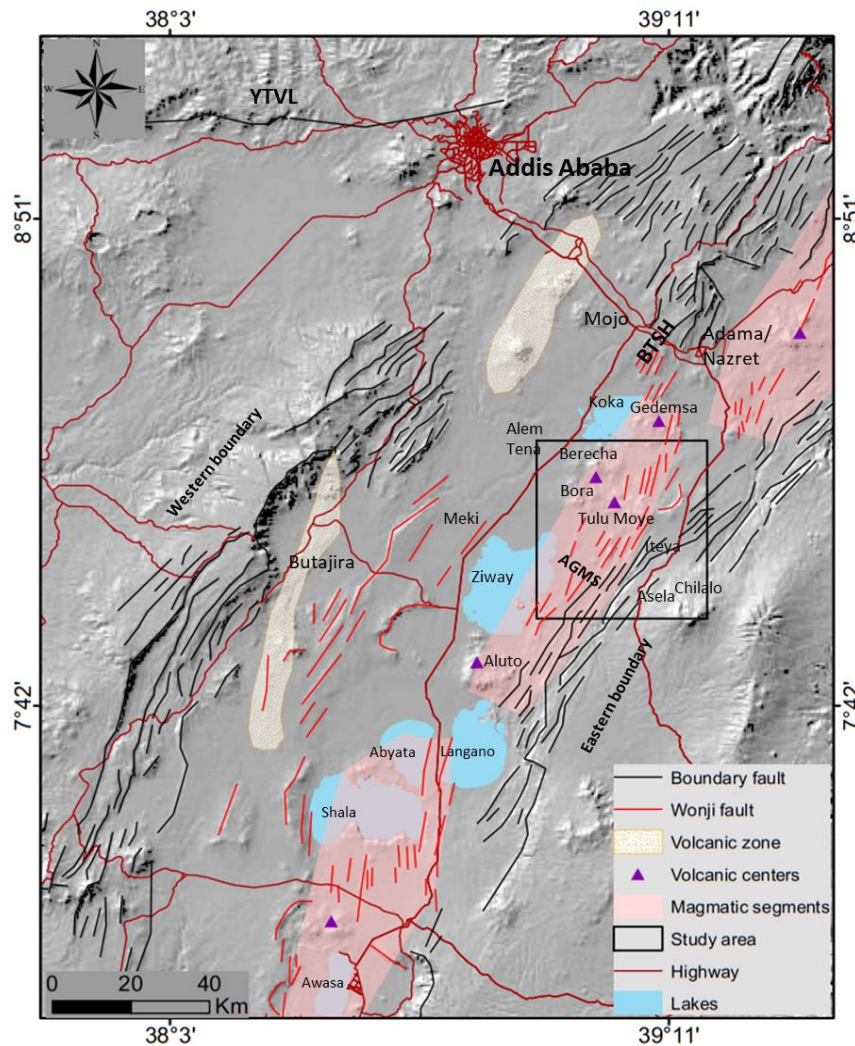


Figure 6. Overview map of the central main Ethiopian rift and location of the study area. YTVL: Yerer Tulu Welel Volcanic lineament; BTSH: Boru Toru structural high; AGMS: Aluto-Gedemsa magmatic segment.

3.2 General geology and tectonic setting of the Tulu Moya geothermal and the Ziway- Asela area

3.2.1 Tectonic setting

The Tulu Moya-Ziway-Asela area is situated near the eastern margin of the Ethiopian rift system. The eastern margin is characterized by near vertical high angle, W-dipping normal faults, with an average strike of N30°E-N40°E. The extension direction is thus ~ ESE-WNW, with local variations ranging between E-W and NW-SE (e.g., Boccaletti et al., 1998; Acocella and Korme, 2002; Bonini et al., 2005; Pizzi et al., 2006). Previously the area has been recognized under different sectors of the MER. As an example, Abebe et al. (2005) and

Wolfenden et al. (2004) mapped the area as part of the northern MER. On the other hand, Bonini et al. (2005); Abebe et al. (2010); Woldegabriel et al. (1990); and others considered it to be a part of the central sector, while Agostini et al. (2011b) and Corti, (2009) put the area between the two sectors. In this study, the area will be considered to be a part of the CMER sector for various reasons. Regarding the architecture of both the internal and the marginal faults and the rift trend, the area mainly follows the behavior of the CMER. In addition to this, the YTVL that is situated northeast of the study area, is believed to be a separator between the two sectors (e.g., Keranen and Klemperer, 2007; Bonini et al., 2005) as evidenced from the geophysical investigations. It is confirmed that this separation has an extension up to the mantle lithosphere (Figure 5). Since the study area is situated south of this volcanotectonic feature, it can be considered to be a part of the CMER sector.

Tulu Moye - Ziway/Asela area is bounded by various tectonic elements. To the north, it is bounded by the Gedemsa caldera structure (Figure 6). Further north of this is the ~ N-S trending Boru Turo structural high (Figure 6 and Figure 7), which marks the transition zone between the central and northern MER (Bonini et al., 2005). It is a high relief accommodation zone marking a dextral shift of the main rift axis and change in the trend of the main boundary fault (Figure 7b). It propagates into the rift floor and connects the western margin to the eastern rift margin near Chilalo volcano. In addition, accommodation zones with a dextral transverse displacement bound the area from both in the north and south sides (Figure 7; Woldegabriel et al., 1990; Mohr, 1967). The eastern side is bordered by the notably NE trending eastern escarpment and the off axis Chilalo volcano, which is situated on top of the rift shoulder of the Somali plateau (Figure 6). The western side is wider with a flat topography, characterized by Lake sediments and pyroclastic deposits that have been cut by a few of the NE to NNE oriented normal faults.

The research area encompasses fissures and fault swarms, including both the major boundary faults and the inner WFB and caldera structures. The boundary faults are older structures closely spaced and localized near the escarpment, oriented in the general NE direction. On the other hand, the Wonji fault swarm branched off from the boundary faults and passes along the central part of the area exceeding Gedemsa caldera to mark an oblique en echelon right stepping relation with the nearby Bosetti-Kone magmatic segment. This and southern extension of WFB together forms the Aluto-Gedemsa magmatic segment; one of the volcano-tectonic segments of the MER. All the recent volcanic eruptions of the rift floor as well as the study area are controlled by the Wonji Fault Belt and are localized along these volcanotectonic segments. These magmatic segments are also a site of high heat flow and serve as a geothermal energy source by providing the heat source and permeability for fluid mobility. Besides these, the area is also crossed by NW-SE oriented strike slip faults as reported by Korme (1999).

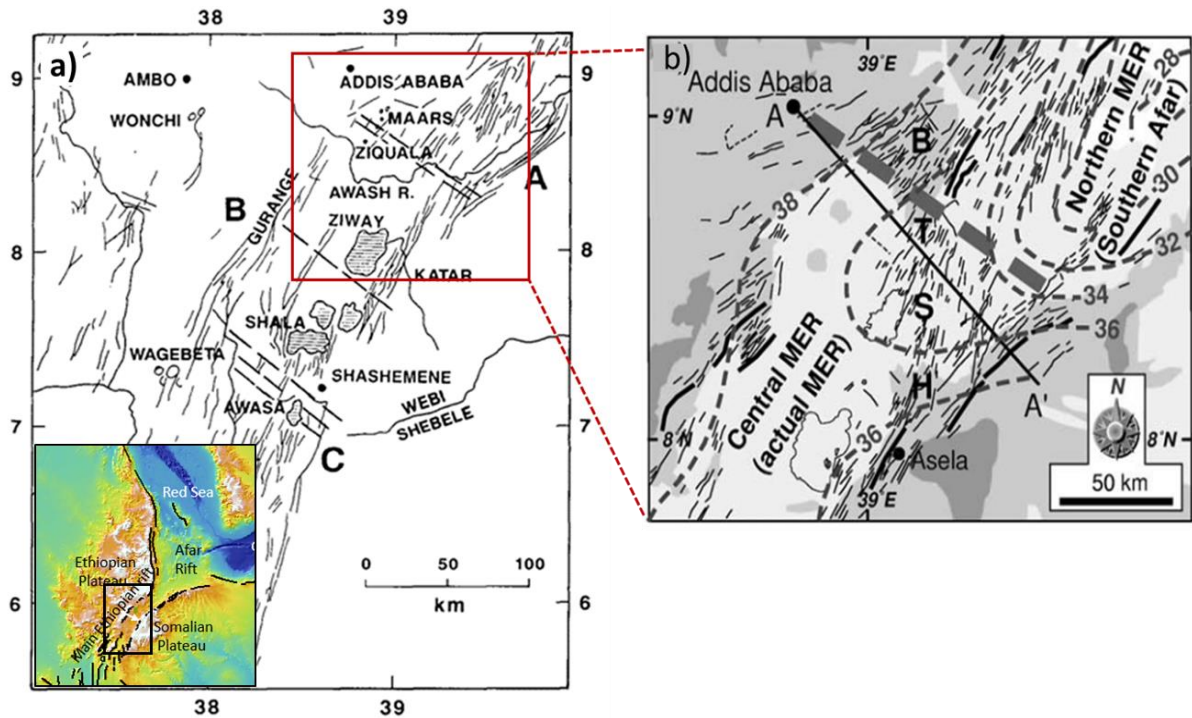


Figure 7. a) Fault traces and accommodation zones (cross rift broken lines) of MER (figure from Woldegabriel et al., 1990). b) Fault traces of part of the Central MER-Northern MER transition zone, BTS (figure from Bonini et al., 2005). Thick dark gray dashed line indicates structures extrapolated from the trend of the Yerer Tullu-Wellel (YTVL).

3.2.2 Lithology

The lithology of the area is characterized by bimodal activity of basaltic and rhyolitic volcanism, as well as by lacustrine sediment deposits. Caldera collapse, craters, eruptive fissures, and cinder cones are the main volcanic features of the area. Volcanism in the area spans from Pliocene to historical (e.g., Di Paola, 1972; Boccaletti et al., 1999). The older deposits are exposed in the southeastern side along the marginal areas. The young deposits are localized along the axial region of the rift floor and represented by effusive and extrusive bimodal volcanism of Holocene to recent age (Figure 8).

The lithological description and stratigraphy of the area are presented below by synthesizing the previous studies and field observations. The previous studies are compiled mainly from Di Paola (1972), Abebe et al. (1998), Korme (1999), Boccaletti et al. (1999) and Abebe et al. (2005). In addition to lithology, the mentioned authors also mapped the tectonic structures of the area in less detailed. According to the combined results of the above-mentioned authors, rocks belong to Tulu Moye-Ziway-Asela area can be categorized chronologically into two major groups (Pliocene-Pleistocene and Pleistocene-Historical groups) and different subgroups as follows:

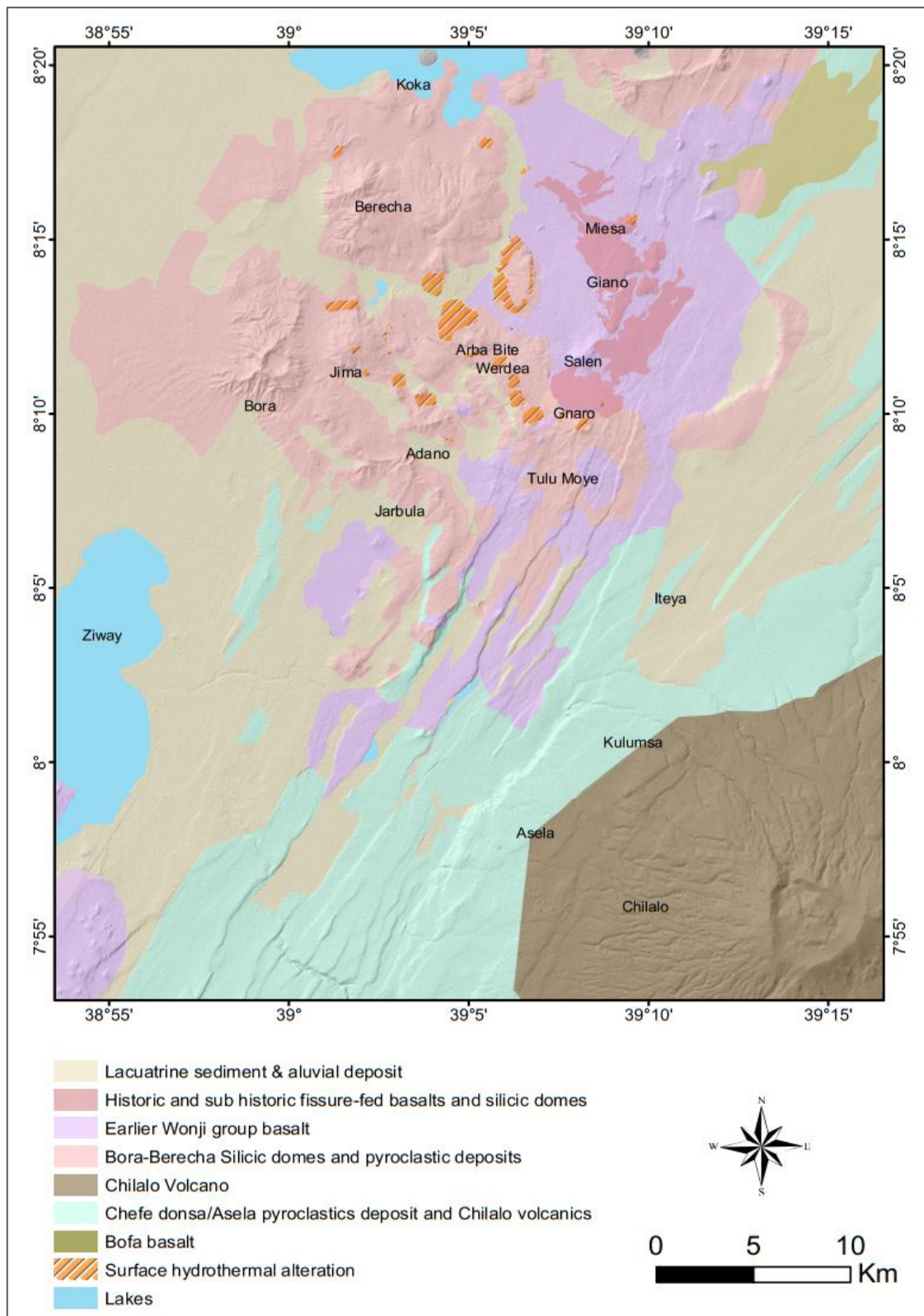


Figure 8. Geological map of the research area showing lithology and distribution of surface hydrothermal alteration activity. Lithology is modified from Abebe et al. (1998), Boccaletti et al. (1999) and Abebe et al. (2005). The surface hydrothermal alteration is modified from Ayele et al. (2002) and field observations.

Pliocene-Pleistocene Group

This group consists of older rocks exposed in the area. It consists of three coeval units: basalt, trachyte and pyroclastic fall and flow deposits. From these, the basalt and pyroclastic rock are well distributed along rest of the CMER and NMER, outside the study area and are given different formational names after the localities.

Bofa Basalt

This basalt unit is the oldest in the study area and is one of the young rift floor fissure-fed basalt flow deposit, dating between 3.5-1.6 Ma (Woldegabriel et al., 1990). It mainly crops out on the floor of the rift above the well-known late Miocene-Pliocene syn rift pyroclastic product, the Nazret unit. It is exposed rarely in the study area, only in the north-eastern part. Compositionally, it is alkaline, quartz tholeiite with a few olivine basalts.

Chilalo volcanics

The other coeval unit under this group is Chilalo volcanics, outcropped on the highest elevation of the study area on the escarpment. This unit incorporates a K-Ar radiometric determined age of 2.3-1.3 Ma rocks. It includes the fissure-fed hawaiiite basalts of the “eastern margin escarpment units” Boccaletti et al. (1999) and associated pantellerite ignimbrite sheets along the eastern fault escarpment and Chilalo basalt lavas. Chilalo composite volcano produces basaltic-trachyandesitic lava flows, associated mugearite basalt and pyroclastic deposits.

The Asela /Chefe donsa unit

This unit is characterized by pantelleritic and strongly to poorly welded ignimbrites. It covers a vast area, mainly localized between Lake Ziway and the eastern escarpment overlying the Eastern margin unit. The eruption centers are located outside the study area. It includes paleosol interbedding within the sections. It is exposed by the main border faults near and on the escarpment and along the rift floor along the graben, horst and half graben forming faults. It is the Asla unit of Abebe et al. (1998) and Chefe donsa of Abebe et al. (2005).

Pleistocene-Historic Group

This group consists of recent products that are associated with the Wonji fault activity of < 1.6 Ma to Holocene age. The products of this group are mainly called the Wonji group (e.g., Meyer et al., 1975). In the research area, these products are confined to the northern and north central parts.

The Bora-Berecha silicic volcanic products

This unit comprises the two sizable central volcanoes, Bora and Berecha and other associated silicic centres (e.g., Mount Tulu Moye, Jima, Werdea). It predominantly consists of pumice dominated pyroclastic eruption deposits and silicic lava domes. The volcanoes are located in the northern part of the study area, between the two Lakes, Ziway and Koka (Figure 8). They reach the highest altitude along the floor of the study area. Bora rises > 2100 m a.s.l. and forms large (> 1400 m) crater on its top (Figure 9). Berecha is fully constructed from unwelded pumice (Di Paola, 1972) and rises > 2200 m a.s.l. A small diameter (500 m) crater forming the Tulu Moye pyroclastic volcano, situated south east of Bora is about 2300 m

a.s.l. A layering of pumice, ash fall, and flow deposits and the associated peralkaline rhyolite and trachyte lava flows and domes of comenditic and pantelleritic composition characterize products of these volcanoes. Part of this product is also exposed on the heavily faulted east central part of the area. It consists of pantelleritic with subordinate comendites pyroclastic deposits with minor lava domes and flows that are related to the caldera collapse (Jarbula?) 115 ka to 1.8 Ma years ago. According to Fontjin et al. (2018), most of these pyroclastic deposits are sourced from ridges and domes east of Bora.

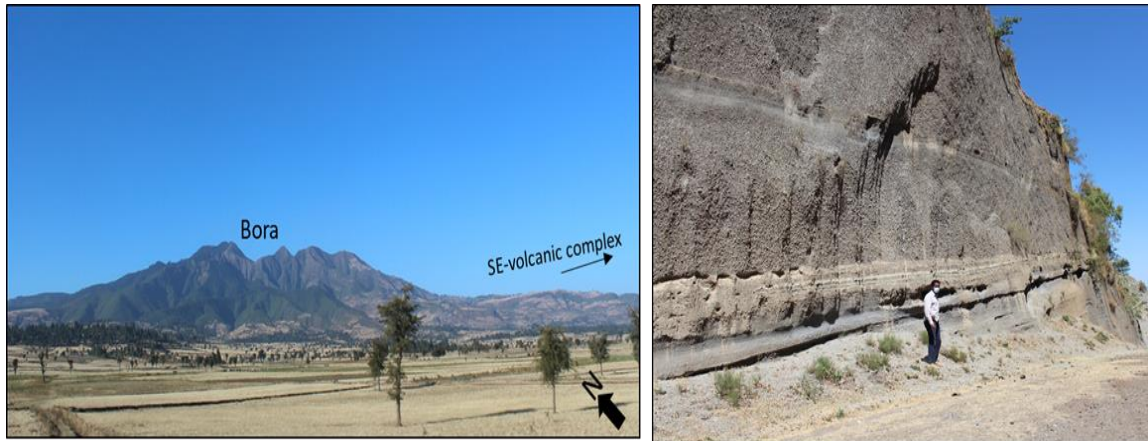


Figure 9. Mt. Bora and the heavily faulted volcanic complex further to the SE (on the left side) and thick succession of stratified pyroclastic deposit near Jarbula crater (on the right).

The Salen-Giano units, the youngest eruptions

Rocks in this group are both felsic and mafic. They are the youngest in the area, erupted mainly through fissures of the WFB. Products of this unit are also called the Wonji group/ Wonji series. The basaltic products and their associated cinder cones cover a vast area.



Figure 10. The NNE aligned Salen-Giano deposit, a view from the heavily dissected half caldera situated in the east.

The most recent basalt is represented by aphyric lava flows, erupted through fissures and cinder cones, while a relatively older member of the lava is porphyritic, with plagioclase grains and mostly erupted through the faults situated along the rift axis. The K-Ar radiometric age of the older member showed an age of 0.29 Ma (Woldegabriel et al., 1990), which might be considered coeval to the Bora-Berecha unit (Figure 11). Besides this, comenditic obsidian lava flows on the rift axis erupted from the same fissure along the Salen-Giano range (Figure 10). The domes are concentric and aligned following the same NNE-SSW striking vents, where Gnaro dome is situated in the south-central part and Giano and Miesa are further to the north (Figure 8). These obsidian domes are the youngest deposits in the area and believed to have erupted around 1900s (Wadge et al., 2016), yet according to Di Paola (1972), the basalts are younger than the obsidians or they are penecontemporaneous. Bizouard and Di Paola (1978) reported that one of the obsidian dome, Giano erupted in late 18th century. The products surrounding the Salen-Giano range get relatively older away from this range in both towards the east and west. The stratigraphic succession of the area is shown in Figure 11 below.

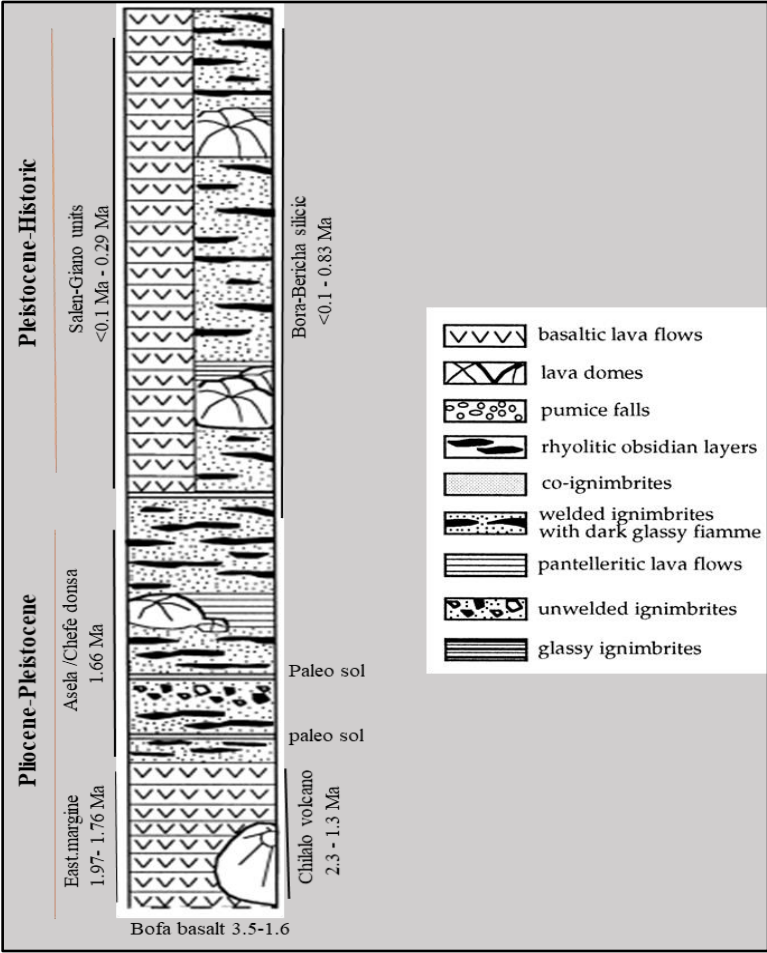


Figure 11. Stratigraphy column of the main rock types outcropping in the study area (Modified from Boccaletti et al. 1999).

Lacustrine sediments and alluvial deposits (late Pleistocene - Holocene)

Lacustrine sediments cover the lower elevated areas; mostly surroundings of Lake Ziway area and north-western part of the research area. It is one of the characterizing feature of the central MER, resulted from the deposit of sediments from the lakes, Lake Ziway-Shala region, which in turn is the result of an environmental/ climatic change over time and tectonism in the MER during late Pleistocene and Holocene time (Benvenuti et al., 2002). They incorporate mainly sand and silt and volcanic origin sediments, such as pumice and volcanic ash, obsidian, rhyolite, and basalt rock fragments (Abebe et al., 2005; Benvenuti et al., 2002). The alluvial sediments are mainly at the lower elevation, also in valleys. They are reworked materials of the local volcanic deposits.

The subsurface geology of the study area is poorly studied due to lack of deep drilling wells. From the five shallow (<170 m depth) temperature gradient wells, Ayele et al., (2002) carried out a study of the shallow subsurface geology and hydrothermal alteration.

3.2.3 Thermal manifestations

The northern part of the study area, where the volcanic complexes are intense, is marked by an extensive hydrothermal activity, which is exposed on the surface (Figure 8). This includes fumaroles, steaming and warm ground, and the altered products of soft clay deposits. Unlike other geothermal sites of the country, Tulu Moye lacks neither hot/warm nor cold spring. The thermal activity affects a widespread area of pyroclastic flow and fall deposits and rhyolite domes situated between the Bora-Berecha and Tulu Moye edifices. Clay deposit is the most common surface thermal manifestation and covers a vast area, resulted mainly from the alteration of the pyroclastic materials (Figure 12).

Apart from the mapped hydrothermal activities, there are several small size surface hydrothermal manifestations distributed throughout the area, predominating in the west central part of the area. Some of these are weak fumaroles and are used by the local people as steam bath and for healing purposes.

The shallow subsurface study reveals the presence of a temperature gradient 40-66 °C/100 m and low to high intensity of alteration throughout the wells and alteration minerals; such as, smectite, stilbite, kaolinite, quartz, calcite, pyrite, albite and so on, from which smectite, kaolinite and quartz are abundant (Ayele et al., 2002). In addition, rocks such as pumice, pumice breccia, ignimbrite, rhyolite, trachyte, scoraceous basalt, basalt lava, and alluvium were identified from the boreholes.



Figure 12. Photos of surface hydrothermal manifestations. The upper photos show fumaroles and the lower are rocks altered to variegated clay deposits. Photo A to C are taken from the western side of Tulu Moye area and photo D to F are taken from the eastern side Arba Bite, between Mt. Jima and Adano.

3.3 Geothermal exploration in Tulu Moye high temperature geothermal field

Tulu Moye geothermal prospect has been investigated for geothermal exploration studies; geology, geochemistry, and geophysics, since the 1980s. Electro Consult (ELC) conducted the first coordinated surface exploration with Geothermica Italiana and Ethiopian Institute of Geological Survey during the year 1985-1987, aiming at the reconnaissance study at Tulu Moye and other selected geothermal sites of the Ethiopian rift system (Ayele et al., 2002; Electro Consult, 1987). During this time, they did studies of geology, soil survey (radon and mercury) and geophysical surveys (gravity and electrical resistivity). Geological Survey of Ethiopia also carried out exploration (geology, geochemistry, and geophysics) on the surface, and borehole geology and hydrothermal studies from the five shallow temperature gradient wells that were drilled in 2001 to construct the shallow depth log of stratigraphy and hydrothermal alteration; and to understand the thermal and hydrogeological history of the geothermal site (Ayele et al., 2002).

The previous studies were not detailed and did not utilize an integrated method until the prospect leased out to Tulu Moye Geothermal Operations Plc in 2014. Tulu Moye Geothermal Operations Plc (TMGO) is operated by a collaboration of Meridiam global investor and asset manager and Reykjavik Geothermal development company, aiming at

installing 520 MWe geothermal power plant by 2025 and 50 MW in the near future, by 2022 (Varet and Birba, 2018).

After a long period of inactivity, improved and detailed exploration studies were done by TMGO, utilizing various methods of surface explorations since 2008 (Varet and Birba, 2018). The results from those studies confirm that the area has a potential geothermal reservoir with a shallow heat source and presumably good permeability suitable for geothermal power production (e.g., Varet and Birba, 2018; Gudbrandsson et al., 2020). Accordingly, the first deep drilling well was drilled for further detailed examination of the geothermal system and power production. Both surface and subsurface exploration studies are currently being done in the area.

In addition to this, other studies have also been done recently which can support the geothermal exploration. An overview of the exploration results from the previous works are described in the section below.

3.3.1 Geochemistry

Since the area lacks springs for sampling, the geochemical analysis are based on steam samples from fumaroles and temperature gradient wells. Despite that, based on Ayele et al., (2002), the water samples from the shallow wells around Tulu Moye prospect area are characterized by an immature, carbonated and low chloride content water with high concentration of CO₂ and H₂S.

According to the internal report of Meridiam (the co-creator of TMGO; Marini, 2018) as reported in Varet and Birba, (2018) the southern part of Salen ridge that is characterized by a steaming ground with high CO₂ concentration and relatively high temperature is identified as an up flow zone. The wide area west of Gnaro dome is suggested to be an outflow zone, characterized by high CO₂ emitting fumaroles and numerous steam bathes. The recent study of gas geothermometers designated that the reservoir temperatures of Tulu Moye geothermal area are over 230 °C (Gudbrandsson et al., 2020).

3.3.2 Geophysical Exploration

Gravity and magnetic surveys

The Geological Survey of Ethiopia from 1991-1992, with an interval of 5 km using trails and dry weather roads did regional gravity and magnetic surveys (Ayele et al., 2002). Results from the magnetic survey show a positive magnetic anomaly in the central and eastern parts and negative anomaly in the north-western part of the area. The gravity survey defines a positive gravity anomaly on the volcanic centers to the western side, near Mt. Berecha, Bora, Jima, Werdea and Adano with an absolute value in excess of 162 mGal. This is interpreted as 4-6 km deep magma intrusions, which are assumed to be a possible heat source of the geothermal system along with a NW-SE aligned volcano-tectonic segment in the area. Negative anomaly is observed around the west and north-western part as well as in the Tulu Moye area and is inferred to be due to densely distributed fractures.

Resistivity

Resistivity mapping was carried out by the Geological Survey of Ethiopia in 1999 and 2000. The result from the collected data reveals a wide zone of NW-SE directed low resistivity anomaly to the western side, over the deposits of unwelded pumice breccia, tuffs and ashes of peralkaline rhyolite composition. This is interpreted as a NW-SE trending volcano-tectonic line of tectonically affected region. This locality is also identified as a widespread alteration zone that is considered an outflow zone of hydrothermal fluids (Ayele et al., 2002).

Magnetotelluric (MT) imaging is among few of the studies carried out recently in the Tulu Moyo geothermal area. 112 stations were occupied between Bora-Berecha and Tulu Moyo volcanoes, aiming at outlining Earth's electrical conductivity structure using naturally occurring low-frequency electromagnetic variations (Samrock et al., 2018). They made 3-D subsurface electrical conductivity model which shows the electrical conductivity of the subsurface at various depths. The model reveals the presence of four distinct electrically conductive zones (C1-C4) (Figure 13).

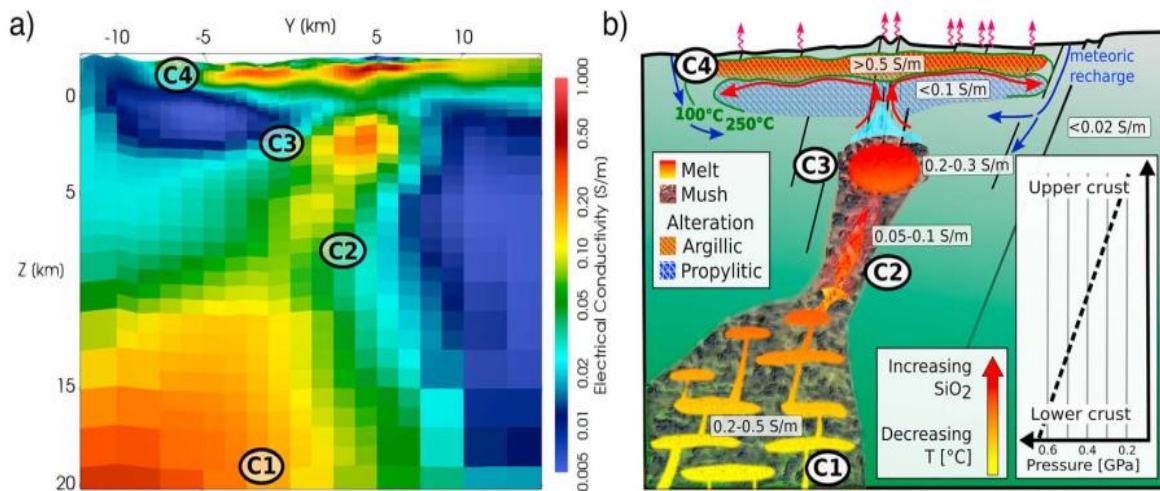


Figure 13. A map showing model of (a) Electrical conductivity along the E-W cross section and (b) the magmatic system transferring from the lower crust into a shallow partial melt zone driving the convecting hydrothermal system (figures from Samrock et al., 2018).

The lower conductive zone, at depths below 14 km, is defined by the highest electrical conductivity (C1, 0.2-0.5 S/m) and represents the lower crust. The upper crust, which is close to the surface (C4) is denoted by high conductivity capping the shallow zone of partial melting, identified as C3. According to Samrock et al. (2018), the deeper lower crustal zone of higher conductivity is inferred as a mantle-derived basaltic melt and the shallow conductivity is caused by the argillic hydrothermal alteration forming highly conductive smectite clays, which is an indicator of convective high-enthalpy hydrothermal system in the area. C3 has the high electrical conductivity (0.2-0.3 S/m) representing a shallow partial melt zone centered at a depth of about 4 km and is taken as the possible source of heat for the geothermal system (Samrock et al., 2018).

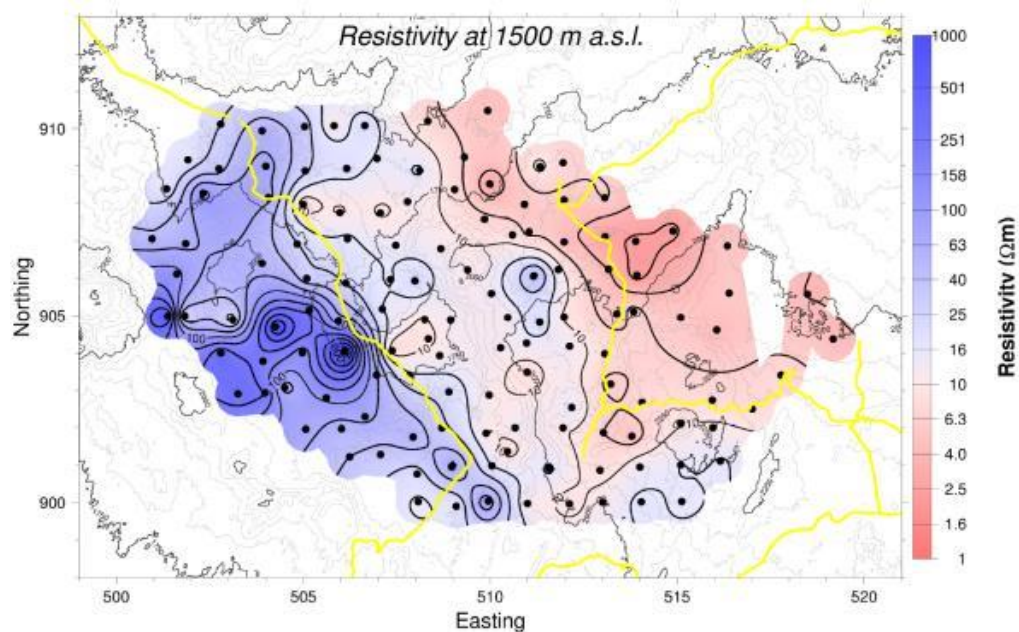


Figure 14. Resistivity map at 1500 m a.s.l. figured from MT survey showing lower resistivity in the eastern part of the survey area, south of Salen Ridge (figure from Varet and Birba, 2018).

A resistivity survey (TEM-MT) also done by TMGO covered a broad area of the southern half section of the prospect, with over 150 stations. The result from the survey indicates the presence of a 500 to 1000 m thick clay cap at a depth of 500-800 m from the surface, and low resistivity anomaly along the southern part of the Salen volcanic range (Varet and Birba, 2018; Gudbrandsson et al., 2020; Figure 14). This low resistivity anomaly is suggested to be shallow depth magma chamber, that can be a heat source of the geothermal system.

Seismic activity

Despite the limited coverage of seismic network in Ethiopia, seismic activity of Bora-Tulu Moyo area was described by Greenfield et al. (2019 a,b). It included the period between February 2016 and October 2017, during which more than 1200 seismic events of local magnitude 0 to 2.3 were recorded. From the earthquake catalogue, three active regions of earthquake swarms are highlighted as shown in Figure 15, where most of the seismicity lies beneath the volcanic centers situated to the west and south-central part of the area, predominantly near Tulu Moyo. The most active region is located between the volcanic centers of Bora and Tulu Moyo, indicated by an east-west elongated cluster of red-colored circles (Figure 15). Lower magnitude events are distributed within a broader region associated with Bora, situated among Bora, Berrecha and Arba Bite. A cluster of seismicity also occurs underneath Tulu Moyo, indicated by yellow-colored circles; denoted as low-frequency earthquakes Greenfield et al. (2019 b).

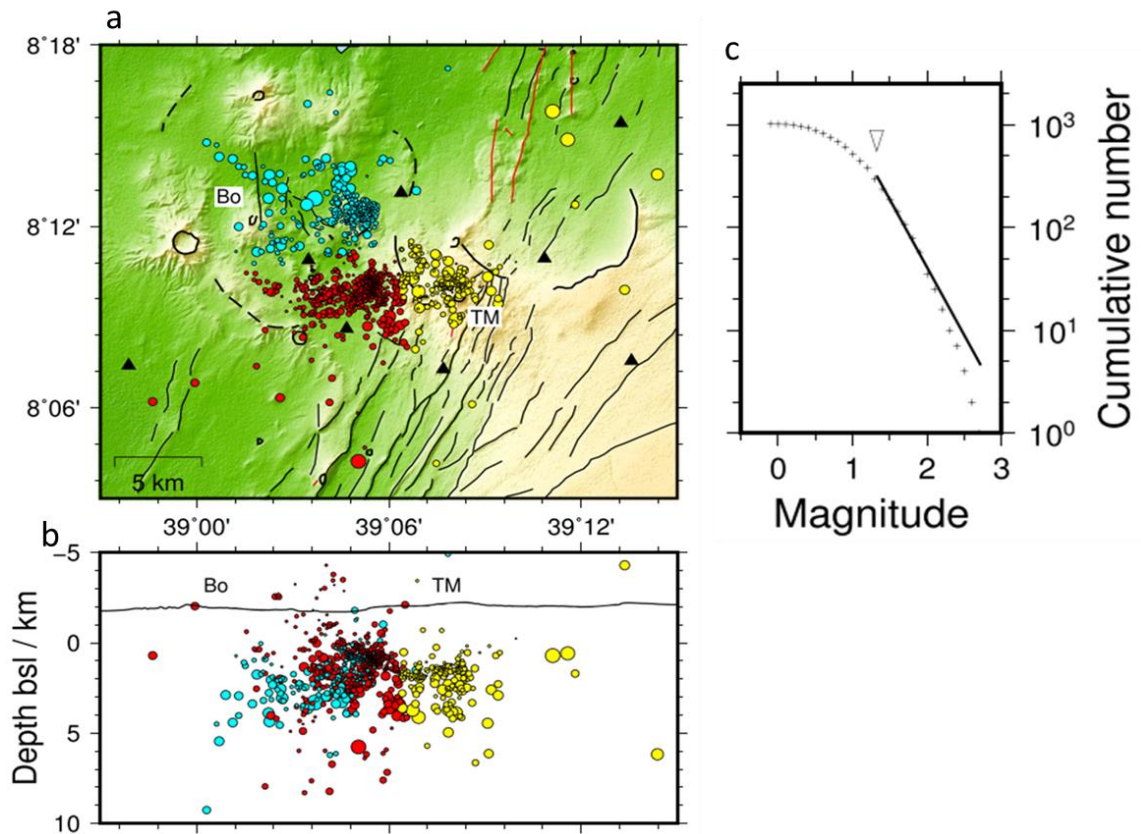


Figure 15. Earthquake epicentres distribution map around the Bora-Tulu Moyo volcanic complex. a) Epicentres indicated by circles that are colored by their cluster location and size of circles denote the magnitude. b) Longitude versus depth cross section of hypocentres. c) Cumulative magnitude distribution. Figure from Greenfield et al. (2019a).

Overall, the study suggested the presence of intense and low magnitude seismic activity beneath the mentioned volcanic centers. The seismic activity is interpreted to be triggered by the hydrothermal fluid circulation that is assisted by a shallow magmatic reservoir. The low-frequency earthquakes beneath Tulu Moyo are assumed to be triggered by high pore fluid pressures (H₂O/CO₂ mixtures) from a shallow magma body (Greenfield et al., 2019b). This has been interpreted as an indication of a magmatic body at a minimum depth of about 4 km underneath the Tulu Moyo edifice. The minimum depth of the brittle-ductile transition is estimated to be 6.5 km.

3.3.3 Recharge

Recharge is one of the basic components of a geothermal system. Aquifers of the geothermal systems along the Ethiopian rift get their recharge from the highlands that bound the rift valley following the regional groundwater flow (e.g., Fentaw and Mihret, 2011). The central main Ethiopian rift system is well identified by the occurrence of the Lake basins that are fed by the rivers originating from the plateaus. The tectonics, geology and topography of the area control the regional groundwater flow in the CMER as well as in the Tulu Moyo geothermal prospect (Figure 16). The CMER is a topographically a low valley restricted by

an elevated plateau recharge area in the east. As a result, both the groundwater and meteoric waters flow from the highlands towards the rift following the slope. Percolation and flow of water through the system is governed by the fracture system of the rocks and lithological boundaries and stratifications, which are means of permeability. Ghiglieri et al. (2020) showed that the main recharge areas are located in the east and west shoulders of the rift; the discharge zones (potential reservoir) take place in the flanks towards the center of the graben, which is the main groundwater reservoir.

Apart from these, the hydrological properties of the rocks also play an important role regarding the movement of the groundwater. Ghiglieri et al. (2020) identified two types of hydrologic aquifer systems in the Lake district area in the central part of the rift, characterized by sedimentary and volcanic units. The sedimentary unit consists of aquifers that are mainly composed of lacustrine, alluvial, and volcano-clastic with moderately productive porous aquifer property. According to the analysis of Fentaw and Mihret (2011), the volcanic aquifers of Eocene–Oligocene basalts, mid-upper Miocene basalts and trachybasalts and Pliocene ignimbrites have moderate productivity, while Pleistocene pyroclastics low to medium and Pleistocene to recent basalts have high aquifer productivities.

The study area is within the CMER and is hydrogeologically bound by the Lake basin (e.g., Benvenuti et al., 2002) to the south, the upper Awash River basin (e.g., Ghiglieri et al., 2020) to the north and the eastern escarpment to the east (Figure 16). From the overall regional groundwater flow, the groundwater recharge to the aquifer system of Tulu Moye will be from the nearby highlands of the eastern escarpment, through the extensive fractures.

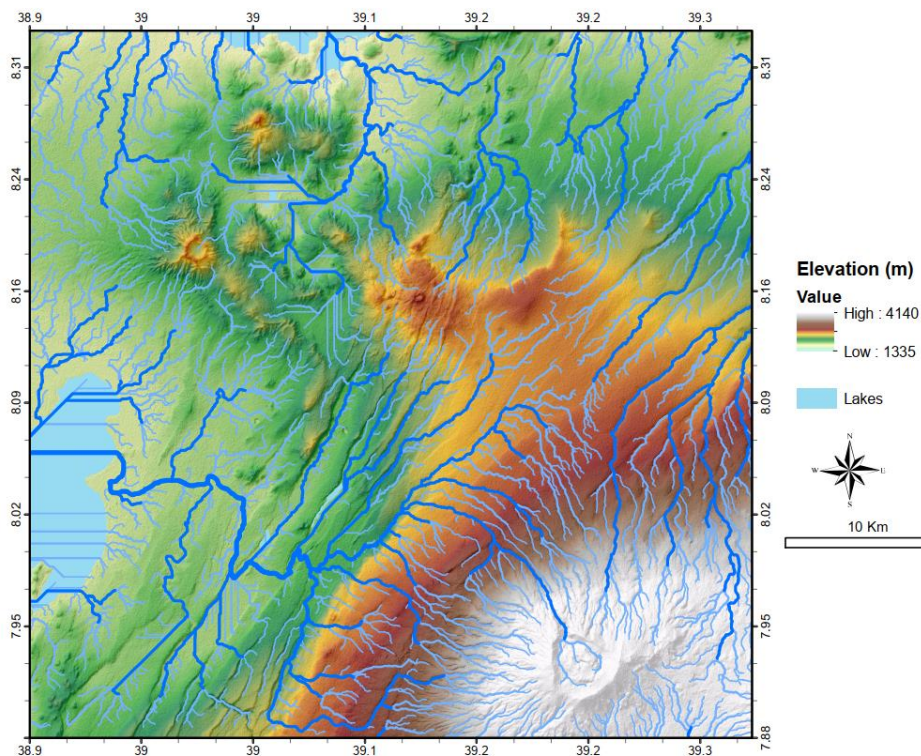


Figure 16. Regional and local hydrological map of the Ziway-Asela area and Tulu Moye geothermal system. The major and minor stream flows are indicated by the thick blue colored lines and thin light-blue colored lines, respectively.

4 Methods

This study involved mapping of the faults, fissures and eruptive fractures, and a field trip. The fieldwork was carried out for one-week duration, from Dec. 23 to 30, 2020 aiming at ground checking.

Garmin GPS and compass were used for finding a location and measuring some of the inclinations and directions of the tectonic features, respectively. A temperature tape was used to measure the temperature of fumaroles and hot grounds.

Mapping of the faults and fissures was performed using aerial photos and LiDAR images only for the northern most part of the research area, which is TMGO's concession. The aerial photo was taken using drones with a resolution of 0.16 x 0.16 m and the LiDAR image has 2 x 2 m of resolution. Both the drone and LiDAR images were accomplished and provided by TMGO for the purpose of the geothermal exploration.

For the southern part of the research area, Sentinel-1 image was accessed from the USGS open source. It was used to cover the area beyond the coverage of LiDAR and aerial photo, the southern section. Sentinel-1 has a 10 x 10 m of resolution and is prepared with 8-bands for mapping the lithology besides the extraction of the tectonic features.

To visualize the digital elevation model of the whole rift outline and the regional tectonic image, and to make the profile sections of the faults, the free online application called GeoMapApp was used.

The RockWork software was used to demonstrate the orientations of the digitized structural outlines in the form of rose diagram. The Grapher software was also used to make the length by orientation graphs of the faults and fissures. The conceptual geothermal model of the area was made by using the application called Inkscape. All the accessed images, the collected data and tectonic features were resolved by using ArcGIS software.

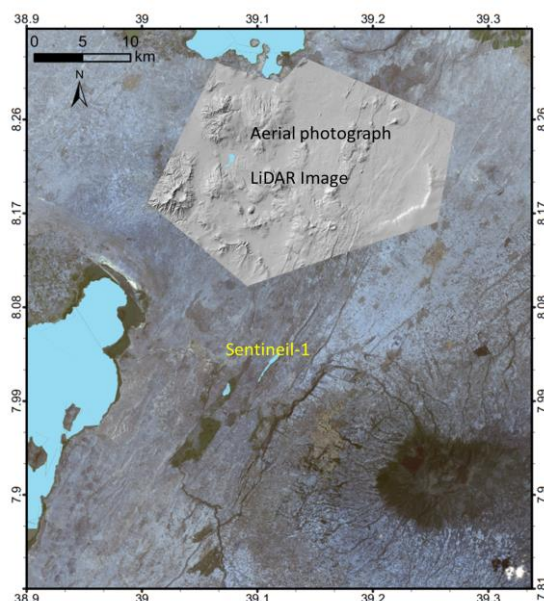


Figure 17. A map showing extent of the areas used by different images and aerial photo.

5 Results

5.1 General overview of structural features in the study area

The tectonic feature and the structural elements of the area can be classified into normal faults, fissures, eruptive fissures, mini-grabens and caldera complex structures (Figure 18). The fissures are confined to the north-eastern part of the mapped area. They are short in length and few in number having an orientation towards NS-NNE. Eruptive fissures are also very few and confined to the northern most part of the study area. They appeared along the recent products of cinder cones and volcanic domes. Normal faults are found throughout the area, displaying different orientations. The dominant orientation is NS-NNE followed by NE-SW and WNW-NW. NE-SW oriented faults are dominantly found at the southern half part of the study area and NS-NNE faults dominate the northern part, while WNW-NW oriented faults are localized in the north-western part of the study area. The faults dominate at the central part of the area and become few away from the centre. Besides their orientations, the faults differ from each other regarding the vertical displacement, dipping direction, and age. Based on such differences of the faults, the mapping area is categorized into three regions. Two mini-grabens and three caldera structures are also identified in the northern section of the study area.

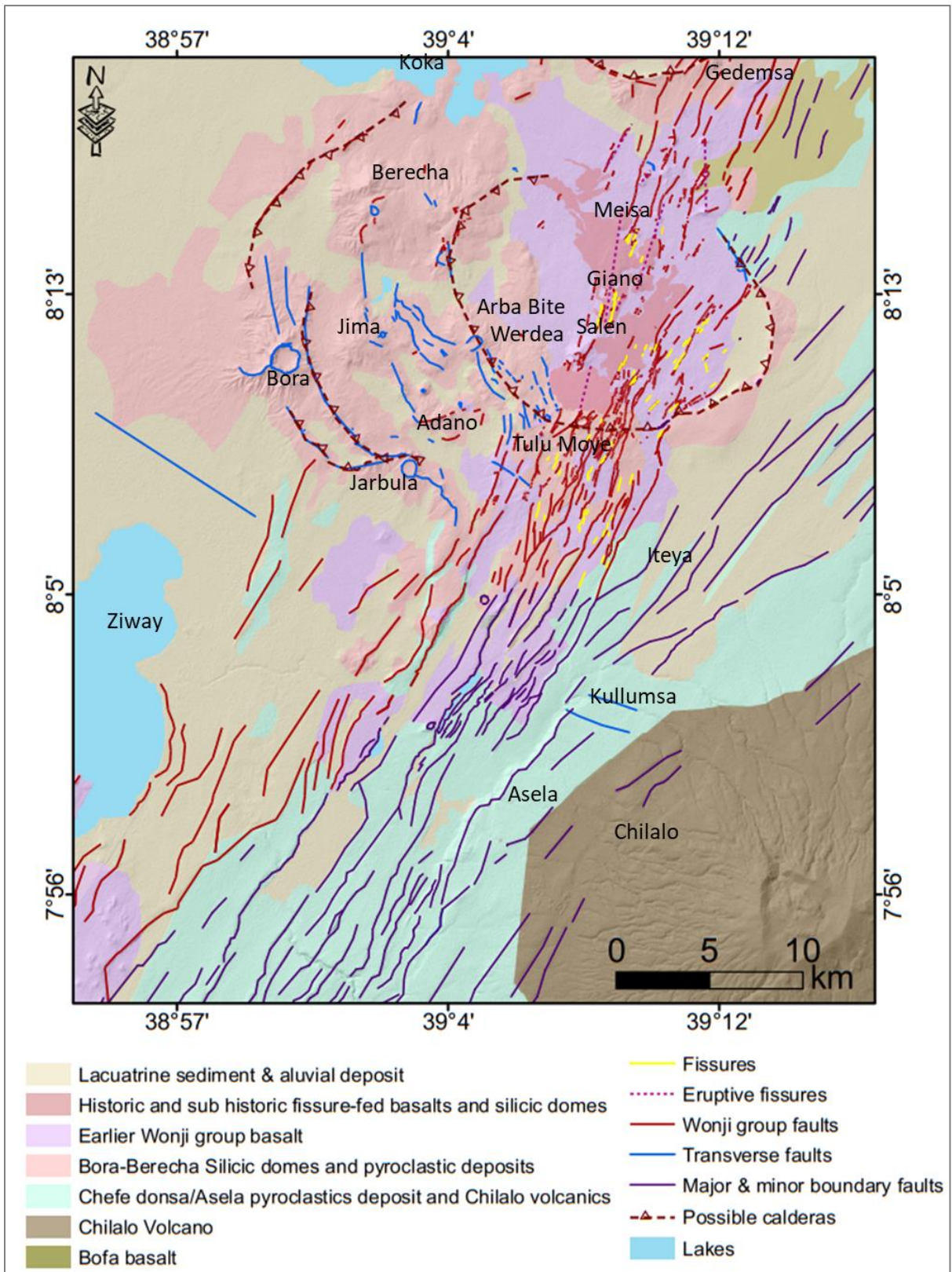


Figure 18. A tectonic map showing a general overview of the structural features together with the lithology of the area. The lithology is modified from Abebe et al. (1998), Boccaletti et al. (1999) and Abebe et al. (2005). The surface hydrothermal alteration is modified from Ayele et al. (2002) and field observations.

5.2 Fissures

Fissures are common in the north-eastern and the central parts of the area situated along with the faults, mainly where the NS-NNE oriented faults are dominant. Commonly, the fissures appear as cracks without vertical displacement, while others show some vertical displacement and are grouped as faults.

Most of them are oriented in the direction of NS to NNE and they are densely populated in the Wonji group basaltic field (Figure 18). A few of them, mainly situated between Mt. Salen and Giano, are oriented in the transverse NNW direction (Figures 17). The strike of most of the fissures is between 0 and \sim N13°E, while the rest of them are oriented up to \sim N55°E (Figure 19).

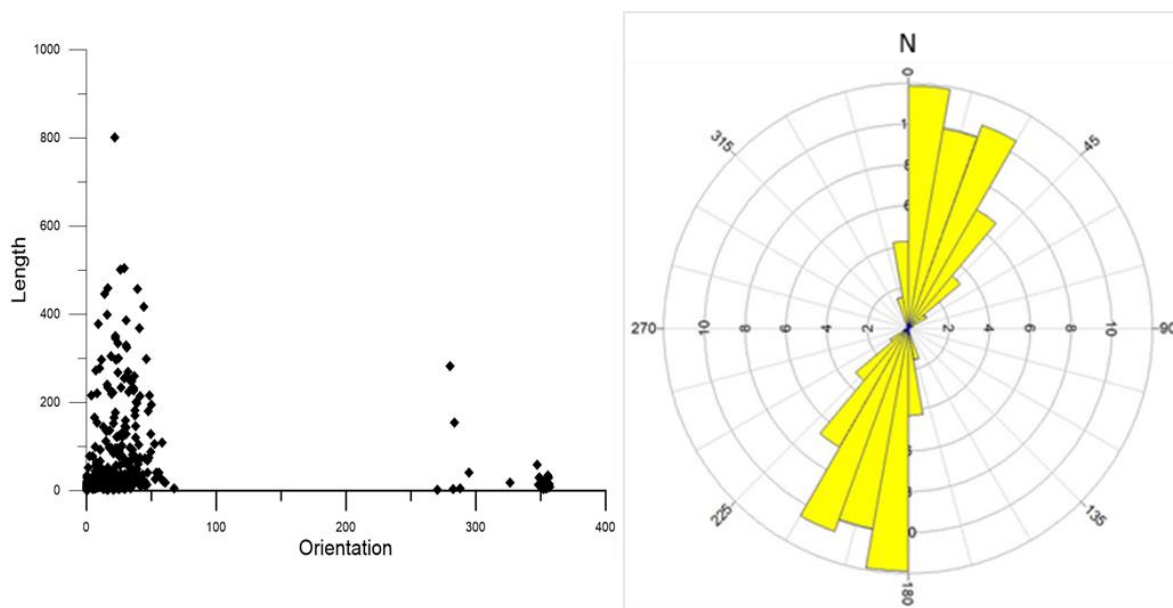


Figure 19. The graph on the left side shows length vs. orientation of the fissures and the rose diagram on right side represents frequency of the total distribution of the fissures with their respective orientations. The small numbers on the X and Y axis of the circles represents the percentage of frequency of the fissures.

Most fissures are short. Shorter fissures always show a small scale of opening and do not show clear evidence of vertical displacement. While the longer fissures are fairly opened laterally and extend to greater depth with slight displacement to create an open fault. The vertical displacement of most of this type of fissures is largest at its centre.

The maximum measured length of the fissures is up to hundreds of meters. The longest fissure is seen on top of the Salen volcanic range extending over 1000 m (Figure 20). It is oriented to the NNE and has a slight dip-slip movement near the center where the extension is largest. The opening fluctuates from cm scale to about 7 m.

The opening of the fissures reaches from a few cm to ~10 m; and the largest one is observed on the open tensional faults (fissures with a relative vertical displacement; Figure 21). These measurements were obtained during the fieldwork.

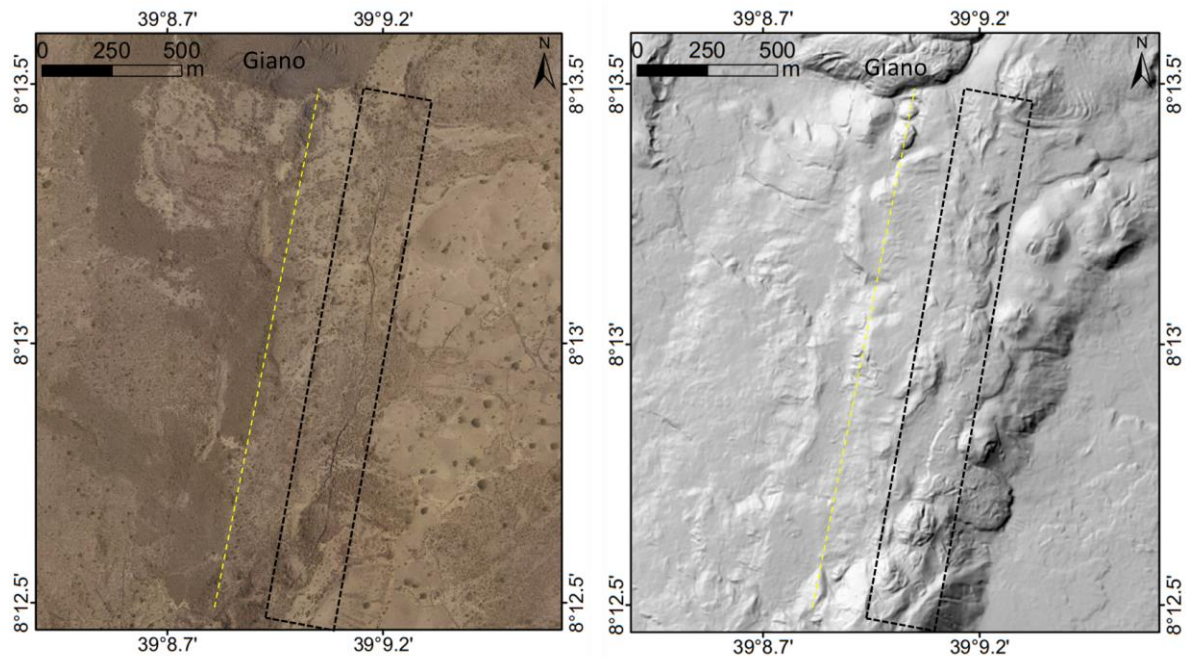


Figure 20. An aerial photo and DEM showing the longest fissure of the area (in the black dashed rectangle) and eruptive fissure (a dashed yellow color) formed during the historic eruption on the Salen spreading axis.

Most of the fissures are vegetated which is their typical identifying character both in the field and on aerial photo.

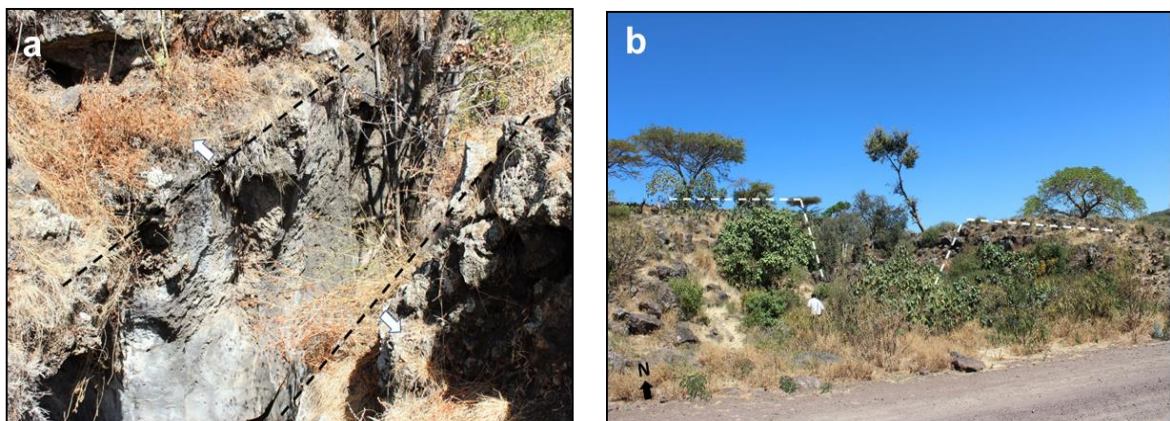


Figure 21. Photo of an extension fissure (a) south east of Giano dome, about 3 m opening towards the direction of the general extension of the MER. (b) a fissure developed an open fault with an opening of ~10 m in the basaltic field of the Wonji group, further south east of Mt. Tulu Moyo.

5.3 Eruptive fissures

The eruptive fissures are very few and limited to the northern part of the study area. They were formed during the Pleistocene-Holocene and during historical eruptions near, and along the active Salen volcanic range/axis (Figure 18). They are elongated in the ~NS direction, along the cinder cones and domes.

5.4 Faults

5.4.1 General pattern

Faults are the most prominent tectonic features in the area, as they are in general within the Main Ethiopian Rift (MER). They show similarities with the other active sites of the MER, in terms of their mode of formation, architecture, age and orientations. The fault density map in Figure 22 shows that faults are found throughout the study area. They are densely distributed along the central part, flooring the axis of the rift and mainly positioned close to the young volcanic activities (Figure 18). The general pattern of the faults shows a narrowing tendency from the southern part towards the north. In particular, the area northeast of Lake Ziway shows a decrease in length, vertical displacement and spacing between the faults.

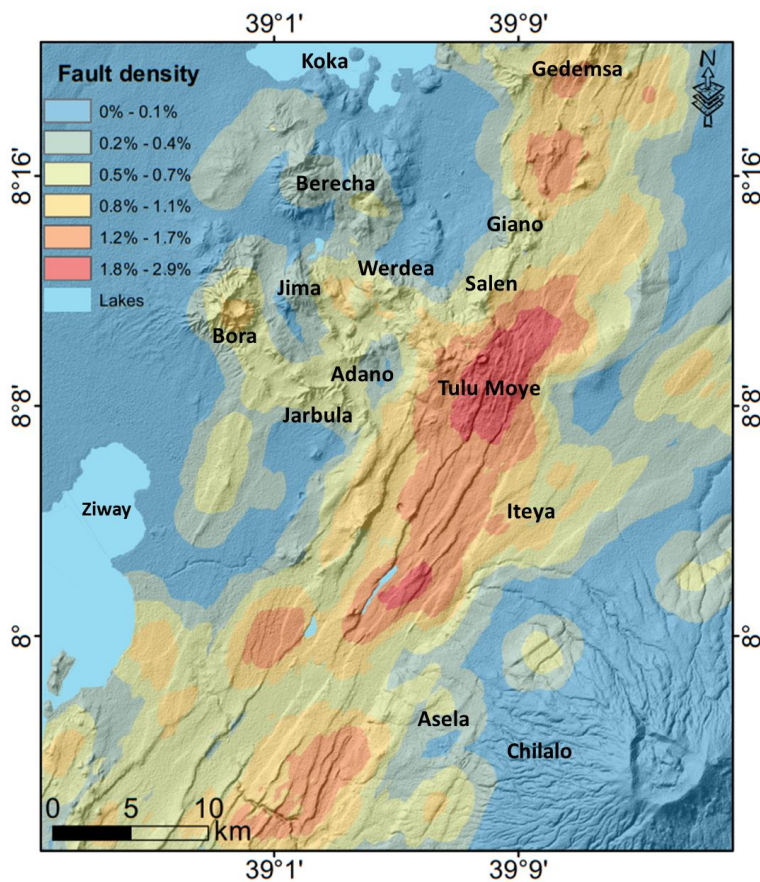


Figure 22. The fault density distribution map of the study area.

The fault swarms are mainly oriented towards N-NE, while a few of them have an orientation towards WNW-NW (Figure 23). As shown on the length vs. orientation graph and the rose diagram below, most of the fault swarms in the area have a trend of 0°-N50°E with the high peak between ~N10°E-N40°E, while few of them have an azimuth extended to about N80°E. Most of the faults have a length less than 2000 m, but the WNW-NW faults are much shorter than the northeasterly striking faults.

Faults in the research area show different characteristics at different localities. They are classified here broadly into two groups based up on their orientation directions and their patterns at different localities.

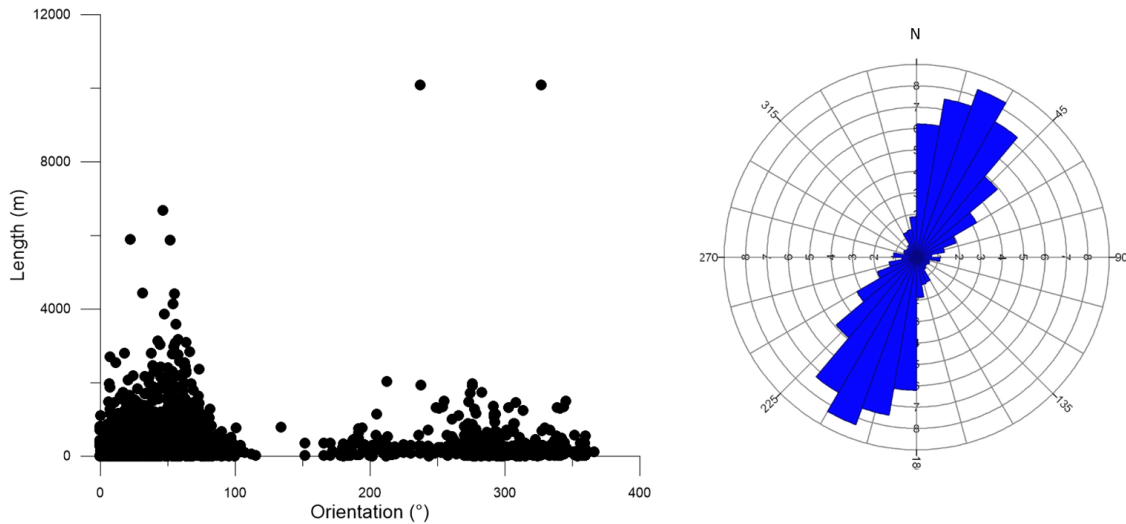


Figure 23. Quantitative data representation of the faults in the study area. Length vs. orientation graph (the left hand side) and rose diagram (the right side) of the faults in the study area. The color bars on the rose diagram represent the frequency of the faults over their orientations. The small numbers on the X and Y axis of the circles represent the percentage of the frequency.

5.4.2 Types of faults based on orientation

Faults in the area have variable orientations. They can be classified into three groups: NE-SW, NS-NNE and WNW-NW trending faults. The major boundary faults of the Main Ethiopian rift system have a general direction of NE, mainly framing the trend of the rift. However, the faults on the rift axis are N to NNE oriented younger faults, affecting the young formations (Figure 18). In addition, some rift crossing faults are also identified within the study area, having a general strike direction of WNW to NW. Below, these fault populations will be described in more detail.

NE-SW striking faults

The NE striking faults are one of the dominant ones in the area; mainly confined to the southern and the eastern parts, between Lake Ziway and Asela/ on and near Chilalo central volcano; exposing mainly older volcanic deposits. Some of them are major marginal and escarpment forming faults in the eastern central MER rift, bounding the rift from the east mainly as parallel horst and graben/ half graben structures. They have big dipping angle, the

greatest length, and the largest vertical displacement of the faults in the study area. They mainly trend between N20°E and > N50°E and the striking angle is higher on the eastern part of the area.

NS-NNE striking faults

These faults are mostly located within the Wonji Fault Belt (WFB). They are mainly restricted to the central, south eastern and northern parts of the area, striking between 0° and N40°E and in a few cases up to N50°E. Relative to the boundary faults, these are shorter, fewer and mostly have smaller vertical displacements. The vertical displacements of these faults at the central section of the study area are large. The dominant faults are confined to the strike direction between 0° and N30°E. They mainly associate with the cinder cones, spatter cones and fissure eruption activities (Figure 18) and rarely affect the lacustrine deposit.

WNW-NW striking faults

Transverse faults are few and restricted to the area between Lake Ziway and Lake Koka, on the north-western part of the area, cross cutting the Pleistocene-Holocene deposits. A NW-striking parallel faults with small throws are also observed near Gnaro obsidian dome at the north central part (Figure 18). It mainly affects the recent Wonji fault related pyroclastic deposits and its associated silicic products, except the ones near northern Lake Ziway and Kulumsa, north of Asela on the escarpment (Figure 18). The extensive hydrothermal activity of the area follows the same direction as this fault system (Figure 24).

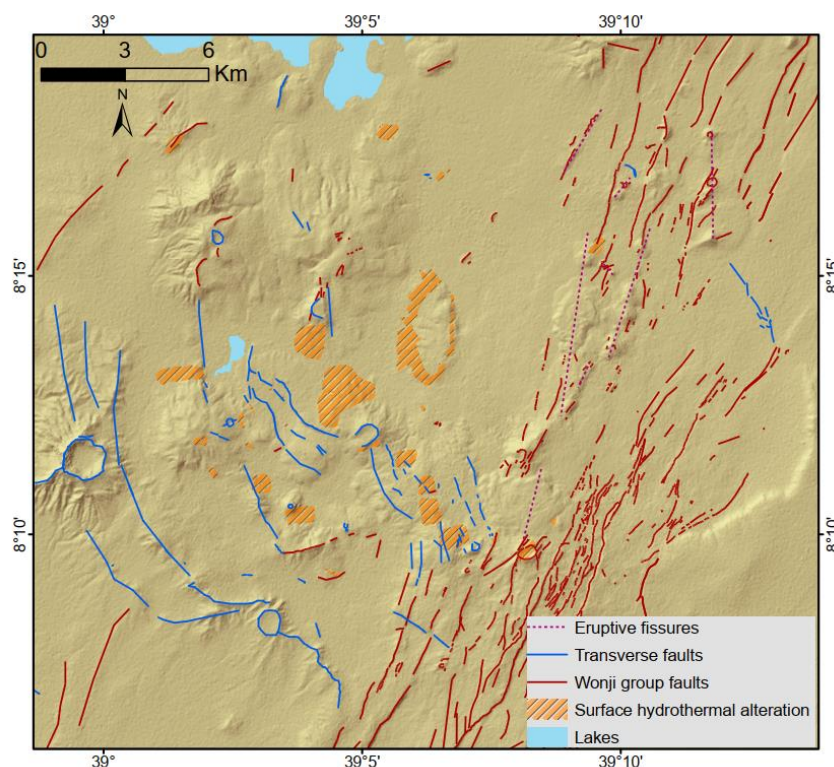


Figure 24. Map showing the relationship between the WNW-NW striking faults and surface hydrothermal activity. Information on the hydrothermal activity is modified from Ayele et al. (2002).

5.4.3 Types of faults based on their localities

The fault swarms at the Tulu Moye - Ziway area show different physical characteristics at different localities. Therefore, the areas are categorized into different regions based on the similar characterizing features of the faults (e.g., orientation, vertical displacement); as southern, northeastern, and north-western regions. Here, the physical properties of the faults will be discussed from the image analysis and field observation.

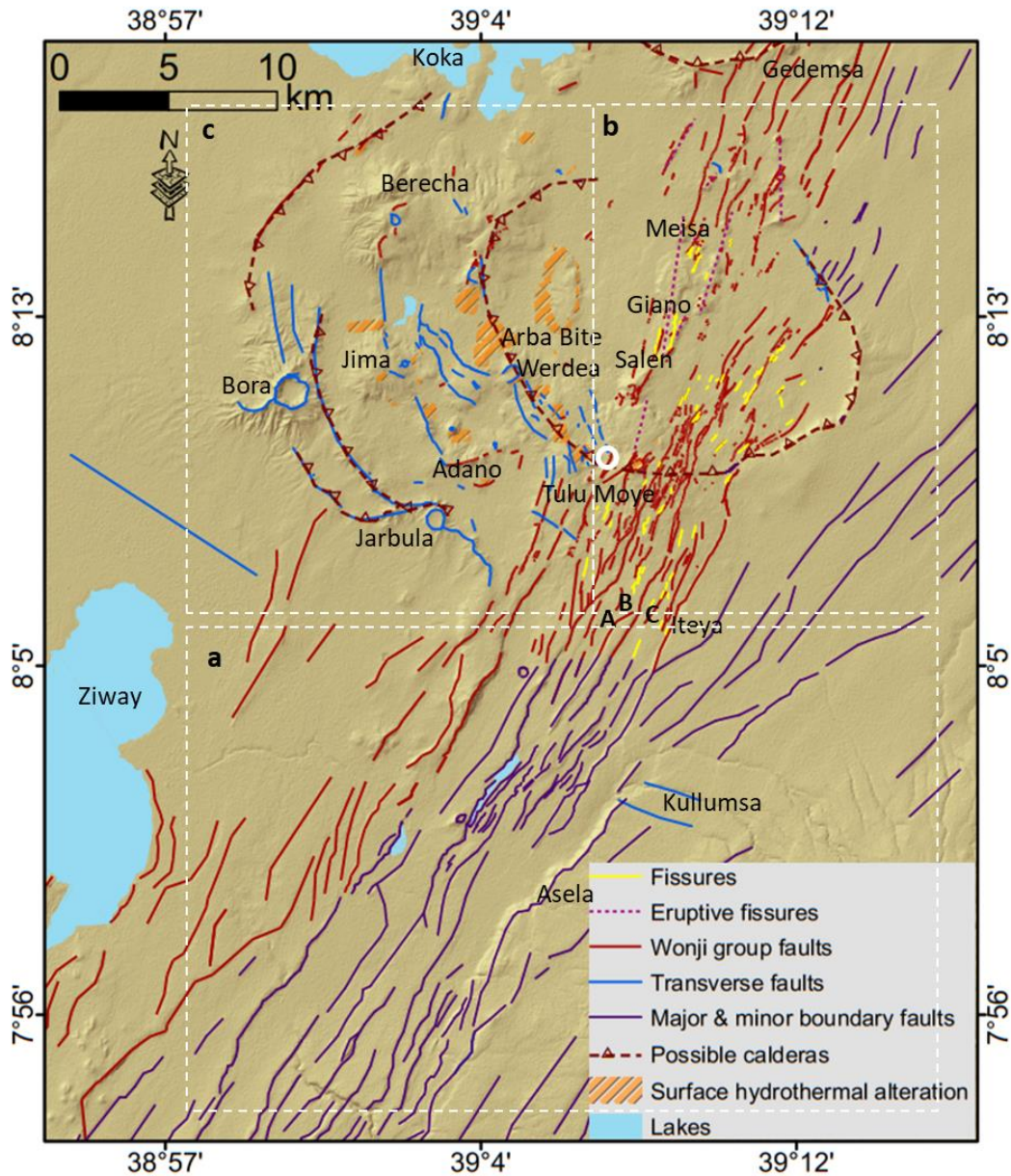


Figure 25. Structural map of the research area showing faults, hydrothermal activity and the categorized regions as identified by the white dashed lines. a) the southern region, b) the north-eastern region, c) the north-western region. The letters A, B and C represent the location of pictures used in this report. The white circle shows the highest measured temperature of surface surface manifestation.

The southern region (Ziway-Asela fault swarm)

This group of faults includes the area between Lake Ziway and Asela/Mt. Chilalo, south of the caldera region (Figure 25). The faults in this area are mainly characterized by the northeasterly striking major boundary fault system. It belongs to the older border fault system of the MER, except a very few of the Wonji faults that appeared nearby the eastern side of Lake Ziway and the northern most part of this sub area with an orientation between 0 and N20°E. The rest of faults in this region have a general azimuth of 20-45° to the NE direction, while few of them show an increment on their azimuth extending up to N70°E; near the escarpment area and north-eastern parts in and outside the study area (Figure 26 and Figure 25). The longer faults have a strike ~N40°E to N60°E and rarely ~N80°W.

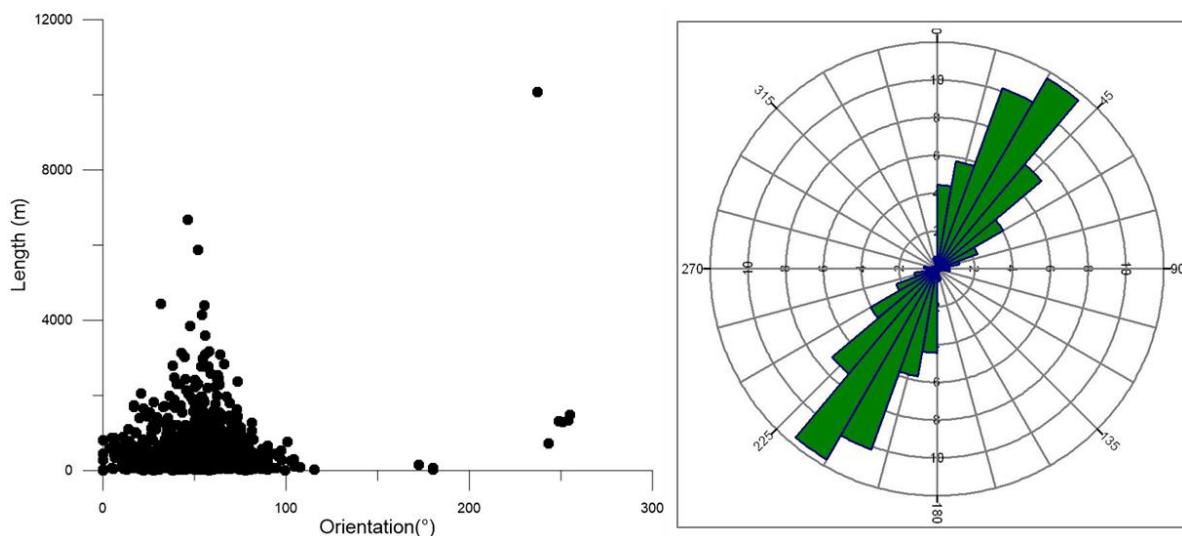


Figure 26. Length vs. orientation graph (the left hand side) and rose diagram (the right side) of the faults in the southern region. The color bars on the rose diagram represent the frequency of the faults over their orientations. The numbers on the X and Y axis of the circles represent the percentage of the frequency.

This fault system largely is located in the older Plio-Pleistocene deposits of the Asela/Chefe Donsa and Chilalo formation and in the Wonji group basalt (Figure 18). No transverse fault is observed in the southern region, except the one on the escarpment north of Asela. From the field survey, a small throw (2-5 m) southerly dipping fault in the older deposit on the escarpment were also identified on the Asela escarpment.

The faults are commonly bordered by grabens and horst/ half graben structures. They mainly dip to the west and have large vertical displacements (Figure 27). In order to measure the vertical displacement distribution of the southern region, above 590 measurement points were selected from the faults, and represented by circles (Figure 27). The measurement shows that the largest vertical displacement is confined to the east, on the eastern escarpment reaching over 550 m. This is found on a westerly dipping major boundary fault that strikes towards the ~ N35°E. The vertical displacement shows lowest values near the lake, at the central and northern parts of the region.

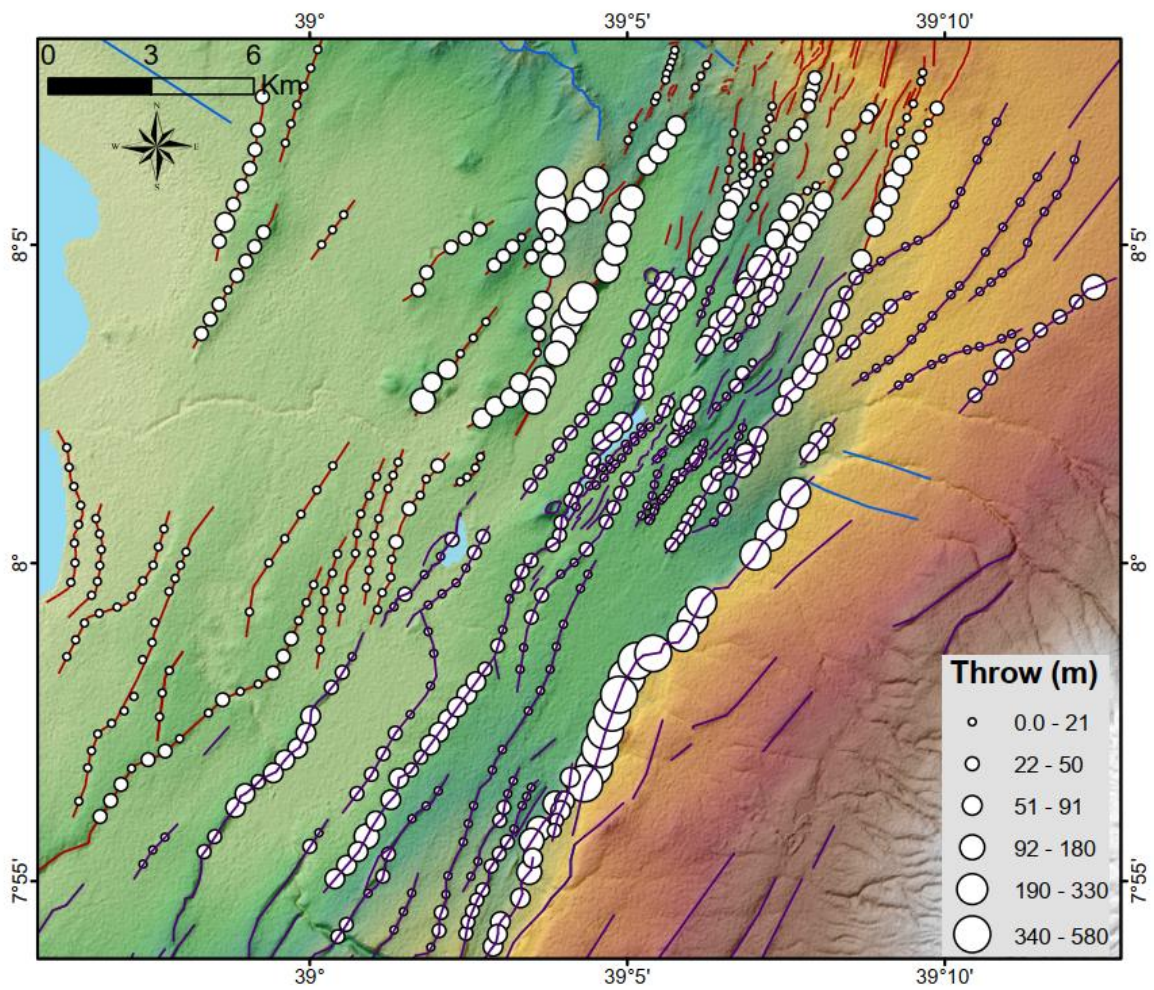


Figure 27. Map of the throws distribution in the southern region.

The length of individual faults reaches up to more than 20 km extending to the south outside the study area. The faults extends further to the south, outside the study area. The width of individual horsts does not exceed 2 km and grabens are always less than 3 km wide (Figure 28).

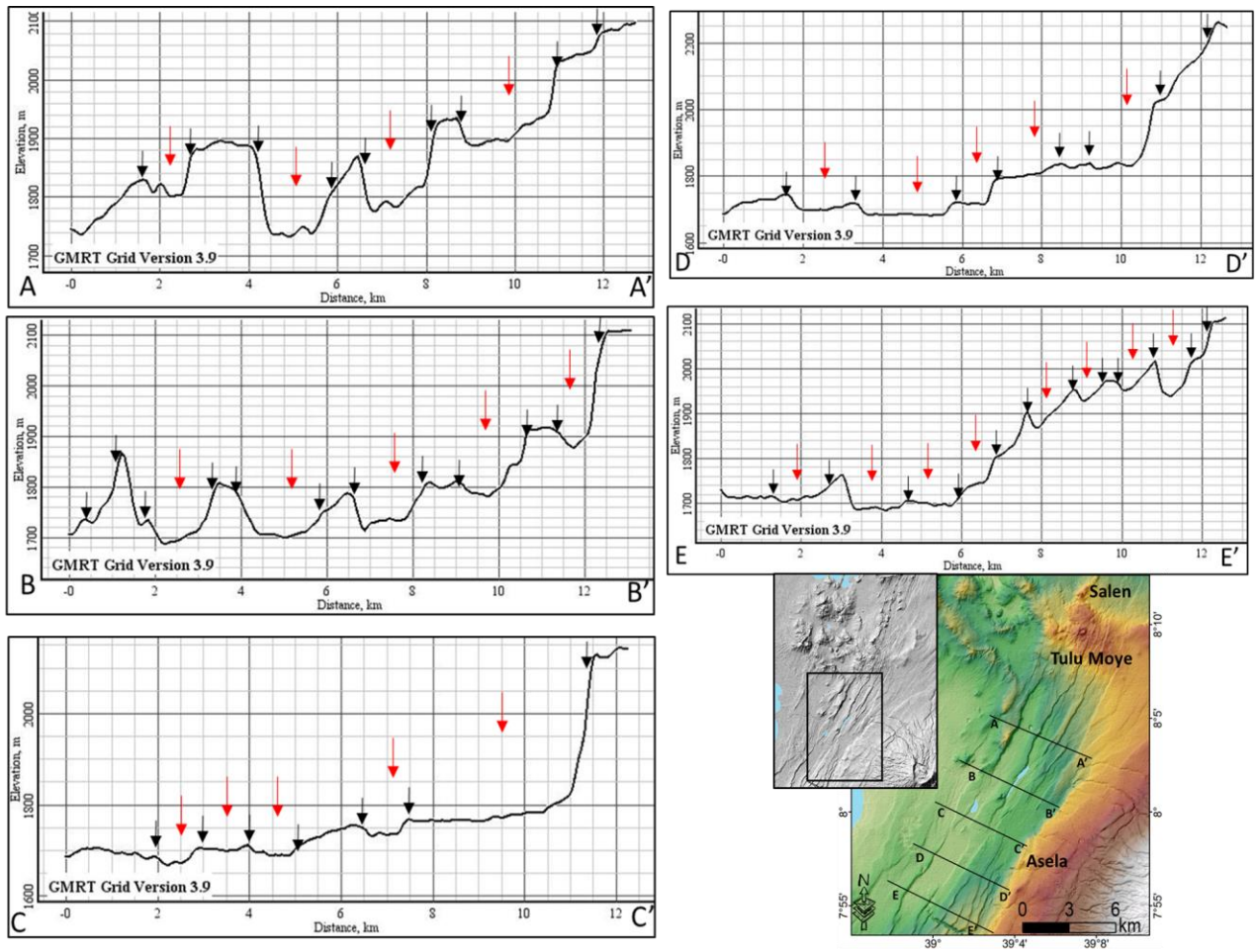


Figure 28. Profiles across the faults in the southern region of the research area. The faults and graben/half grabens are indicated by the black and red arrows, respectively.

The general overview of this region shows a gradual deepening of the topography towards the central part from the east and west. In other words, throws of the graben become less towards the center as shown from the profiles in Figure 28. As a result, the central part appears to be one of the lowest altitude (~1680 m asl.) graben in the region and is filled by a seasonal waterbody and swamp. This graben has a maximum width of about 2 km and the throw of its border faults is up to 50 m. The graben continues northward reaching the tectonically active Salen volcanic ridge with a decreasing throw and width and is finally replaced by thick young volcanic deposits (Figure 29).

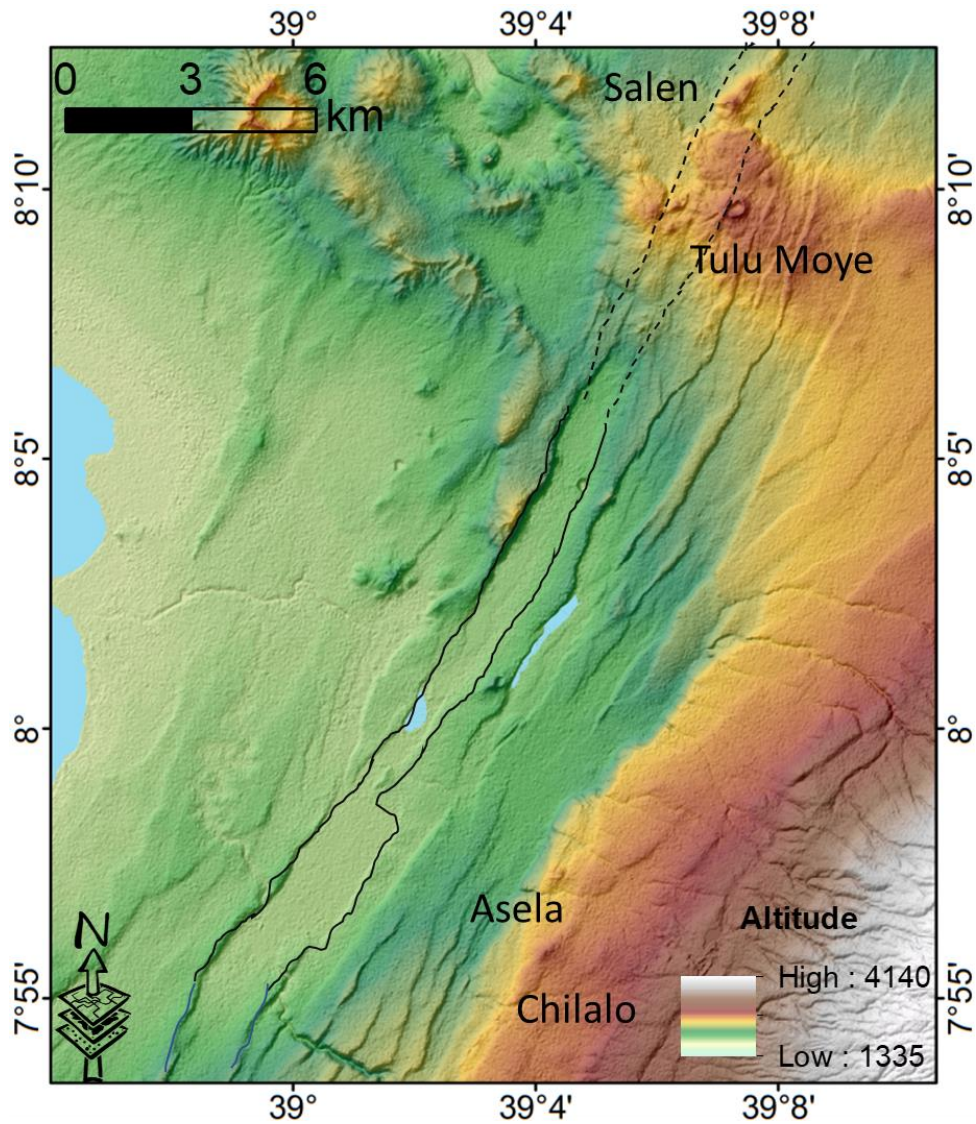


Figure 29. A map showing the lowest elevated graben (indicated by the black line) between Lake Ziway and Asela and its northern extension towards the Salen volcanic ridge (axis of ridge).

The north-eastern region (Tulu Moye fault swarm)

The general structural trend of this area shows a tendency from NE towards the NS direction, displaying mainly the Wonji type of fault swarms that affect both the basaltic field and silicic products of younger deposits. Both NE and NNE to NS striking faults are observed in the region, where the dominant ones are the NNE-NS oriented faults (Figure 30). As the rose diagram below shows, the highest frequency of the faults are observed between 20 to N35°E. The length of the faults in the north-eastern region ranges from a few meters to ~ 6 km, oriented to ~N10°E-N50°E (Figure 30). Few transverse faults are also observed in this region. They are more closely spaced, shorter, and with less throw compared with the faults in the southern region. The horst and graben/ half graben are few and appear at the boundary of the southern and northern regions, displaying a relatively small throws and width compared to the southern region.

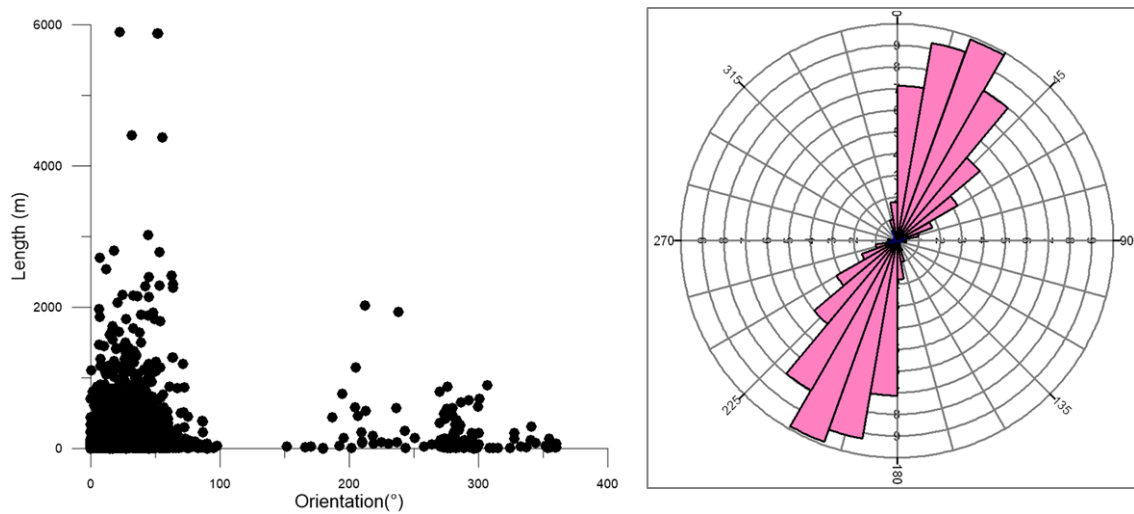


Figure 30. Length vs. orientation graph (the left side) and rose diagram (the right side) of the faults in the north-eastern region region. The color bars on the rose diagram represent the frequency of the faults over their orientations. The numbers on the X and Y axis of the circles represent the percentage of the frequency.

The faults at this boundary have measured vertical displacement between 3 and 150 m with a maximum measured dip of 85°, dipping mostly towards west and few of them dip to the east. In addition, some open tensional faults, eruptive fissures and fissures are displayed in this region. These fault swarms essentially affect the Wonji group porphyritic basalt, Pleistocene trachyte and rhyolite lavas and minor ignimbrites (Figure 31).

Apart from the common normal faulting structures, different fault related tectonic features are observed in this region; this includes mini graben structures, an intra-rifting spreading axis (Salen), and caldera wall.



Figure 31. Photo showing some of the NE and NNE striking faults in the southernmost part of the north-eastern region. The white arrows indicate the faults. Their location is indicated as A, B and C in Figure 25.

The Salen intra-rift spreading axis

The Salen-Giano ridge or the Salen volcanic range is a NNE aligned ridge, behaving as an intra-rift spreading axis along the Gedemsa-Aluto active magmatic segment. It is about 3 km wide and ~12 km long ridge, as measured from Tulu Moye volcanic centre to Meisa obsidian dome (Figure 32). It is an active part of the rift extending from the southern region of the lowermost elevated graben as discussed previously. It is made up of structurally controlled bimodal magma products. Younger volcanic products characterize the central part of the ridge, while the older deposits are distributed farther away from the ridge (e.g., Abebe et al., 2005; Boccaletti et al., 1999) and the caldera complex surrounds it further from the east and western sides (Figure 8). The youngest products are fissure-fed obsidian domes of historical eruptions and their coeval or penecontemporaneous basalt that erupted from the same fissure (Di Paola, 1972).

Fissures rather than larger faults characterize the structural activity of this spreading axis. The faults are located mainly to the eastern side of the spreading axis, while its western side is dominated by the young silicic volcanic edifice.

The tectonic structures along the ridge are aligned slightly oblique to the trend of the ridge (Figure 32). The general trend of the whole ridge is between ~N15°E and N20°E, which is

oblique to the main spreading direction of the rift and the fractures on the ridge trend obliquely to the spreading axis itself; between $< 10^\circ$ and 30° towards north east with few transversing fissures. The appearance of these oblique fractures along with the general trend of the ridge displays a sense of transfer fault movement. This tectonic movement has no sign of a continuation away from the axis.

Beside this, the hydrothermal activity also characterizes this locality. At its southern part, near Gnaro dome and Tulu Moye and near Meisa, a surface hydrothermal alteration that follows the NNE-N fractures and its intersection with the NW striking faults is dominant (Figure 24). During the field observation, the hot ground at this locality had measured temperature up to 92°C (see the white circle in Figure 25).

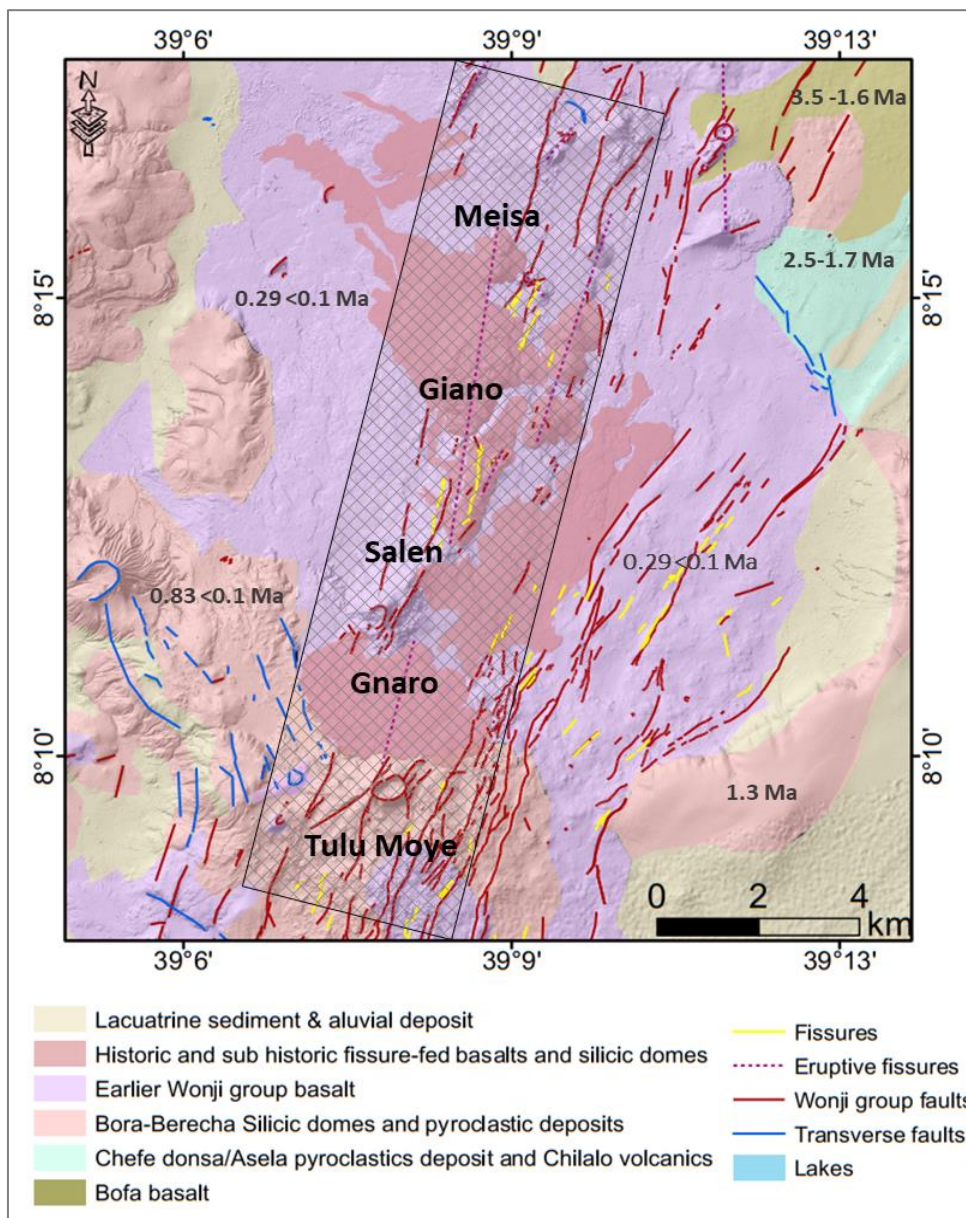


Figure 32. Map of the Salen intra-rift spreading axis (indicated by black dashed rectangle) with lithology and the surrounding fractures. The lithology is modified from Abebe et al. (1998), Boccaletti et al. (1999) and Abebe et al. (2005).

The mini-graben

In this region, two of the volcanic centers, Mt. Tulu Moye and Salen, show mini-graben structures (Figure 33). Both Tulu Moye and Salen are situated along the Salen intra-rift spreading axis, separated by the Gnaro obsidian dome (Figure 32). Tulu Moye is a ~ 650 by 500 m diameter crater forming volcanic center, which is elongated towards northeast and situated at an altitude of 2300 m a.s.l. The crater is ~150 m high from its base. It is made up mostly of pyroclastic deposits (pumice and ash), but with a base mostly made of trachytic and rhyolitic lavas (Di Paola, 1972). It is highly dissected by ~N30°E striking normal fault, to form a mini graben. The mini graben has a width range between 200-300 m and a down throw of about 15-120 m. The fault forming the mini graben extends further to the south. The mini graben is situated facing towards the Tulu Moye geothermal drilling wells pad at southern end of Gnaro dome (Figure 33 a).

Salen volcanic center is an elongated scoracious basaltic cone deposit with the highest peak of > 2200 m a.s.l. on the Salen spreading axis. At the right and left side of the peak, faults form a graben-like topography, although this could also be an erosional effect. The graben looking structure at the north-eastern side of the peak shows a sharp flat vertically thrown topography having about 150 m width, facing toward NW-SE direction perpendicular to the Salen axis as seen from the image and photo in Figure 33b.

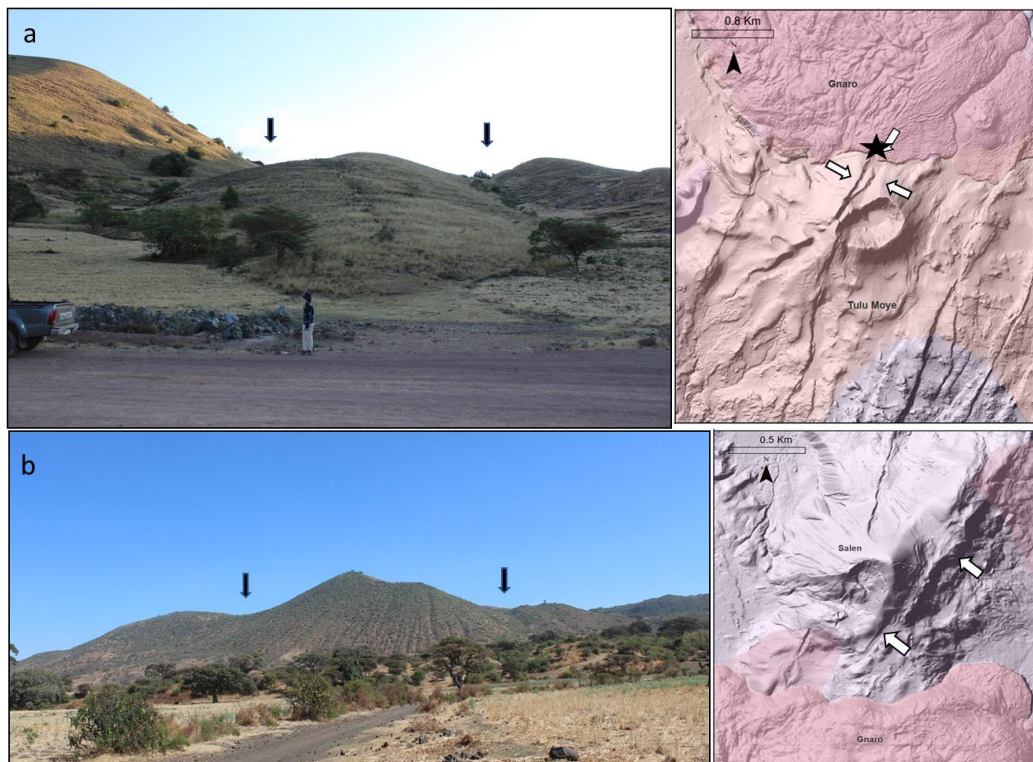


Figure 33. A photo and image showing the mini graben structures of Tulu Moye (a) and Salen (b) volcanic centres. The white and black arrows on the photo and image point to the mini graben structures. The current drilling site is represented by the black star on the up right image.

The north-western region (Bora-Tulu Moye area)

The north-western part of the study area is dominated by the transverse faults, striking towards NW and nearly EW direction. The area also consists of minor N-NE oriented faults, mainly in the northern section forming a caldera rim feature (Figure 25). The faults are characterized by uneven length; they are dominantly short and are oriented mainly between 0 and N70°W (Figure 34). The highest frequency of the faults is seen between N30°W-N20°W. These faults affect mainly the youngest, Pleistocene silicic deposits (Figure 18).

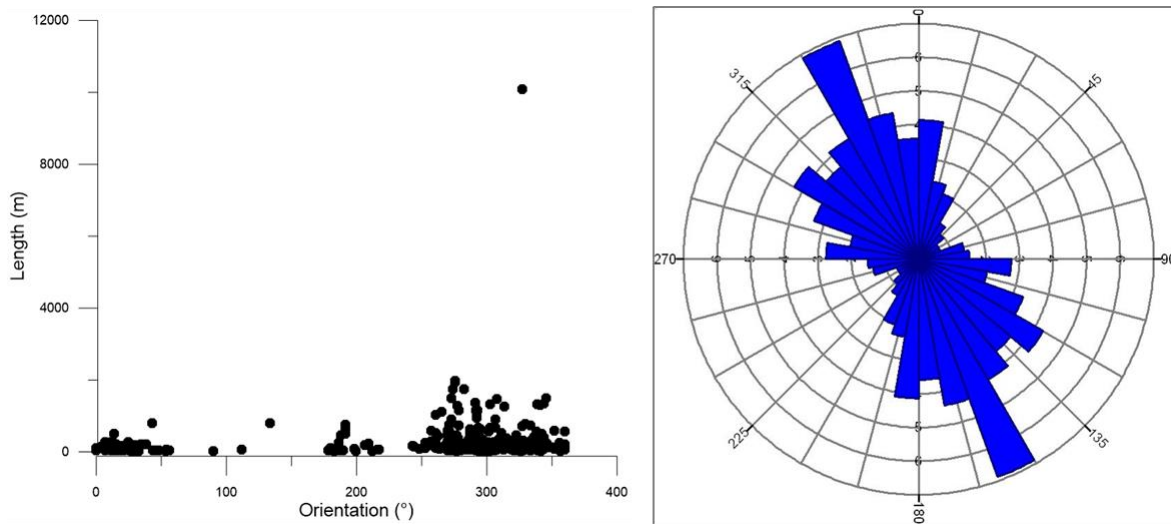


Figure 34. Length vs. orientation graph (the left side) and rose diagram (the right side) of the faults in the north-western region. The color bars on the rose diagram represent the frequency of the faults over their orientations. The numbers on the X and Y axis of the circles represent the percentage of the frequency.

The major transverse faults are restricted between the area SE of Mt. Bora and Berrecha (Figure 35). The one which extends from Mt. Bora towards the SE, to the Jarbula crater, is a caldera rim forming fault that has the highest vertical displacement (~500 m) in the northern part of the study area. This fault dip towards the northeast with a general orientation of ~ N50°W and extends for > 10 km (Figure 34). Southeast of Mt. Bora, this fault shows branching into two ~5 km long faults with the same orientation (Figure 25 and Figure 35).

About 1.4 km east of mount Jima, there are rather well defined half grabens, which have formed across the rift faults, oriented towards the northwest, approximately parallel with the faults between Bora and Jarbula. The grabens are closely spaced, parallel and dip towards each other, having a width of greater than 1 km (Figure 35 a, b). They extend further towards Tatesa, west of Tulu Moye further southeast. The maximum vertical displacement of these faults is 80 m and increases to ~130 m near Mt. Arba Bite.

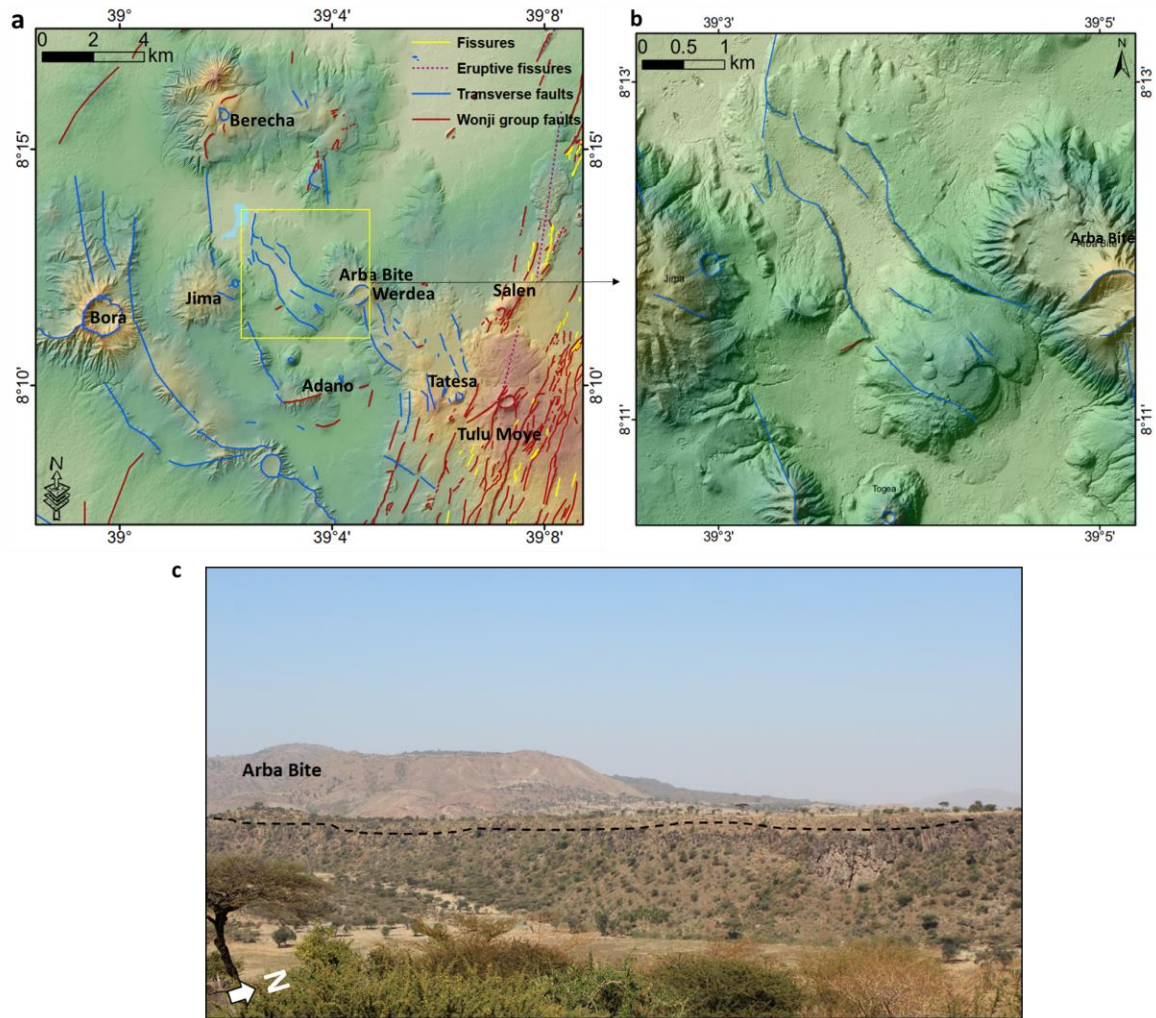


Figure 35. a) Map of the half graben and the surrounding transverse faults at Bora-Arba Bite area. b) The zoomed map of the yellow box on map a, showing the graben. c) A photo showing a transverse fault (black dotted line) near the extensively altered mount Arba Bite.

Short, transverse faults with a very small throw are also found near the Giano obsidian dome (Figure 32 and Figure 35). They strike $\sim N20^{\circ}W$, affect the Wonji basalt and fall-out deposits, and are not well visible in the field.

The clay deposits, indicating the geothermal activity are seen extensively covering the region along the fault lines. During the field observations, it was verified that the clay deposits of Jima-Arba Bite, around Jima edifice, appeared as cold ground with no indication of thermal anomaly. The temperature of the steaming ground and weak fumaroles that were measured during the fieldwork, particularly from the surroundings of Tulu Moye volcanic center show maximum temperature up to $92^{\circ}C$ (the area between Gnaro and Tulu Moye).

6 Discussion

6.1 The crosscutting relationships and volcano-tectonic interaction

Unlike the southern region, the northern region of the study area has a vast number of cinder cones and silicic domes to infer the interaction between the fractures and volcanic activity. The crosscutting relationships between the fractures as well as volcanic features (cinder cones and silicic domes) reveal the relative age relationship. In the northern and southern part of this region, the N-NNE running faults and fissures intersect most of the cones and silicic lava domes as shown in Figure 36. Some of the cones are faulted with clear vertical displacement and some are affected by fissures; implying that some of the tectonic features post-dates the volcanic features, particularly in the northern section (Figure 36). The eruptive fissures are also seen along the Salen spreading axis and on its northern part, serving as a conduit for the magmas to erupt. The Holocene-historical silicic domes, Mt. Gnaro, Salen, Giano and Meisa that are situated along the Salen axis are good examples of this and infer the presence of fracture controlled volcanic activity in the area.

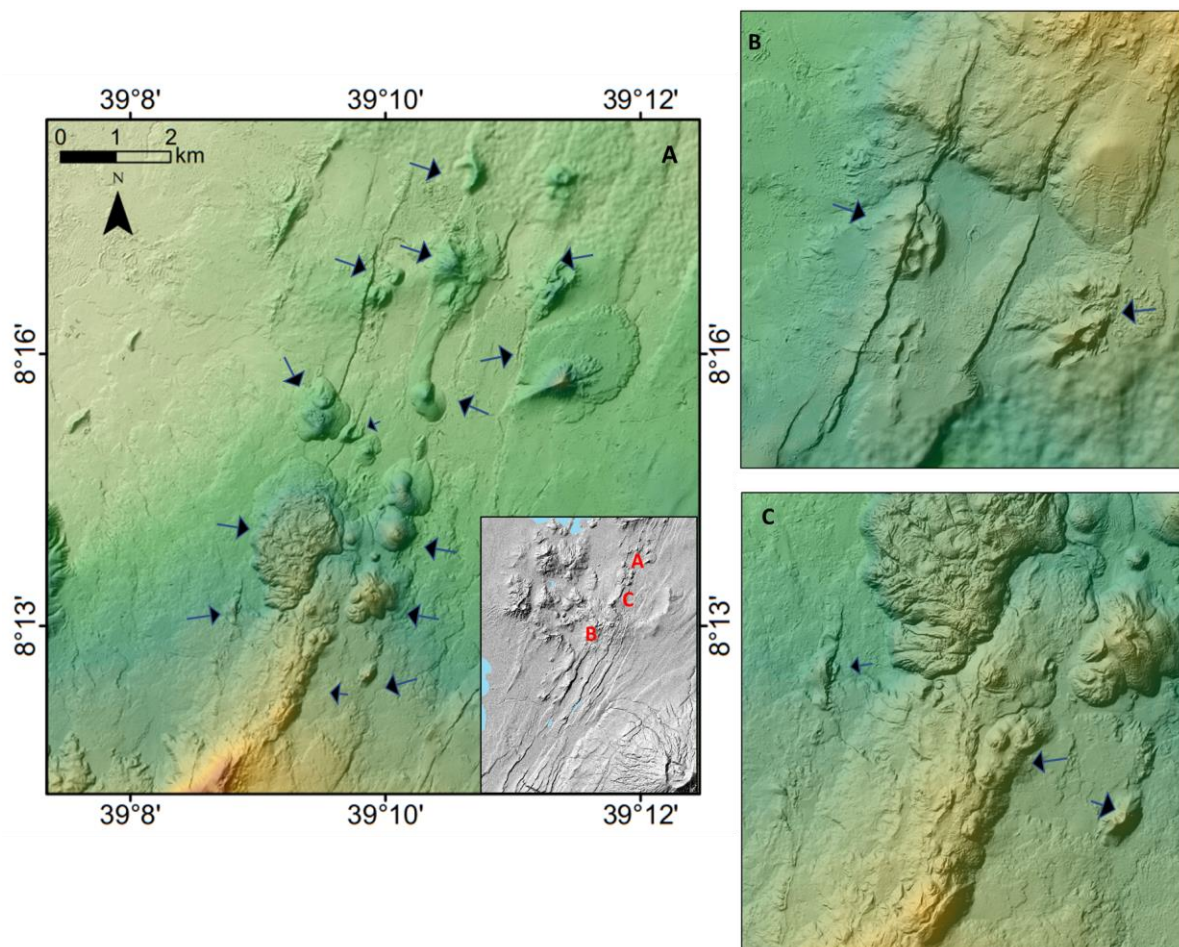


Figure 36. DEM showing examples of the interaction of fractures and faults with the cinder cones and silicic domes at different localities as indicated in the inset map.

Regarding the cross cutting relationship apart from what is described above, faults of different orientations intersect each other in this region. Under normal condition, the NNE to N faults are the younger Wonji fault system and formed after the development of the NE trending older border fault system. Yet, in the study area, at the right side of Gnaro and Gudure obsidian domes, the 30° to 40° NE striking faults crosscut the NNE-N (0 to 30°) oriented faults on the Wonji group basaltic field (Figure 37 a). This might indicate that deformation on border fault system is not completely ceased. Or else, it might be due to a short period change in the local extension direction. This might again be caused by the reactivation of the Mio-Pliocene NE trending major faults that are prone to be influenced by the recent volcano-tectonic activity of this area.

Further southwest of the Gnaro dome, another cross-cutting relationship of the faults are observed. As shown in Figure 37 b, the transverse faults that strikes about N40°W cross cuts the ~N20°E trending Wonji faults. This is shown from the physical appearance of the faults on the image (Figure 37 b) and implies that the transverse faults at this locality are younger than the NNE-N oriented faults. However, the fact that the youngest tectonic features are NNE striking fissures and open tensional faults that are situated on the Holocene lavas along the Salen axis (Figure 32) will not be denied.

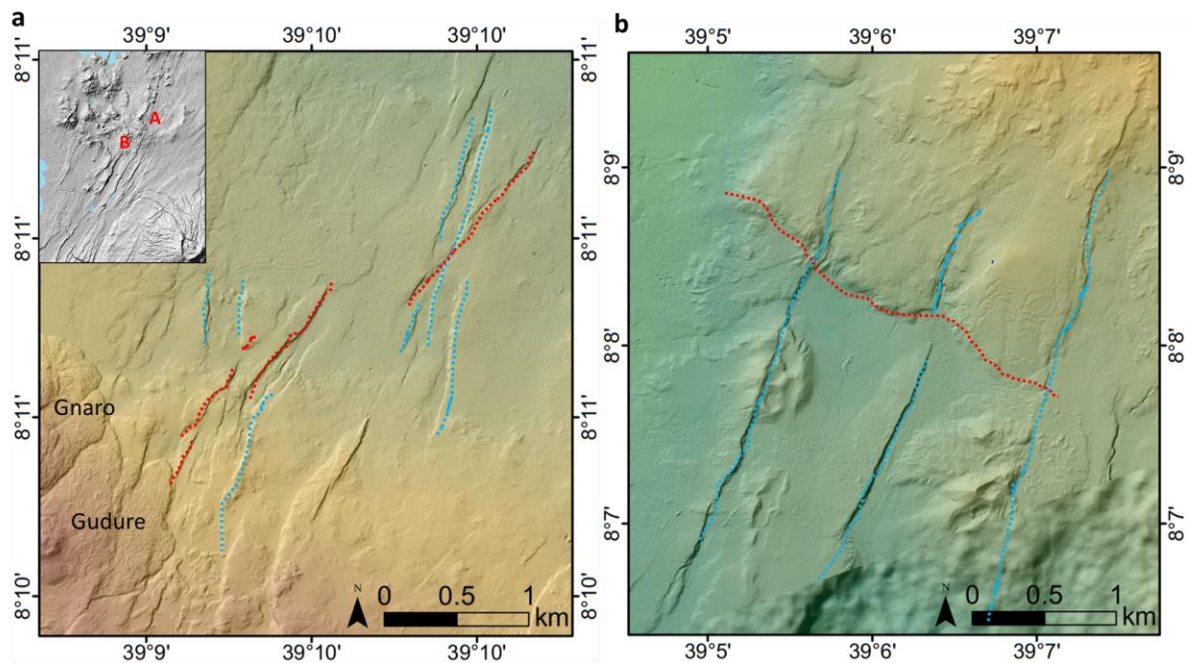


Figure 37. DEM image showing crosscutting relationships of the fractures at the northern region; in the southern (b) and in the south-western (a) side of Gnaro dome. The red and blue dotted lines represent the younger and relatively older faults, respectively. Location of the areas are indicated in the inset map.

A crosscutting relationship is also observed between the Wonji group fractures and the caldera-1 rim (discussed in the next chapter), where the faults, fissures and eruptive fissures intersect the caldera rim structure following the regional stress field. This interaction implies that the fractures postdates the caldera structure. This infers the reactivation of recent NNE

oriented structures took place after the development of the calderas following the Wonji fault stress directions. As a result, the surface hydrothermal manifestations emanates following the south-western rim of this caldera. The intersection also shows that deformation is more localized towards the east-central part of the study area, near the Tulu Moye volcano.

6.2 Tulu Moye caldera complex structures

Calderas are common volcanic structures of the volcanic environment. They differ from place to place based on their mode of formation and development, depending on the tectonic activity of the area, morphology, the type of magma erupted and collapsing and so on. It is one of the typical structure found throughout the whole rift system of Ethiopia, mainly focused on the axial zone and associated with pyroclastic eruptions. In the study area, particularly in the northern part, poorly defined caldera structures are observed. The calderas are outlined by following the possible caldera rim structure. They are three in number and named as caldera-1, 2 and 3.

Caldera-1, Tulu Hayat caldera of Abebe et al. (1998; Figure 38), in the north-eastern part is a well defined highly faulted block of half caldera rim (~300 m thick), displaying a stratigraphic succession of ignimbrite, pumaceous breccia and pumice and ash deposits. According to Boccaletti et al. (1999), the age of the rock under this group of rock is 1.3 ± 0.3 Ma; which makes it somewhat older than the other proposed calderas in the area. Apart from the well defined part of it, the rest of this caldera seems to be eroded and covered by more recent products. The possible extension of this caldera could reach about 18 km to the west promoting north westerly elongation, leaving the Salen spreading axis at the center of the caldera (Figure 38 and Figure 39). The NS to NE oriented fault swarms and fissures crosscut the north and south portion of the caldera rim and its floor. Beside these, the south-western part of the rim is highly affected by surface hydrothermal alteration, which is also related to the NW striking fracture system.



Figure 38. A photo showing the remenant of the half caldera-1 seen from the top center.

About 8.5 km southwest of the western rim extension of this caldera, there exists another possible caldera rim structure (caldera-2) passing from the foot of the Bora volcanic complex through Jarbula crater. It extends towards the south east with a length of about 13 km. It is

made up of thick pyroclastic deposit and silicic lavas with a down throw up to 500 m. As shown on the map, the full portion extent of this rim is not noticeable, but part of the caldera wall can easily be detected from the highly faulted block that appears most likely as a heavily faulted arcuate transverse fault.

About 1.5 km west of this caldera there is a collapse structure following the same direction and appearance as caldera-2. It is situated between Bora and Jarbula and is about 7.5 km long. It shows a clear collapse structure in a similar rock formation as caldera-2. It can be defined as a separate caldera, but it is more like a part of the caldera-2 collapse.

The last caldera, caldera-3 is situated at the northern side of caldera-2 and Bora central volcano. It has a poorly defined caldera rim, which is about 14 km long. It has no sharp faulted blocks like the previous ones; instead, the patchy aligned faults and the volcanic deposits that are erupted along the arcuate caldera identify it. Both the faults and the volcanic deposits follow the same direction and give a sense of a caldera rim morphology. This caldera, and caldera-2 border the volcanic deposits of the main volcanic area from the west and it appears that there are no recent eruptions from these calderas.

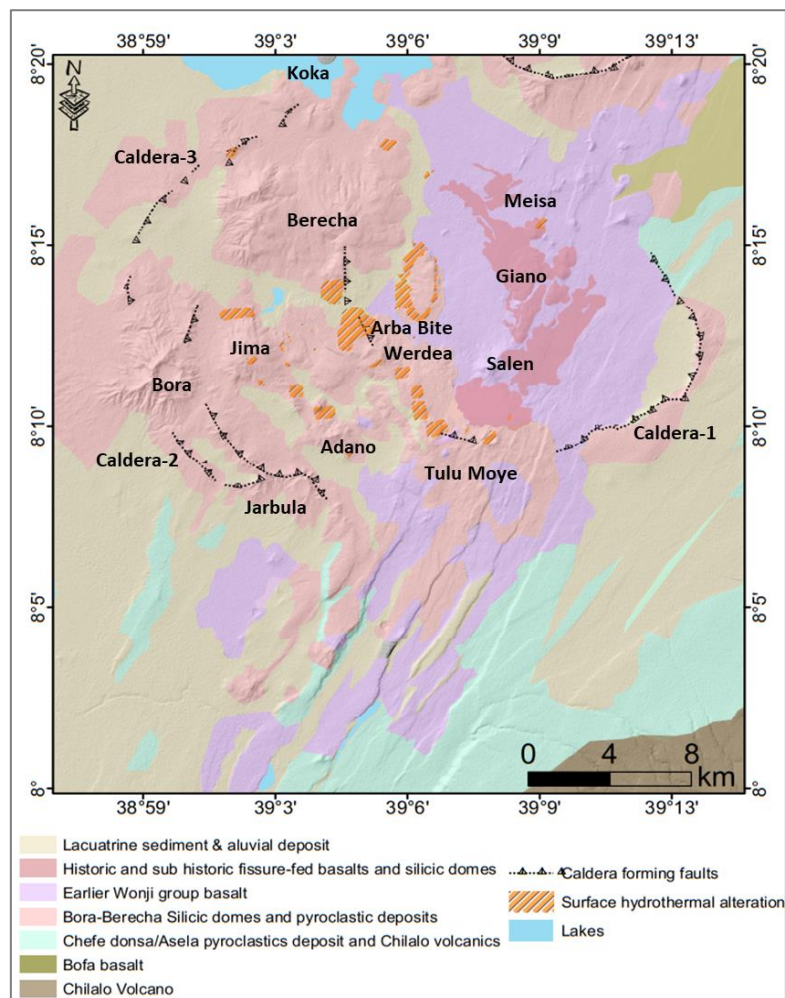


Figure 39. Map of the proposed caldera complex structures and the lithology. The lithology is modified from Abebe et al. (1998), Boccaletti et al. (1999) and Abebe et al. (2005). The surface hydrothermal alteration is modified from Ayele et al. (2002) and field observations.

6.2.1 Scenarios for the mode of collapse of the proposed caldera complex

The Tulu Moye caldera complex seems of to consist of nested or overlapping calderas of different ages. All the calderas have few well visible caldera rims while the rest of the calderas are not visible neither on the aerial images nor in the field. This could occur as late volcanic deposits cover and modify the caldera structures. Furthermore, since the dominant rocks forming the existing caldera wall are loose pyroclastic deposits, surface processes (erosion) can easily modify it. In this study, by combining the data (age of the rocks, lithology and physical morphology), scenarios have been proposed for the collapse structure of the caldera complex. The scenarios would have been more reliable if detailed studies (e.g., volcanic history of the area, number of the magma chamber, gravity survey and so on) had been available in the area.

Caldera-1 (Figure 39) seems to form by a collapse due to a large-scale magma withdrawal earlier than the rest of the proposed calderas. Its possible diameter is about 18 km, depicting the subsidence of a large block of rock along a ring fault. This kind of collapse is observed from the plate or piston type of caldera collapse (e.g., Lipman, 1995; Cole et al., 2004). A plate (piston) collapse is the subsidence of a coherent block of rock into an empty magma chamber bounded by a set of arcuate sub-vertical collapse ring faults. These calderas are associated with voluminous eruptions from large shallow magma chambers (Lipman, 1995; Figure 40).

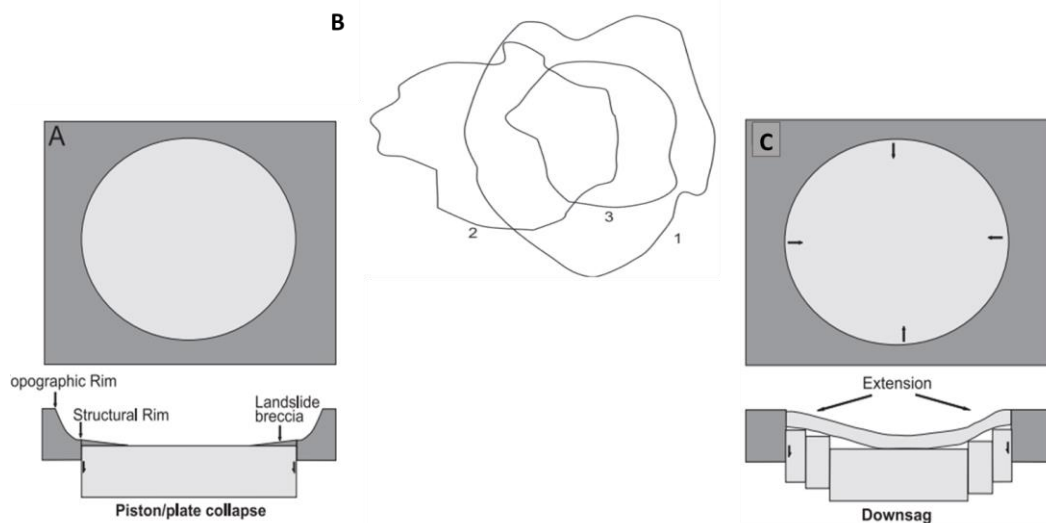


Figure 40. Type of caldera collapses A) Piston/Plate B) Piecemeal C) Downsag. Figures from Cole et al. (2004).

According to the terminology given by Cole et al. (2004) this type of caldera structure can be called a cauldron, which is an eroded caldera in which most of the caldera collapse has been removed by erosion. The rest of the caldera can also be categorized as cauldrons, but unlike caldera-1, their morphology seems more due to collapse effect rather than a complete caldera that has been eroded.

The eastern portion of caldera-1 is affected by the young NS-NE, dominantly NNE oriented fault swarms and fissures. The active Wonji fault might also play a role to widen the caldera ~E-W direction. This could also be taken as another possibility to explain the extended diameter of the caldera. This appearance of caldera widening by the post caldera extensional fractures makes caldera-1 comparable with the calderas in other parts of the world, such as Krafla caldera of Iceland, along the mid-Atlantic ridge.

The Krafla caldera is located in the northern part of Iceland within the northern volcanic zone, where the plates (Eurasian and American) diverge ~E-W. It is an ~8 km wide caldera formed by the lava flows and hyaloclastite. The caldera rim is only exposed in a few places, and is intersected by fissures swarms that extend through the caldera aligned the NNE-SSW direction (Hjartardottir et al., 2012). The extensional structures play a role in the widening of the caldera about 2 km in east-west direction (Sæmundsson, 1991). In addition to this, the Torfajökull rhyolitic volcano that is located in south central Iceland also has a similar appearance. The fissure swarm and feeder dykes cuts across the caldera-forming volcano in the direction of NE-SW (Sæmundsson, 2012).

The rest of the caldera structures seem to be formed by a piecemeal type of collapse (Figure 39), where all areas of the collapse take place during one eruptive episode. This collapse might took place during one eruptive episode or nearly coeval episodes. According to Cole et al. (2004), the collapse might be due to several reasons. This includes multiple magma chambers with overlapping eruption times in which eruption of one may trigger eruption of the other; where tectonically controlled faults break the caldera floor into numerous blocks prior to eruption and control collapse location; or where the entire caldera floor has been rendered a mega breccia. Besides these, successive collapse might also be caused by propagation of magma away from the magma chambers into fractures. A good example of this is Askja. Askja volcanic system is located in the northern volcanic zone, south of Krafla central volcano/fissure swarm. It is formed by hyaloclastite ridges and fissure lavas, and consists of three nested calderas (namely Kollur, Askja and Öskjuvatn). Volcanic fissures and tectonic fractures are either oriented away from or concentric with the calderas, with N-S to NNE-SSW orientations (Figure 41; Trippanera et al., 2018; Hjartardóttir et al., 2009) as in the case of Krafla. The calderas are formed at different times, and the collapses are suggested to have been formed by a lateral magma drainage from a reservoir beneath Askja caldera (Sigurdsson and Sparks, 1978). The same applies to the Bárðarbunga volcano in Iceland (e.g., Sigmundsson et al., 2015; Gudmundsson et al., 2016) and Kilauea caldera collapses in Hawaii (e.g., Tepp et al., 2020).

Apart from caldera formations, the volcanic fissures and tectonic fractures in the fissure swarms of both Krafla, Askja and Bárðarbunga (2014-2015) are formed when magma intrudes fractures to form dikes and even feeds fissure eruptions (Hjartardóttir et al., 2009) along the diverging plate. This marks an additional similarity between the development of the WFB and the fissure swarms of the north Iceland volcanic zone.

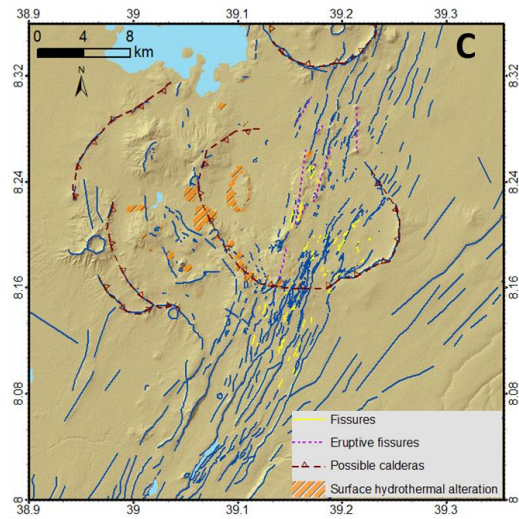
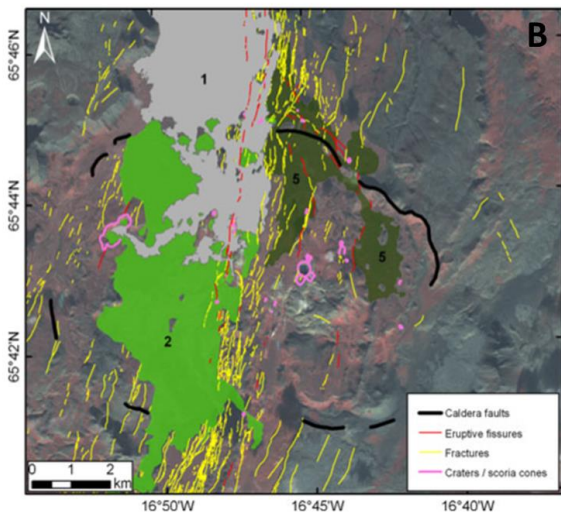
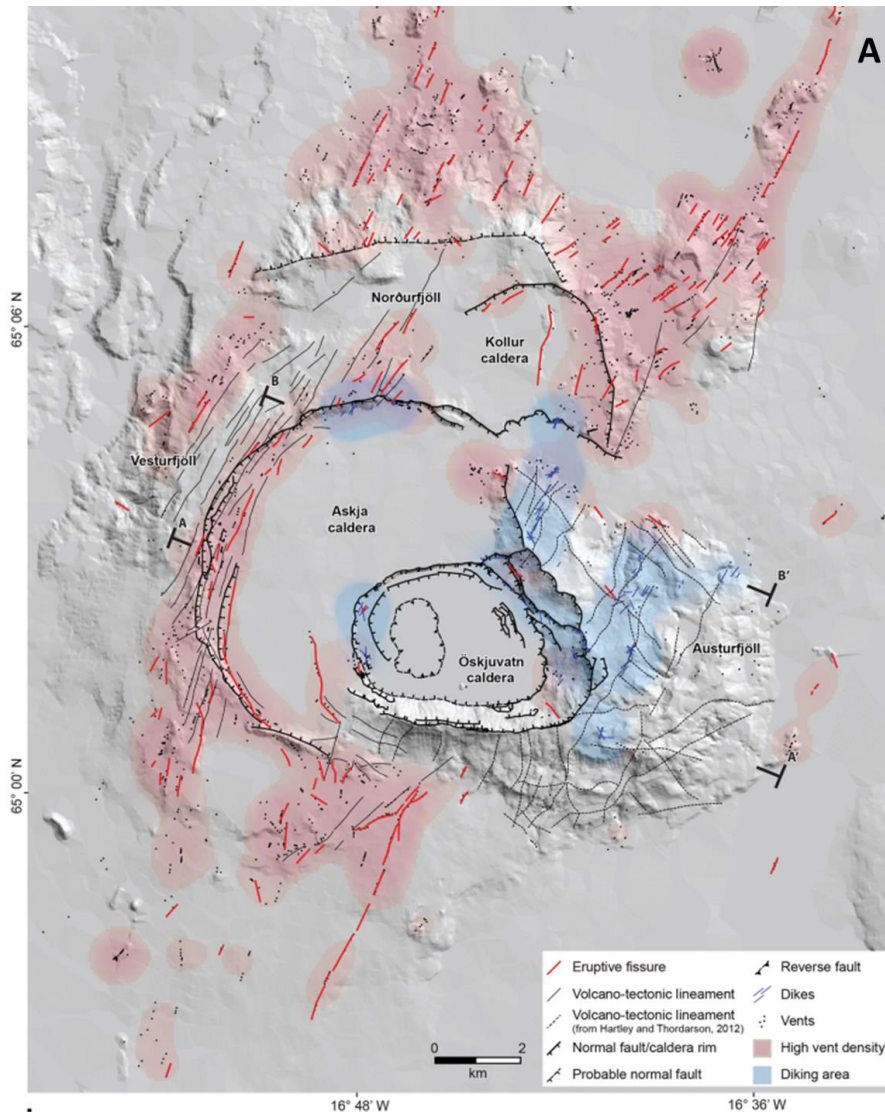


Figure 41. A) A structural map of Askja central volcano showing the most important tectonic and magmatic features (from Trippanera et al., 2018); B) The fissure swarm crossing Krafla caldera, (from Hjartardottir et al., 2012); C) Map of the fault swarm and fissures crossing an elongated caldera of Tulu Moye area.

The structure of caldera-3 suggested that it may be formed by downsag collapse (Figure 40). The collapse structure is not clear and affected by erosion except the patchy arcuate appearance of the faults near the volcanic centres. It seems that the volcanic centers erupted following the pre-existing rim and experienced a downsag type of collapse, resulting in modification of the pre-existing caldera structure by the newly erupted deposits that has the age of Aluto-Bereccia units (0.83 ± 0.10 Ma; Boccaletti et al., 1999).

In addition to these scenarios, the contribution of regional extension also plays an important role on the development of the caldera complex. The collapses, particularly caldera 2 and 3 are developed in association with the north-westerly oriented transverse structures. Moreover, the elongation direction of caldera-1 is also towards the north-west. This is in agreement with the typical caldera structures of the Ethiopian Rift. Acocella et al. (2002) illustrated that most calderas that are developed along the axial zone of the WFB have E-W elongation, caused by the pre-existing tectonic structures that controls the collapse geometry. It is also demonstrated that the E-W-trending fractures were partly reactivated during rifting; possibly controlling the emplacement of the magma chambers at depth and the development of the E-W elongation of the calderas would be the surface expression of such control. The Tulu Moya volcano, erupted on the southern rim of caldera-1 also has a north-easterly elongated crater on its top.

6.3 The WNW-NW fracture system

The north-western part, Bora-Tulu Moya area is characterized by normal faults of multiple orientations and caldera collapses. The dominant faults are oriented in the WNW-NW direction crosscutting the general trend of the rift with subordinate NNE faults (e.g., Figure 35 and 34). This transverse fault system might be formed following the caldera collapse events. This area is also noted by an extensive surface hydrothermal activity (dominantly clay) that implies the existence of an active volcanism and magmatism. However, as confirmed from the field observation, the clay deposits between Bora and Arba Bite appeared as cold following the transverse faults with no or slight temperature change compared to the Mt. Tulu Moya area. This might indicate the less or partial deactivation of tectonic activity in this particular area. Previous studies have shown that the area between Tulu Moya and Bora is active in terms of deformation as well as seismic activity (Biggs et al., 2011; Samrock et al., 2018; Greenfield et al., 2019 a, b), which is thought to be caused by the triggering of the hydrothermal activity at shallow depth. Greenfield et al., (2019 a) also stated “*Seismicity around B-TM is closely associated with the expression of volcanism, being centered around TM, rather than the tectonically generated features within the WFB*”. Thus, the north-western portion of the area might be getting tectonically deactivated. There might be several reasons for the reduced tectonic activity; two scenarios are proposed here. The first scenario is that after the eruption of Pleistocene-Holocene silicic magma (Bora-Berecha silicic products) and caldera collapses, the magma migrated towards the eastern side following the transverse fractures. This is also confirmed from the presence of historical eruptions, which are confined to the east along the Salen spreading axis. The geophysical studies also indicated that the magma chamber is situated at a shallow depth underneath the Tulu Moya volcano (e.g., Samrock et al., 2018). Because extension along the Wonji magmatic segments is assisted by the dyke intrusion (e.g., Ebinger and Casey, 2001; Keir et al., 2006), the migration of the magma from this locality will affect the extensional tectonic activity.

The second scenario is that a local change in the extension direction for a short period. For such reasons the north-western portion of the research area is considered as a gradually deactivated volcano-tectonic area. However, Samrock et al. (2018) identified this region as the low electrical conductivity zone (Figure 13) and interpreted this low electrical conductivity as a highly resistive rock matrix due to the presence of high-temperature alteration minerals and significant steam fraction in the pore fluids.

6.4 Seismicity and its relationship with fractures

Seismic activity and fractures are directly associated. In the MER, the seismic zone is restricted between 20-30 km width across the WFB, corresponding with Quaternary faults, fissures, and chains of eruptive centers (Figure 42; e.g., Keir et al., 2006). The Wonji fault activity is driven by magma intrusions into the mid to upper crust, which trigger faulting and dyke intrusion in the brittle upper crust. This activity controls the locus of seismicity and faulting, where low-magnitude swarms (e.g., Keir et al., 2006) characterize the seismicity.

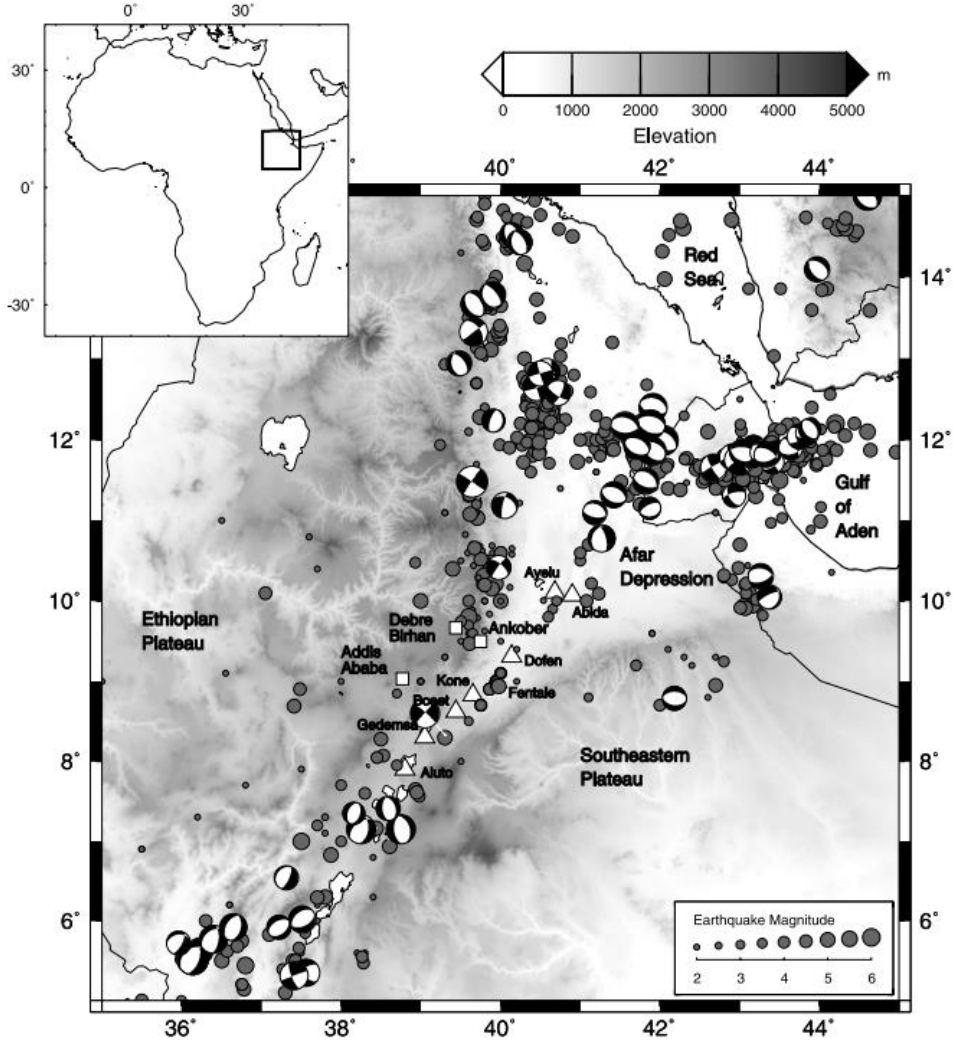


Figure 42. Seismic activity of the Ethiopia since 1960. The triangles show the Quaternary volcanoes in the MER. The image is taken from Keir et al. (2006).

In the study area, a historical earthquake with $M > 6$ were recorded near the rift boundary (Pizzi et al., 2006). In the northern section of the study area, variable orientations of fractures were identified and the fault plane solutions indicated mostly normal faulting (Greenfield et al., 2019 b). The study also confirms the presence of the normal faults that follow the Wonji fault orientation and few of an oblique angle (Figure 43). The earthquake swarms are believed to be driven by the hydrothermal fluid circulation that is assisted by a shallow magmatic reservoirs (< 6 km), underneath the Tulu Moye volcano (Greenfield et al., 2019 a, b).

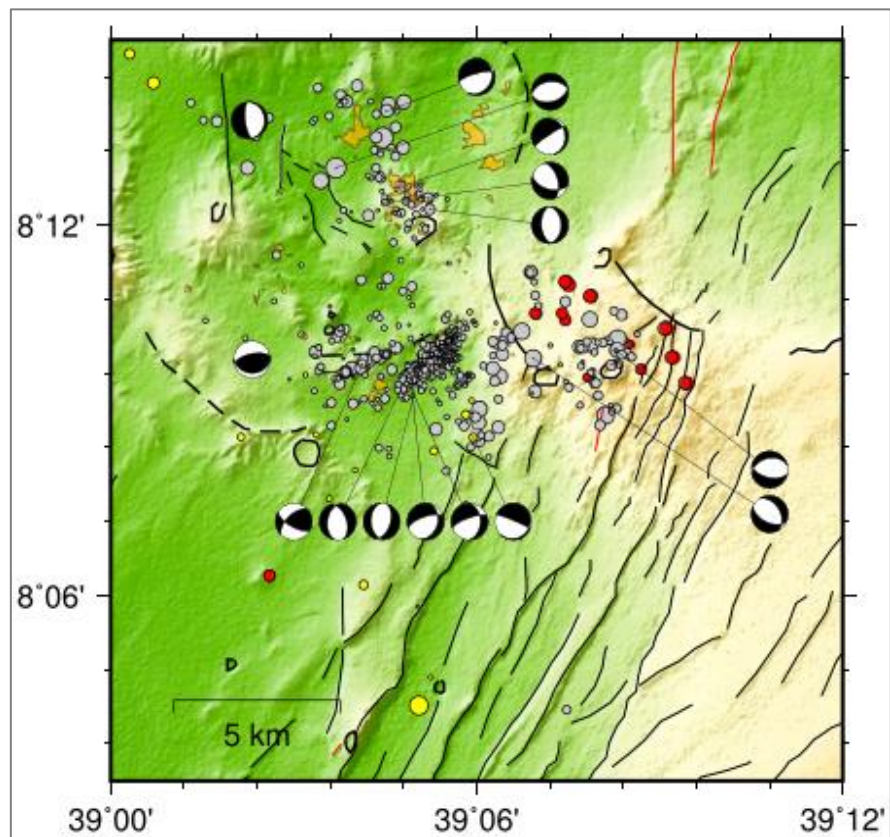


Figure 43. A seismic map showing the distribution of focal mechanisms (from Greenfield et al. 2019a)

By using the data from Greenfield et al. (2019 a,b), here the epicentral distribution of the area is remapped based on magnitude. The structural lineaments best fitting the trends of the seismic swarm are outlined. These structural trends as the orientation of the faults in the area. The orientations are shown by a yellow line on the map (Figure 44). They are located near the intensely altered Arba bite and Werdea volcanoes, the Tulu Moye volcanic center, and along the southwestern rim of the proposed caldera-1. One possible lineament is also observed in the graben structure to the west side of Arba bite. Besides the trends of transverse structures, north-easterly oriented swarm is observed near mount Adano. All the seismicity defined orientations are in line with the existing faults on the surface and the caldera rim, as well as the surface hydrothermal activities. This locality is well defined by extensive

hydrothermal activity that is manifested on the surface mainly in the form of fumaroles and clay deposits following fractures. The surface manifestations also follow the transverse fault system, the caldera-1 rim and the NNE faults (e.g., near Mt. Tulu Moye; Figure 44). This also shows the interaction between the structures, surface thermal manifestations and seismic activity. Such interaction along the south-western rim of caldera-1 suggests the presence of possible geothermal core besides from the area near Tulu Moye volcano.

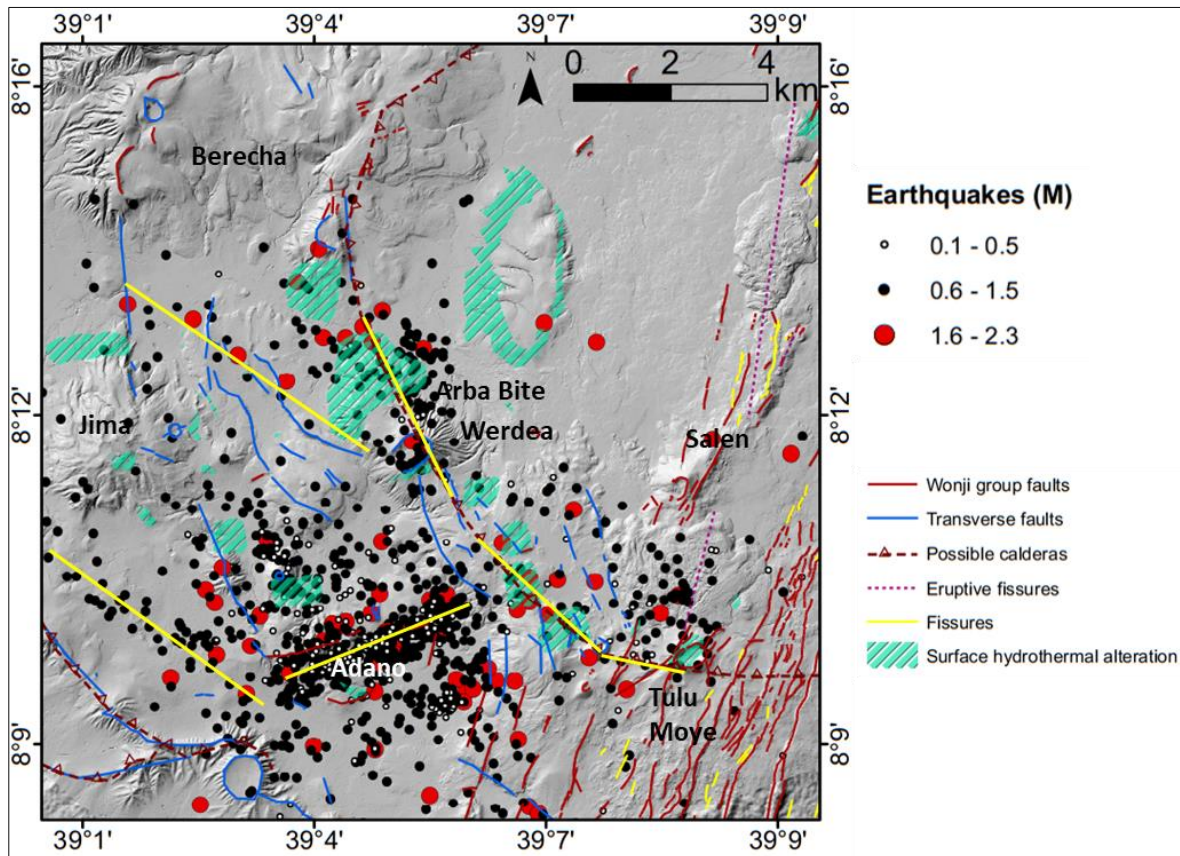


Figure 44. Epicentral map with magnitude showing the association of the existing surface structures with the distribution of the earthquakes (indicated by yellow lines) and surface alteration (The seismic data are provided by the TMGO expert, and the surface alteration is from Ayele et al., 2002 and field observation).

6.5 Tectonic structures and its relationship with the geothermal system

The tectonic structure is one of the most important aspects of a geothermal system. Fractures play a role in relation with permeability. They are paths for the movement of fluid in and out of the reservoir. In the Tulu Moye geothermal area, the fractures are extensive and densely distributed, making an important path for the movement of the fluid in the system. This is confirmed by the structural mapping and previous geophysical studies.

The permeability in the study area is commonly controlled by the fractures and expected to be intense at the intersection of different fracture systems and the caldera rim. This fracture network of the area creates suitable permeability conditions for the recharge into the reservoir. Despite this, unlike the other geothermal systems of Ethiopia, Tulu Moye has no hot/cold springs as well as streams observed on the surface. This apparent lack of recharge can happen for a number of reasons. It might be related to the elevation of the prospect area, which is situated on a highly elevated zone from the surrounding plane; as a result, the groundwater table will be deep seated. The other factor for the absence of the springs in the area might be related to the intense volcanic eruptions. The subsequent volcanic eruptions together with the caldera collapses might cause the faults to be buried, which in turn reduces the hydraulic properties of the system and disrupts the proper subsurface stratification of the aquifer creating a barrier for the movement of the ground water (e.g., Heath, 1983). In this case, the main recharge for the Tulu Moye geothermal system will be meteoric water channelled through the fractures, while the deeper recharge is from the eastern escarpment. Greenfield et al., (2019 a) also concluded that the fluids involved in the hydrothermal circulation of Tulu Moye reservoir could be sourced directly from the degassing of a magmatic body or indirectly via meteoric water. This is also consistent with the idea that the bulk of the water found in hydrothermal fluids of the MER is sourced from rainwater (Darling et al., 1996).

Since the area lacks deep exploration wells, the groundwater system of the Tulu Moye area has not been studied in detail and the subsurface hydrogeological property has not been examined. The current deep well drilling will help to understand this and other subsurface behaviour of the geothermal system in the near future.

Overall, the current drilling targets are located between Mt. Tulu Moye and the Gnaro dome, targeting to cross the Wonji fault and fissure system. Based on the evidences from the exploration studies, the Tulu Moye high temperature geothermal prospect presumably be considered as a good geothermal system.

6.6 Characterisation of the study area with respect to the MER

From the structural and geological information, the research area can be considered as two tectonically distinct settings; each represented by different stages or phases of rifting. As mentioned earlier these are defined by the development of the north easterly striking older border fault system, which is also marked by a non-magmatic (pure tensional) tectonism and the younger magmatically assisted NNE trending Wonji fault system that floors the axis of the rift (e.g., Corti, 2009). These phases are then represented in the research area as the northern (Bora-Tulu Moye) and the southern (Ziway-Asela) areas. The stages of rifting in these two distinct areas are determined typically from the volcano-tectonic relation and pattern of the faults, which in turn is caused by their mode of deformation and age of the tectonic activity. The fractures in the northern section are younger and densely distributed than the southern, implying the presence of active tectonism and higher extension rate in the northern part.

This first phase of relatively older rifting activity characterizes well the northeasterly trending border fault system of the research area as well as the CMER. Apart from the

models and geophysical findings to argue for the non-magmatic rifting along the rift boundaries, Pizzi et al. (2006) used the physical properties and seismicity characteristic to suggest non-magmatic deformation in the Asela area. The mountain front morphology, large vertical displacements, fault length and morphology of the tilted blocks are among the fault features and the brittle-seismic faulting from the historical seismic activity of magnitude > 6 in this region was used to support a tectonic origin of the boundary fault in the southern part of the area.

Further support is also found in the tectonic nature of the central part of the research area. On the Salen axis in its southern extension, the area between Lake Ziway and the Asela escarpment is defined by the north easterly striking and < 2.2 km wide flat lain graben (Figure 29) that has been replaced by the active Wonji fault system of the Salen spreading axis further to the north. At the Salen spreading axis, the angle of extension direction changes and the fractures strike toward N-NNE (Figure 29). This zone might represent the main rift zone of extension and it displays both non-magmatic and magmatic supported deformation on the south and north, respectively. The Salen spreading axis in this area is taken as the locus of active spreading center.

6.7 Conceptual models of the developmental phases of the study area

The conceptual model of the developmental phases of the study area is presented in the context of the MER based on the information from the structural data interpretation, stratigraphic succession and relative age of the rocks, and the theories of the evolution of the MER (Figure 45).

Phase I: Initial rifting and border fault development

The first phase (Figure 45a) represents the primarily rifting in the MER that commenced along the rift border during Miocene (e.g., Woldegabriel et al., 1990) forming alternating half-grabens. The border faulting is resulted from pure extensional movement. In the CMER, the development of the NE-SW striking border faults commenced in Pliocene (e.g., Bonini et al., 2005; Chernet et al., 1998). At this stage of rifting, no volcanism was encountered on the rift floor.

Phase II: Rift shoulder volcanism

The rift continues to deepened and volcanic eruptions started in the eastern plateau on the shoulder of the rift during Pliocene (e.g., Badda, Kecha, Chilalo volcanoes; Woldegabriel et al., 1990; Figure 45b). At this stage, basaltic lava and extensive silicic pyroclastic materials erupted and cover most of the MER floor and continues to Pleistocene (Di Paola, 1972; Woldegabriel et al., 1990). The near escarpment, southern portion of the study area, which is mainly covered by silicic deposit and NE-SW trending horst and graben developed at this time.

Phase III: Quaternary volcano-tectonism (WFB)

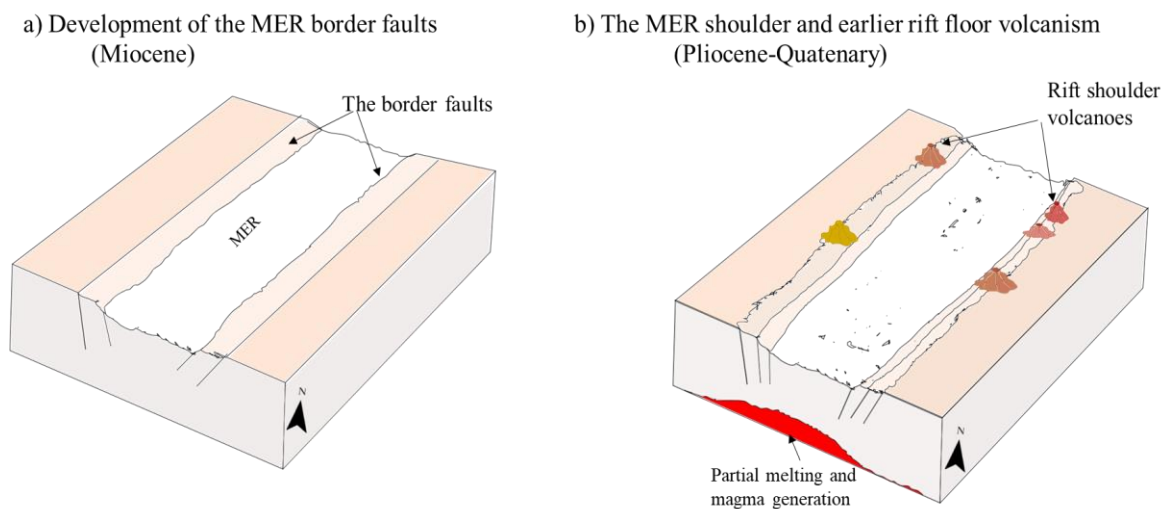
The third phase is considered as an important change in the evolution of the rift. It is marked by the development of the Quaternary (< 2 Ma) rifting (Wonji faulting) on the floor of the rift. In the CMER, this activity is situated near the eastern boundary and on the western boundary (Butajira and Debrezeyit-Silti volcanic zone; e.g., Mohr, 1962; Di Paola, 1972). Unlike the first phase, rifting at this phase involves the magmatic activity and extension is oblique to the general rift trend, arranged in an echelon fashion (e.g., Corti, 2009). At this stage, volcanism took place following the new rifting along the axis (Figure 45c). In the northern section of the study area, the volcanic center forming the Caldera-1 were erupted at this epoch (1.3 Ma; Boccaletti et al., 1999).

Phase IV: The Pleistocene-Holocene activity of the study area

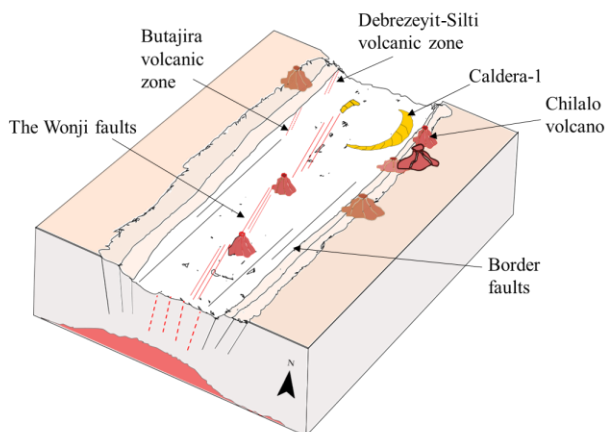
In Pleistocene-Holocene, volcanism and tectonism became more intense in the study area, resulting the thick succession of pyroclastic deposits; including the SE-pyroclastic succession (115 ka-1.8; Bigazzi et al., 1993), Bora, Berecha and Tulu Moya silicic deposits (0.8-0.3 Ma) and the Wonji group basalt lava flows and cinder cones (0.25 Ma) (Woldegabriel et al., 1990; Figure 45d). The proposed caldera collapses (caldera-2 and 3) and the development of the NW striking transverse faults might also have developed at this stage. The late Pleistocene- Holocene is also marked by the development of a basin along the WFB and a large Lake, which is responsible for the lacustrine deposit, which filled most part of the MER (Benvenuti et al., 2002; Di Paola, 1972). The basin occupied large areas of the MER floor, dominantly the CMER.

Phase V: Holocene activities and historical eruptions

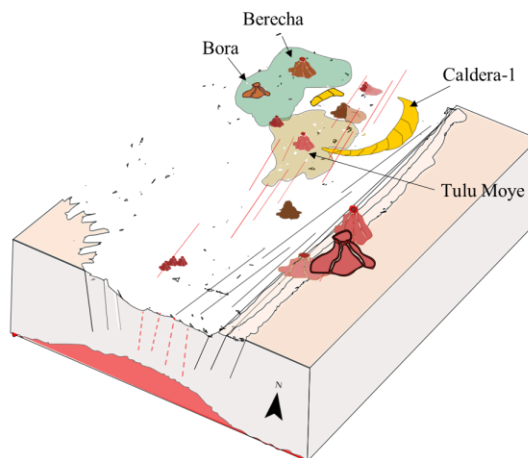
In the last phase of the evolution, the large Lake was separated to form individual Lakes, such as Lake Ziway. This phase marks the continued formation of Lake sediment in the CMER. In the study area, besides the faulting and fracturing, the last historical bimodal fissure eruptions occurred along the Salen ridge were recorded.



c) Volcano-tectonic activity, the development of the WFB in the MER (Pleistocene)



d) The volcano-tectonic activity of the study area (Pleistocene-Holocene)



e) Holocene activities and historical eruptions in the study area

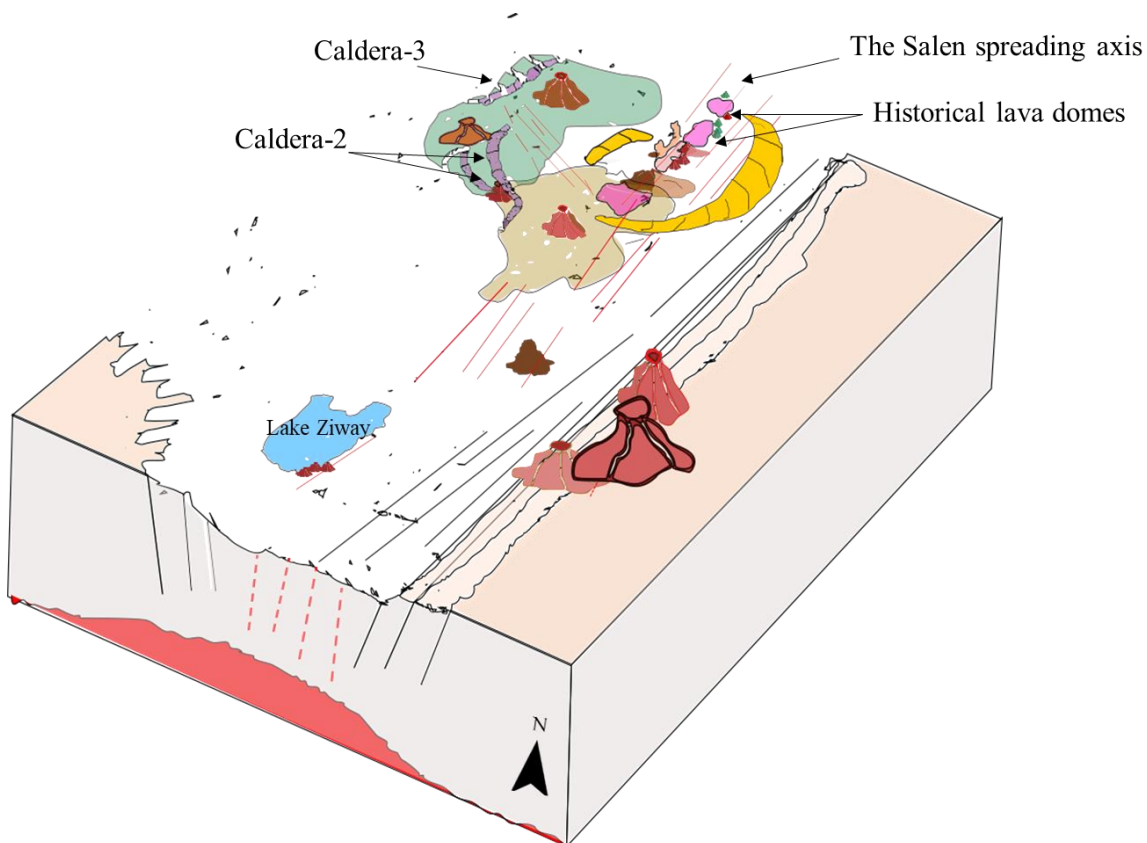


Figure 45. Conceptual models showing the development of the study area in the context of the MER.

7 Conclusions

By using various images and field observations, a detailed structural analysis has been done in the Tulu Moye-Ziway area. The research area can be divided into two distinct regions (northern and southern regions), based on their formation, time of development, age of the deformed rocks and the distribution of the tectonic structures.

The southern region was formed earlier, with a well-developed fault system which includes the major faults of the eastern escarpment. It fulfils the description given for the intermediate stage of rift evolution in the MER. The northern region is an active part of the WFB system, representing the latest activity defined by the interaction of tectonism and magmatism. This behaviour is more correlated with the NMER magmatic segments, yet due to the location of the area, which is in the CMER this locality is concluded to be a transitional area between the CMER and NMER and in a transitional stage of evolution from intermediate (CMER type) to matured (NMER).

From the image analysis, a total of three caldera structures are identified in the northern section. Like the other calderas of the MER, the first caldera, caldera-1 shows an elongation towards the NW, opposite to the elongation direction of the common caldera elongation direction in MER, as seen in the Tulu Moye crater. This depicts the presence of trans-rift extensions. The trans-rift extensions are manifested by several faults in the western part of the north region, where the hydrothermal activities also emanated following their orientations. However, because the hydrothermal manifestations are colder in this part of the study area this locality is considered as tectono-magmatically deactivated. The earthquake data and the surface hydrothermal alterations are overlapped with the rim of caldera-1 structure, suggesting the occurrence of geothermal target in the southwestern rim of the caldera.

Two mini-graben structures are also identified on Mt. Tulu Moye and Salen. It is one of the manifestation of intense tectonism in the area.

The other finding is localized in the north central sector, marked by the presence of the Salen spreading axis. It is a spreading center situated within the Aluto-Gedemsa magmatic segment, where deformation is active and the volcanic activity is expressed by historical fissure eruptions. The geothermal reservoir is also situated along this line. It is characterized by shallow heat source, good permeability that is caused by the network intersection between the structural features.

Overall, the research has confirmed that the tectonic structure of Tulu Moye-Ziway area and the geothermal system of Tulu Moye is comparable to the tectonic features of the Ethiopian rift system in various parameters. It also has various parameters making it comparable with the divergent tectonic settings in the other part of the world, like the Mid-Oceanic ridge, Iceland.

8 Recommendations

The Tulu Moye area is one of the promising geothermal sites in Ethiopia and detailed investigations are still ongoing. In order to support the geothermal exploration and exploitation process and also to define the geology of the area in a better way, it is recommended to do more geophysical studies and geochemical analysis of the rocks. This will also benefit to better define and comprehend the caldera structures as well as the activity of the transverse structures and the connection to the geothermal system. In addition, further investigation is recommended along the south-western rim of the caldera-1 rim, where the promising geothermal core is evaluated in this study.

It is also recommended to do a detailed work on the reconstruction of volcanic history of the whole area.

Since recharge is the necessity for the geothermal system, the hydrology system of the area, particularly the geothermal system needs to be studied in more detail.

It is recommended to study the subsurface geology of the area in detailed and conceptualize the geothermal model in a better way from the deep drilling wells that are currently undergoing drilling.

References

- Abbate, E., Sagri, M., (1980). Volcanites of Ethiopian and Somali Plateaus and major tectonic lines. *Atti Convegna Lincei* 47, 219–227
- Abebe B., Boccaletti M., Mazzuoli R., Bonini M., Tortorici L., Trua T. (1998). Geological Map of the Lake Ziway-Asela Region (Main Ethiopian Rift). 1:50,000 scale. A.R.C.A Map, Florence.
- Abebe, B., Acocella, V., Korme, T., Ayalew, D., (2007). Quaternary faulting and volcanism in the Main Ethiopian Rift. *J. Afr. Earth Sci.* 48, 115–124.
- Abebe, T., Mazzarini, F., Innocenti, F., Manetti, P. (1998). The Yerer–Tullu Wellel volcanotectonic lineament: a transtensional structure in Central Ethiopia and the associated magmatic activity. *Journal of African Earth Sciences* 26, 135–150. [https://doi.org/10.1016/S0899-5362\(97\)00141-3](https://doi.org/10.1016/S0899-5362(97)00141-3)
- Abebe, T., Manetti, P., Bonini, M., Corti, G., Innocenti, F., Mazzarini, F., Pecskey, Z., (2005). Geological map (scale 1:200000) of the northern main Ethiopian rift and its implication for the volcano-tectonic evolution of the rift. Geological Society of America, Boulder Colorado, USA, Maps and Charts series, MCH094.
- Abebe, T., Laura, M., Balestrieri, M.L., Bigazzi, G., (2010). The Central Main Ethiopian Rift is younger than 8 Ma: confirmation through apatite fission-track thermochronology. *Terra Nova* 22, 6, 470–476. <http://doi: 10.1111/j.1365-3121.2010.00968>

- Acocella, V., Korme, T., (2002). Holocene extension direction along the Main Ethiopian Rift, East Africa. *Terra Nova* 14, 191–197
- Acocella, V., Korme, T., Salvini, F., Funicello, R., (2002). Elliptic calderas in the Ethiopian Rift: the control of pre-existing structures. *J. Volcanol. Geotherm. Res.* 119, 189– 203
- Agostini, A., Bonini, M., Corti, G., Sani, F., Manetti, P., (2011a). Distribution of Quaternary deformation in the central Main Ethiopian Rift, East Africa. *Tectonics* 30, TC4010. <http://dx.doi.org/10.1029/2010TC002833>.
- Agostini, A., Bonini, M., Corti, G., Sani, F., Mazzarini, F., (2011b). Fault architecture in the Main Ethiopian Rift and comparison with experimental models: implications for rift evolution and Nubia–Somalia kinematics. *Earth PlanetSci. Lett.* 301, 479–492. [10.1016/j.epsl.2010.11.024](http://dx.doi.org/10.1016/j.epsl.2010.11.024)
- Ayele, A., Teklemariam, M. and Kebede, S. (2002). Geothermal Resource Exploration in the Abaya and Tulu Moye-Gedemsa Geothermal Prospects, Main Ethiopia Rift. Internal report, Geological Survey of Ethiopia, Addis Ababa, Ethiopia, 172 pp.
- Bastow, I.D., Stuart, G.W., Kendall, J.M., Ebinger, C.J., (2005). Upper mantle seismic structure in a region of incipient continental breakup: northern Ethiopian rift. *Geophysical Journal International* 162 (2), 479–493.
- Benvenuti, M., Carnicelli, S., Belluomini, G., Dainelli, N., DiGrazia, S., Ferrari, G., Iasio, C., Sagri, M., Ventura, D., Atnafu B. (2002). The Ziway–Shala Lake basin (main Ethiopian rift, Ethiopia): a revision of basin evolution with special reference to the Late Quaternary. *J. Afr. Earth Sci.*, 35, pp. 247-269, [10.1016/S0899-5362\(02\)00036-2](http://dx.doi.org/10.1016/S0899-5362(02)00036-2).
- Berhe, S.M., (1990). Ophiolites in northeast and East Africa: implications for Proterozoic crustal growth. *Journal of the Geological Society of London* 147, 41–57.
- Beyene, A., and Abdelsalam, M., (2005). Tectonics of the Afar Depression: a review and synthesis. *Journal of African Earth Science*. 41: 41-59.
- Bigazzi, B., Bonadonna, F.P., Di Paola, G.M., Giuliani, A., (1993). K-Ar and fission track ages of the last volcano tectonic phase in the Ethiopian Rift Valley (Tullu Moye' area). *Geology and Mineral Resources of Somalia and Surrounding Region*, pp. 311–322.
- Biggs, J., Bastow, I. D., Keir, D., & Lewi, E. (2011). Pulses of deformation reveal frequently recurring shallow magmatic activity beneath the Main Ethiopian Rift. *Geochemistry, Geophysics, Geosystems*, 12, Q0AB10. <https://doi.org/10.1029/2011GC003662>.
- Bizouard, H., Di Paola, G.M., (1978). Mineralogy of the Tullu Moje active volcanic area (Arussi: Ethiopian Rift Valley). In: Neumann, E.R., Ramberg, I.B. (Eds.), *Petrology and Geochemistry of Continental Rifts*. Reidel Publishing Company, Dordrecht, Holland, pp. 87–100.
- Boccaletti, M., Bonini, M., Mazzuoli, R., Abebe, B., Piccardi, L., Tortorici, L., (1998). Quaternary oblique extensional tectonics in the Ethiopian Rift (Horn of Africa). *Tectonophysics* 287, 97–116.

Boccaletti, M., Bonini, M., Mazzuoli, R., Trua, T., (1999). Pliocene-Quaternary volcanism and faulting in the northern Main Ethiopian Rift (with two geological maps at scale 1:50000). *Acta Vulcanologica* 11, 83–97.

Bonini, M., Corti, G., Innocenti, F., Manetti, P., Mazzarini, F., Abebe, T., Pecskey, Z., (2005). The evolution of the Main Ethiopian Rift in the frame of Afar and Kenya rifts propagation. *Tectonics* 24, TC1007. doi:10.1029/2004TC001680

Chernet, T., W. Hart, J. Aronson, and R. Walter, (1998). New age constraints on the timing of volcanism and tectonism in the northern Main Ethiopian Rift—Southern Afar transition zone (Ethiopia), *J. Volcanol. Geotherm. Res.*, 80, 267– 280.

Chorowicz, J., Collet, B., Bonavia, F., Korme, T., (1994). Northwest to north-northwest extension direction in the Ethiopian rift deduced from the orientation of extension structures and fault-slip analysis. *Geological Society of America Bulletin* 105, 1560–1570. [https://doi.org/10.1130/0016-7606\(1994\)105<1560:NTNED>2.3.CO;2](https://doi.org/10.1130/0016-7606(1994)105<1560:NTNED>2.3.CO;2)

Chorowicz, J., (2005). The East African Rift System. *Journal of African Earth Sciences* 43, 379–410. doi:10.1016/j.jafrearsci.2005.07.019

Cole, J. W., (1969). The Gariboldi volcanic complex. *Bull. Volcanol.* 33, 566–578. doi: 10.1007/BF02596525

Cole, J.W., Milner, D.M., Spinks, K.D. (2004). Calderas and caldera structures: a review. *Earth-Science Reviews* 69, 1 –26.

Corti, G. (2008). Control of rift obliquity on the evolution and segmentation of the main Ethiopian rift, *Nat. Geosci.*, 1(4), 258– 262. doi:10.1038/ngeo160.

Corti, G., (2009). Continental rift evolution: from rift initiation to incipient break-up in the Main Ethiopian Rift, East Africa. *Earth Sci. Rev.* 96, 1–53.

Darling, W. G., Gizaw, B., Arusei, M. K. (1996). Lake-groundwater relationships and fluid-rock interaction in the East-African Rift Valley: Isotopic evidence. *Journal of African Earth Sciences*, 22(4), 423–431. [https://doi.org/10.1016/0899-5362\(96\)00026-7](https://doi.org/10.1016/0899-5362(96)00026-7)

Di Paola, G.M., (1972). The Ethiopian Rift Valley (between 7°00' and 8°40' lat. North). *Bulletin of Volcanology*, 36, 517–560.

Dugda, M.T., Nyblade, A.A., Julia, J., Langston, C.A., Ammon, C.J., Simiyu, S., (2005). Crustal structure in Ethiopia and Kenya from receiver function analysis: implications for rift development in eastern Africa. *J. Geophys. Res.* 110, B01303. doi:10.1029/2004JB003065.

Ebinger, C.J., Yemane, T., Woldegabriel, G., Aronson, J.L., Walter, R.C., (1993). Late Eocene-Recent volcanism and faulting in the southern main Ethiopian rift. *Journal of the Geological Society of London* 150, 99–108.

Ebinger, C.J., Casey, M., (2001). Continental breakup in magmatic provinces: an Ethiopian example. *Geology* 29, 527–530.

Electroconsult, (1987). Geothermal reconnaissance study of selected sites in the Ethiopian Rift Valley. Internal final report. Ethiopian Institute of Geological Survey. 172 p. 20p.

Fentaw, B., Mihret, M., (2011). Hydrogeological map of Akaki–Beseka 1:250.000 scale (Ethiopia), sheet NC 37-14. Geological Survey of Ethiopia, Addis Ababa, Ethiopia, internal report.

Fontijn, K., Keri M.N., Amdemichael, Z. T., David, M. P., Firawalin, D., William, H., Tamsin, A. M., Yirgu, G., (2018). Contrasting styles of post-caldera volcanism along the Main Ethiopian Rift: Implications for contemporary volcanic hazards. *Journal of Volcanology and Geothermal Research*, 356, 90-113.

Gani, N.D., Abdelsalam, M.G., Gani, M.R., (2007). Blue Nile incision on the Ethiopian Plateau: pulsed plateau growth, Pliocene uplift, and hominin evolution. *GSA Today* 17, 4–11.

Ghiglieri, G., Pistis, M., Abebe, B., Azagegn, T., Engidasew, T., Pittalis, D., Soler, A., Barbieri, M., Navarro-Ciurana, S., Carrey, R., Puig, R., Carletti, A., Balia, R., Haile, T. (2020). Three- dimensional hydrostratigraphical modelling supporting the evaluation of fluoride enrichment in groundwater: Lakes basin (Central Ethiopia). *Journal of Hydrology: Regional Studies* 32, 100756. <https://doi.org/10.1016/j.ejrh.2020.100756>

Greenfield, T., Keir, D., Kendall, J.-M., & Ayele, A. (2019a). Seismicity of the Bora-Tulu Moyo volcanic field, 2016–2017. *Geochemistry, Geophysics, Geosystems*, 20. <https://doi.org/10.1029/2018GC007648>

Greenfield, T., Keir, D., Kendall, J.-M., & Ayele, A. (2019b). Low-frequency earthquakes beneath Tulu Moyo volcano, Ethiopia, reveal fluid pulses from shallow magma chamber. *Earth and Planetary Science Letters* 526. <https://doi.org/10.1016/j.epsl.2019.115782>

Gudbrandsson, S., Eysteinnsson, H., Mamo, T., Cervantes, C., Gislason, G., (2020). Geology and Conceptual Model of the Tulu Moyo Geothermal Project, Oromia, Ethiopia. *Proceedings World Geothermal Congress Reykjavik, Iceland*, 7p.

Gudmundsson, M.T., K. Jónsdóttir, A. Hooper, E. P. Holohan, S. A. Halldórsson, B. G. Ófeigsson, S. Cesca, K. S. Vogfjörð, F. Sigmundsson, Th. Högnadóttir, P. Einarsson, O. Sigmarsson, A. H. Jarosch, K. Jónasson, E. Magnússon, S. Hreinsdóttir, M. Bagnardi, M. Parks, V. Hjörleifsdóttir, F. Pálsson, T. R. Walter, M. P.J. Schöpfer, S. Heimann, H. I. Reynolds, S. Dumont, E. Bali, G. H. Gudfinnsson, T. Dahm, M. Roberts, M. Hensch, J. M.C. Belart, K. Spaans, S. Jakobsson, G. B. Gudmundsson, H. M. Fridriksdóttir, V. Drouin, T. Dürig, G. Adalgeirsdóttir, M. S. Riishuus, G. B.M. Pedersen, T. van Boeckel., (2016). Gradual caldera collapse at Bárðarbunga volcano, Iceland, regulated by lateral magma outflow. *Science*, 353, aaf8988 Doi: 10.1126/science.aaf8988.

Heath, R.C., (1983). Basic groundwater hydrology. US Geological Survey, Reston, VI, 86 pp.

Hayward, N.J., Ebinger, C.J., (1996). Variations in the along-axis segmentation of the Afar Rift system. *Tectonics* 15, 244-257. <https://doi.org/10.1029/95TC02292>

Hjartardóttir Á.R., Einarsson, P., Sigurdsson, H., (2009). The fissure swarm of the Askja volcanic system along the divergent plate boundary of N Iceland. *Bull Volcanol* 71, 961–975. <https://doi.org/10.1007/s00445-009-0282-x>

Hjartardóttir Á.R., Einarsson, P., Bramham, E., Wright, T. J., (2012). The Krafla fissure swarm, Iceland, and its formation by rifting events. *Bull Volcanol* 74, 2139–2153. DOI 10.1007/s00445-012-0659-0

Kebede, S., (2014). Geothermal exploration and development in Ethiopia: country update. Short Course IX on Exploration for Geothermal Resources. UNU-GTP, GDC and KenGen, Kenya. <https://orkustofnun.is/gogn/unu-gtp-sc/UNU-GTP-SC-19-1002.pdf>

Keir, D., Ebinger, C. J., Stuart, G. W., Daly, E., & Ayele, A., (2006). Strain accommodation by magmatism and faulting as rifting proceeds to breakup: Seismicity of the northern Ethiopian rift. *Journal of Geophysical Research*, 111, B05314. <https://doi.org/10.1029/2005JB003748>

Keranen, K., Klemperer, S.L., (2007). Discontinuous and diachronous evolution of the Main Ethiopian Rift: implications for the development of continental rifts. *Earth PlanetSci. Lett.* 265, 96–111. doi:10.1016/j.epsl.2007.09.038

Keranen, K., Klemperer, S.L., Julia, J., Lawrence, J.L., Nyblade, A., (2009). Low lower-crustal velocity across Ethiopia: is the Main Ethiopian Rift a narrow rift in a hot craton? *Geochemistry, Geophysics, Geosystems* 10, Q0AB01. doi:10.1029/2008GC002293.

Korme, T., (1999). Lithologic and structural mapping of the north east Lake Ziway area, Ethiopian Rift with the help of Landsat TM data. *SINET, Ethiopian Journal of Science*, 22, 151 – 174.

Lipman, P.W., (1995). Subsidence of ash-flow calderas; role of magma chamber geometry. *IUGG Gen. Assem.* 21, 452.

Mackenzie, G.D., Thybo, H., Maguire, P.K.H., (2005). Crustal velocity structure across the main Ethiopian Rift; results from two-dimensional wide-angle seismic modelling. *Geophys. J. Int.* 162, 994–1006. <https://doi.org/10.1111/j.1365-246X.2005.02710.x>

Maguire, P.K.H., Keller, G.R., Klemperer, S.L., Mackenzie, G.D., Keranen, K., Harder, S O'Reilly, B., Thybo, H., Asfaw, L., Khan, M.A., Amha, M.,(2006). Crustal structure of the Northern Main Ethiopian Rift from the EAGLE controlled source survey; a snapshot of incipient lithospheric break-up. In: Yirgu, G., Ebinger, C.J., Maguire, P.K.H. (The Afar Volcanic Province within the East African Rift System: Geological Society Special Publication, 259, 269–291

Mahatsente, R., Jentzsch, G., Jahr, T., (1999). Crustal structure of the Main Ethiopian Rift from gravity data: 3-dimensional modeling. *Tectonophysics* 313, 363–382

Marini, L., (2018). “Fluid geochemistry of the Tulu Moye Geothermal prospect (and nearby areas) Ethiopia”. *Géo2D* internal report to Meridiam, 61p

- Mazzarini, G., Corti, G., Manetti, P. & Innocenti, F., (2004). Strain rate and bimodal volcanism in the continental rift: Debre Zeyt volcanic field, northern MER, Ethiopia. *Journal of African Earth Sciences*, 39, 415–420
- Meyer, W., Pilger, A., Rosler, A., and Stets, J., (1975). Tectonic evolution of the northern part of the Main Ethiopian Rift in southern Ethiopia, *in* Pilger, A., and Rosler, A., eds., *Afar Depression of Ethiopia*: Stuttgart, Germany, Schweizerbart, Scientific Report 14, p. 352–362.
- Mickus, K., Tadesse, K., Keller, G.R., Oluma, B., (2007). Gravity analysis of the main Ethiopian rift. *Journal of African Earth Sciences* 48, 59–69.
- Mohr, P., (1962). The Ethiopian Rift System. *Bull. Geophys. Obs. Addis Ababa* 5, 33–62
- Mohr, P., (1967). The Ethiopian Rift System. *Bull. Geophys. Obs. Addis Ababa* 11, 1–65
- Pizzi, A., Coltorti, M., Abebe, B., Disperati, L., Sacchi, G., Salvini, R., (2006). The Wonji fault belt (main Ethiopian Rift): structural and geomorphological constraints and GPS monitoring. In: Yirgu, G., Ebinger, C.J., Maguire, P.K.H. *The Afar Volcanic Province within the East African Rift System: Geological Society Special Publication*, vol. 259, pp. 191–207. DOI:10.1144/GSL.SP.2006.259.01.16
- Ring, U., (2014). The East African Rift System. *Austrian Journal of Earth Sciences*, 107, 1.
- Rooney, T., Furman, T., Yirgu, G., Ayelew, D., (2005). Structure of the Ethiopian lithosphere: evidence from mantle Xenoliths. *Geochemica et Cosmochimica Acta* 69, 3889–3910.
- Samrock, f., Alexander, V., Eysteinnsson, H., and Saar, M., (2018). Magnetotelluric image of transcrustal magmatic system beneath the Tulu Moye geothermal prospect in the Ethiopian Rift. *Geophysical Research Letters* 45, no. 23, 12-847. <https://doi.org/10.1029/2018GL080333>.
- Sæmundsson, K., (1991). Geology of the Krafla Volcanic system (Jarðfræði Kröflukerfisins in Icelandic). *Náttúra Mývatns*, 1, 24-95
- Saemundsson, K., (2012). Torfajökull, iceland – a rhyolite volcano and its geothermal resource. Short Course IX on Exploration for Geothermal Resources. UNU-GTP, GDC and KenGen.
- Sigmundsson, F., A. Hooper, S. Hreinsdóttir, K.S. Vogfjörð, B.G. Ófeigsson, E.R. Heimisson, S. Dumont, M. Parks, K. Spaans, G.B. Guðmundsson, V. Drouin, T. Árnadóttir, K. Jónsdóttir, M.T. Gudmundsson, T. Högnadóttir, H.M. Fridriksdóttir, M. Hensch, P. Einarsson, E. Magnússon, S. Samsonov, B. Brandsdóttir, R.S. White, T. Ágústsdóttir, T. Greenfield, R.G. Green, Á.R. Hjartardóttir, R. Pedersen, R.A. Bennett, H. Geirsson, P.C. La Femina, H. Björnsson, F. Pálsson, E. Sturkell, C.J. Been, M. Möllhoff, A.K. Braiden & E.P.S. Eibl, (2015). Segmented lateral dyke growth in a rifting event at Bárðarbunga volcanic system, Iceland. *Nature*, 517, 191-195, doi:10.1038/nature14111.

Sigurdsson, H., Sparks, R.S.J., (1978). Rifting episode in north Iceland in 1874–1875 and the eruption of Askja and Sveinagja. *Bulletin of Volcanology* 41, 149–167.

Tepp, G., Hotovec, E.A., Shiro, B., Johanson, B., Thelen, W., Haney, M., (2020). Seismic and geodetic progression of the 2018 summit caldera collapse of Kīlauea volcano. *Earth and Planetary Science Letters*, 540,116250, ISSN 0012-21X, <https://doi.org/10.1016/j.epsl.2020.116250>.

Trippanera, D., Ruch, J., Acocella, V., (2018). Interaction between central volcanoes and regional tectonics along divergent plate boundaries: Askja, Iceland. *Bull Volcanol* 80, 1. <https://doi.org/10.1007/s00445-017-1179-8>

United Nations Development Programme (UNDP) (1973). Investigation of geothermal resources for power development. *Geology, Geochemistry and Hydrogeology of hot springs of the East African Rift System within Ethiopia*. DP/SF/UN 116-technical internal report.

Varet, J., Birba, E., (2018). Tulu Moye Geothermal Project (Oromia, Ethiopia). *Proceedings 7th African Rift geothermal Conference Kigali, Rwanda*, 14p.

Wadge, G., Biggs, J., Lloyd, R., and Kendall, J., (2016). Historical volcanism and the state of stress in the East African Rift System. *Frontiers in Earth Science* 4, 86.

Woldegabriel , G., Aronson, J.L., Walter, R.C., (1990). Geology, geochronology, and rift basin development in the central sector of the Main Ethiopia Rift. *Geol. Soc. Am. Bull.* 102, 439–458

Wolfenden, E., Ebinger, C., Yirgu, G., Deino, A., Ayale, D., (2004). Evolution of the northern Main Ethiopian rift: birth of a triple junction. *Earth PlanetSci. Lett.* 224, 213–228.

Zanettin, B., Justin-Visentin, E., Nicoletti, M., Petrucciani, C., (1978). Evolution of the Chenchu escarpment and the Ganjiuli graben (Lake Abaya) in the southern Ethiopian rift. *Neues Jahrbuch fur Geologie und Palaontologie. Monatshefte* 8, 473–490.